

PEOPLE'S DEMOCRATIC REPUBLIC OF ALGERIA
MINISTRY OF HIGHER EDUCATION AND SCIENTIFIC RESEARCH
UNIVERSITY OF BLIDA 1
Faculty of Technology
Process Engineering Department



DOCTORAL THESIS

Process Engineering

Specialty: Materials Engineering

ALKALI METAL FERRATES; BIO-SUPEROXIDANTS: SYNTHESIS AND
APPLICATION IN WASTEWATER TREATMENT

By

BENNACER nour el houda

Before the jury composed of :

O.BOURAS	Professeur	SDB 1 University	Président
A.KHADRAOUI	Professor	khemis meliana University	Examiner
Z.CHEMAT DJENI	Professor	SDB 1 University	Examiner
M.W.NACEUR	Professor	SDB 1 University	thesis supervisor
H.HAMITOCHE	MCA	SDB 1 University	thesis Co-supervisor

ACKNOWLEDGEMENTS

First and foremost, I express my gratitude to Almighty Allah for granting me the health and determination to successfully complete this PhD journey.

I would like to thank my esteemed supervisor **Pr. Mohamed Wahib NACEUR** for his invaluable supervision, support and tutelage during the course of my PhD degree. My gratitude extends to my co-supervisor **Dr. Houria Hamitouche** for her invaluable advice, continuous support, patience, and encouragement throughout these years of study and research. Their unwavering presence and dedication to our growth, coupled with their willingness to share their experience, have been truly remarkable. I am eternally grateful for the trust and interest they have shown in me during this period.

I would like to extend my heartfelt gratitude to **Pr. Rachid ISAADI**, the director of the Laboratory “Energetic Application of Hydrogen (EAppH), University of Saad Dahleb Blida 1 for receiving me in his laboratory over all the years of my PhD. I would like to extend a warm thank to **Dr. Nadjjet TAOUALITE** for the support and the help she gave me over my PhD experiments.

A special thanks to **Pr. Omar BOURAS**, the director of the Laboratory “water environment and sustainable development EEDD” for all the advices you gave me, the moral support and motivation to move forward in my journey I appreciate every word you said.

A deep thank to my sister **Dr. Amel BENNACER** for the support with chemical products material and analysis you were my supplier over years I’m grateful for the help you gave me.

I would like to thank mister **Nabil BERKANE** for the important help and support.

I would like to express my gratitude to engineers team of the central laboratory of SEAAL, Kouba : Houa, Fifi, Imen, Nasria, Zina, Mahdia, Riadh as well as ONA WWTP (beni mered) laboratory team chadouli and benamirouche for the help and the support during my training period.

I would like to thank my friends, lab mates, colleagues: Asma, Wissem, Ouafa, Nousaiba, Asma for all the moments we share in lab with ups and downs.



SCAN ME

DEDICATIONS

To my pieces of heaven on earth, my *mum* and *dad* without both of you I would not get to this stage of knowledge thank you for having faith in me over all those years ,I'am thankful to have a parents like you and grateful that you finely see me a doctor.

To my soulmate my gift from god, *my husband* thank you for helping me with all you have, the constant moral support through the sleepless night writing my thesis and the encouragement your belief in me kept me going through this PhD journey I am blessed to have you by my side.

To my sister doctor *Amel BENNACER* your support throughout my doctoral journey made a big difference in my work I am thankful for having such a caring and loving sister

To my little brother *Soheib Aimen* my best friend your support will always have a fingerprint in my life.

To my little sister *Nesrine* my besty your advices and support comes always in the right time thank you to be the best part of the family

To the memory of *my father* in law you will always be in our hearts (17/09/2023)

To *my mother* in law you are such a pure caring women

To my brothers in law: *Imad ,Housseem and Hamza*

To my sisters in law: *Ahlem , Farah and Hiba*

To my nephews in law: *Mohamed and Amira*

To my best friend: *Soumiya*

LIST OF ABBREVIATIONS

ABTS	: 2,2-azino-bis (3- ethylbenzothiazoline-6-sulfonic) acid
Abs	: absence
CFU	: colony-forming unit
DDA%	: degree of deacetylation
E. coli	: Escherichia coli
GCI	: gray cast iron
OS	: ordinary steel
T _d	: drying temperature
tr	: reaction time
WCI	: white cast ion
WWTP	: wastewater treatment plant
w :v	: ratio weight: volume
WHO	: world health organization

LISTE OF FIGURES

Figure 1.1	Presentation of the ferrate molecule $[\text{FeO}_4]^{2-}$.	6
Figure 1.2	Hybrid resonance structure of the Fe (VI) ion.	7
Figure 1.3	Approximate $E=f(\text{pH})$ diagram of the most common iron compounds (1 atm; 25°C).	8
Figure 1.4	Ferrate (VI) color in powder form and in aqueous solution.	10
Figure 1.5	Vibration modes of the ferrate molecule.	11
Figure 1.6	Electrochemical cell for ferrate production.	17
Figure 1.7	The electrochemical method for ferrate synthesis in a two-compartment cell with salt bridge separation.	22
Figure 1.8	Chemical structure of chitin.	23
Figure 1.9	Chemical structure of chitosan.	24
Figure 3.1	The process of electro-generation of ferrate (VI). (1) DC power supply, (2) electrical wire, (3) iron electrodes, (4) double compartment electrochemical cell, (5) chitosan membrane, (6) magnetic stirrer.	46
Figure 3.2	Experimental setup used for the synthesis of ferrates by the dry route. 1-Mechanical stirrer, 2-Double-walled cell, 3-Water bath.	49
Figure 3.3	experimental setup of the chromite method	52
Figure 3.4	Beni Messous station from above (Algiers, 2025).	53
Figure 3.5	Beni Mered WWTP view from above (Blida, 2025).	55
Figure 3.6	Reagent tube LCI500 of COD (left) and the spectrophotometer used (right).	56
Figure 3.7	The SP50 SKALAR robot for BOD ₅ analysis (central laboratory SEAAL, Algiers)	57
Figure 3.8	Continuous flow analyzer (central laboratory SEAAL, Algiers).	59
Figure 3.9	LCK 339 reagent for nitrate analysis.	60
Figure 3.10	Bacterial filtration system (microbiology laboratory, SEAAL).	61
Figure 4.1	From red shrimp shells to chitosan membrane.	63
Figure 4.2	FTIR spectra of the extracted chitosan membrane.	64
Figure 4.3	XRD spectra of the chitosan powder and membrane.	65
Figure 4.4	Thermogravimetric analysis (TGA) of chitosan membrane.	66

Figure 4.5	Differential scanning calorimetry (DSC) of the chitosan membrane.	67
Figure 4.6	Ferrate (VI) concentration and current efficiency in different NaOH concentrations at 60 mA/cm ² over 1 h of electrolysis at 25 °C ± 0.5 synthesized chitosan (CS) membrane.	69
Figure 4.7	Evolution of the consumed energy (kWh/kg) in different NaOH concentration for chitosan membranes.	69
Figure 4.8	Ferrate (VI) concentration and current efficiency as a function of different current density (mA/cm ²) in 20 M NaOH over 1h electrolysis at 25 °C ± 0.5, synthesized with chitosan membrane.	70
Figure 4.9	Evolution of the consumed energy (kWh/kg) in function of current density for chitosan membranes.	71
Figure 4.10	Ferrate (VI) concentration and current efficiency at different temperature in 20 M NaOH at 60 mA/cm ² for 1h electrolysis synthesized with chitosan (CS) membrane.	72
Figure 4.11	Evolution of the consumed energy (kWh/kg) in function of different reaction temperature for chitosan membranes.	72
Figure 4.12	Impact of electrode composition on the concentration of generated ferrate (VI), and current efficiency using both chitosan membrane.	73
Figure 4.13	Evolution of the consumed energy (kWh/kg) for different electrodes types for chitosan membranes.	74
Figure 4.14	Ferrate (VI) concentration and current efficiency by electrolysis duration (min) in 20 M NaOH at 60 mA/cm ² in 25 °C ± 0.5 for chitosan membrane.	75
Figure 4.15	Evolution of the consumed energy at different electrolysis times for Chitosan membranes.	76
Figure 4.16	Variation of ferrate purity (VI) (%) as a function of drying time for iron sulfate heptahydrate and particle diameter of iron sulfate heptahydrate/calcium hypochlorite.	77
Figure 4.17	Variation of ferrate (VI) purity (%) as a function of drying temperature of iron sulfate heptahydrate.	78

Figure 4.18	Variation of ferrate (VI) purity (%) as a function of reaction time (min).	79
Figure 4.19	Variation of ferrate (VI) purity (%) as a function of reaction temperature (C°).	80
Figure 4.20	Variation of ferrate (VI) purity (%) as a function of Fe (VI) drying time (min).	80
Figure 4.21	Potassium sulfate ferrate (VI) after drying	81
Figure 4.22	Variation of ferrate (VI) purity (%) as a function of Fe (VI) drying temperature.	82
Figure 4.23	Variation of ferrate (VI) purity (%) as a function of Fe (VI) number of washes.	82
Figure 4.24	Potassium sulfate ferrate (VI) for characterization	83
Figure 4.25	UV-Visible spectrum of synthesized potassium sulfate-ferrate (VI).	83
Figure 4.26	IR spectrum of potassium sulfate ferrate (VI) obtained.	84
Figure 4.27	DRX spectrum of potassium sulfate ferrates (VI)	85
Figure 4.28	Sodium ferrate (VI) powder synthesized with electrochemical method.	85
Figure 4.29	The UV–visible spectrum of the synthesized ferrate (VI).	86
Figure 4.30	FTIR spectra of synthesized sodium ferrate powder in transmittance mode.	86
Figure 4.31	XRD patterns of synthesized sodium ferrate powder.	87
Figure 4.32	Cyclic voltammogram of ordinary steel 0.12%C in optimal conditions of ferrate (VI) synthesis at a scan rate 50 mv/s.	89
Figure 4.33	TGA spectrum of solid ferrate (VI).	90
Figure 4.34	SEM photo of ferrate (VI) powder.	90
Figure 4.35	Wastewater sample before, during and after ferrate (VI) treatment.	91
Figure 4.36	COD removal efficiency with both ferrate (VI) synthesized with electrochemical and dry method for Beni Messous WWTP.	92
Figure 4.37	BOD ₅ removal efficiency with both ferrate (VI) synthesized with electrochemical and dry method for Beni Messous WWTP.	93
Figure 4.38	Nitrite (NO ₂ ⁻) elimination efficiency with both ferrate (VI) synthesized with electrochemical and dry method for Beni Messous WWTP.	94

Figure 4.39	Nitrate (NO_3^-) elimination efficiency with both ferrate (VI) synthesized with electrochemical and dry method for Beni Messous WWTP.	95
Figure 4.40	Ammonium (NH_4^+) elimination efficiency with both ferrate (VI) synthesized with electrochemical and dry method for Beni Messous (Algiers) WWTP.	96
Figure 4.41	Treated samples and witness (case of E.coli and coliforms) using ferrate (VI) (Beni Messous WWTP).	97
Figure 4.42	Treated samples and witness (case of intestinal enterococci) using ferrate (Beni Messous WWTP).	98
Figure 4.43:	COD removal efficiency with both ferrate (VI) synthesized with electrochemical and dry method for Beni Mered WWTP (Blida).	99
Figure 4.44	BOD ₅ removal efficiency with both ferrate (VI) synthesized with electrochemical and dry method for Beni Mered WWTP (Blida).	100
Figure 4.45	Nitrite (NO_2^-) elimination efficiency with both ferrate (VI) synthesized with electrochemical and dry method for Beni Mered WWTP (Blida).	101
Figure 4.46	Nitrate (NO_3^-) elimination efficiency with both ferrate (VI) synthesized with electrochemical and dry method for Beni Mered WWTP (Blida).	102
Figure 4.47	Ammonium (NH_4^+) elimination efficiency with both ferrate (VI) synthesized with electrochemical and dry method for Beni Mered WWTP (Blida).	103
Figure 4.48	Treated samples and witness (case of E. coli and coliforms) using ferrate (VI) (Beni Mered WWTP).	104
Figure 4.49	Treated samples and witness (case of intestinal enterococci)) using ferrate (VI) (Beni Mered WWTP).	105

LIST OF TABLES

Table 1.1	The different state of iron oxidation	4
Table 1.2	Redox potential of oxidants/disinfectants used in water treatment.	9
Table 1.3	Fields of chitosan applications.	26
Table 2.1	Characteristics of wastewater.	31
Table 3.1	The chemical products used in this study.	40
Table 3.2	The range of parameters studied.	46
Table. 3.3	The different electrodes used for the synthesis.	46
Table 3.4	Studied range of ferrate (VI) dry synthesis parameters.	49
Table 3.5	Dilution factors for BOD ₅ analysis.	58
Table 4.1	Physico-Chemical properties of extracted chitosan.	64
Table 4.2	Ferrate efficiency in bacteria removal (Beni Messous WWTP).	96
Table 4.3	Antimicrobial efficacy of ferrate (Beni Mered WWTP).	103
Table 4.4	Value of different parameter under the optimal concentration of ferrate (VI).	106
Table 4.5	Ferrate removal efficiency (%) for both WWTP studied.	107

ملخص

تهدف هذه الدراسة إلى تحسين ظروف إنتاج الفيرات (VI) باستخدام الطريقتين الجافة والكهروكيميائية. أُجريت عملية الإنتاج الكهروكيميائية في خلية ثنائية المقصورات باستخدام أغشية الكيتوزان ، بينما استخدمت عملية الإنتاج الجافة خلية مزودة الجدار حُجُجًا لاستيعاب المعلمات الرئيسية، مثل كثافة التيار، ودرجة الحرارة، وتركيز الإلكتروليت، وزمن التحليل الكهربائي، ونوع القطب، لكلا الغشائين. أما بالنسبة للطريقة الجافة، فقد قُيِّمَ أيضًا حجم الجسيمات، زمن التجفيف، درجة الحرارة لكل من المادة الأولية وناتج الفيرات (VI) ، زمن ودرجة حرارة التفاعل، وعدد مرات الغسيل.

تم تحديد الظروف المثلى للإنتاج الفيرات (VI) بالطرق الكهروكيميائية والجافة. باستخدام غشاء الكيتوزان، كانت أفضل الظروف الكهروكيميائية هي 210 دقائق من التحليل الكهربائي عند 30 درجة مئوية، بكثافة تيار 60 ملي أمبير/سم² في هيدروكسيد الصوديوم (NaOH) بتركيز 24 مولار وأقطاب من الحديد تركيز 0.12 % كربون، مما أدى إلى إنتاج 0.19 مولار من الفيرات (VI). أما بالنسبة للطريقة الجافة، فقد استخدمت العملية المثلى جزيئات كبريتات الحديد بحجم 160-200 ميكرومتر، جُففت مسبقًا عند 90 درجة مئوية لمدة 10 دقائق، وتفاعلت عند 30 درجة مئوية لمدة 60 دقيقة، ثم جفف الفيرات (VI) الناتج عند 100 درجة مئوية لمدة 15 دقيقة، بعد غسله بالميثانول ثلاث مرات. وقد تم تحقيق أقصى قدر من نقاء الفيرات (VI) بنسبة 98.85%.

تم توصيف المنتج الناتج كيميائيًا ونوعيًا باستخدام معايرة الأشعة فوق البنفسجية المرئية، حيود الأشعة السينية XRD، الأشعة تحت الحمراء FTIR، المجهر الإلكتروني الماسح SEM، التحليل الوزني الحراري TGA، الفولتميتر الدوري CV، ومعايرة الكروميت. أظهرت نتائج التوصيف أن المنتج المُصنَّع بكلا الطريقتين هو فيرات (VI). كُشف تحليل الأشعة فوق البنفسجية المرئية عن قِمَم امتصاص مميزة ضمن النطاق النموذجي بين 500 و510 نانومتر، كما أكد نمط XRD وصور SEM على بنية معينة، وأظهرت أطياف FTIR قمة مميزة لرابطة Fe-O. استُخدم الفيرات المُصنَّع لاحقًا في معالجة مياه الصرف الصحي، مما أظهر كفاءة كبيرة وواعدة في إزالة الملوثات الرئيسية. في ظل التركيز الأمثل للفيرات، تراوحت بين [0.08-0.12]٪، ووصلت معدلات الإزالة إلى 94٪ لـ COD، و98٪ لـ BOD₅، و91٪ للنترات، و97.22٪ للنترت، و95.8٪ للأمونيوم، وإزالة البكتيريا بنسبة 100%.

الكلمات المفتاحية: الكيتوزان، الفيرات (VI)، معالجة مياه الصرف الصحي، الطريقة الجافة، التركيب الكهروكيميائي.

RESUME

Cette étude vise à optimiser les conditions de production de ferrate (VI) par voie sèche et électrochimique. La synthèse électrochimique a été réalisée dans une cellule à deux compartiments utilisant des membranes de chitosane, tandis que la synthèse sèche a utilisé une cellule à double paroi. Des paramètres clés tels que la densité de courant, la température, la concentration en électrolyte, le temps d'électrolyse et le type d'électrode ont été optimisés. Pour la méthode sèche, la granulométrie, le temps et la température de séchage pour le précurseur et le produit ferrate (VI), et de la réaction, ainsi que le nombre de lavages ont également été évalués. Les conditions optimales de synthèse du ferrate (VI) ont été établies pour les deux méthodes. En utilisant la membrane chitosane, les meilleures conditions électrochimiques étaient de 210 minutes d'électrolyse à 30 °C, avec une densité de courant de 60 mA/cm² dans des électrodes de NaOH 24 M et de 0,12 % de C, produisant 0,19 M de ferrate (VI). Pour la méthode sèche, le procédé optimal utilisait des particules de sulfate de fer de 160 à 200 µm, préséchées à 90 °C pendant 10 minutes, mises à réagir à 30 °C pendant 60 minutes, puis lavées au méthanol séchées à 100 °C pendant 15 minutes. Cela a permis d'obtenir une pureté maximale de ferrate (VI) de 98,85 %.

Le produit obtenu a été caractérisé quantitativement et qualitativement à l'aide des techniques UV-Vis, XRD, FTIR, SEM, TGA, CV et titrage de chromite. Les résultats de la caractérisation révèlent que le produit synthétisé à l'aide des deux méthodes est du ferrate (VI). L'analyse UV-Vis a révélé des pics d'absorption caractéristiques dans la gamme typique de 500 à 510 nm, le diagramme XRD et les images SEM confirment une structure orthorhombique, et les spectres FTIR montrent un pic distinct de la liaison Fe-O. Le ferrate synthétisé a ensuite été appliqué dans le traitement des eaux usées, démontrant une efficacité prometteuse dans l'élimination des principaux polluants. Dans des conditions optimales, avec des concentrations de ferrate comprises entre 0,08 et 0,12 %, les taux d'élimination ont atteint 94 % pour la DCO, 98 % pour la DBO₅, 91 % pour les nitrates, 97,22 % pour les nitrites, 95,8 % pour l'ammonium et 100 % pour les bactéries.

Mots clés : chitosane, ferrate (VI), traitement des eaux usées, méthode sèche, synthèse électrochimique.

ABSTRACT

This study aims to optimize the conditions of ferrate (VI) production using both dry and electrochemical methods. The electrochemical synthesis was performed in a two-compartment cell using chitosan membranes, while the dry synthesis used a double-walled cell. Key parameters such as current density, temperature, electrolyte concentration, electrolysis time, and electrode type were optimized for both membranes. For the dry method, particle size, drying time and temperature (for both the precursor and the ferrate (VI) product), reaction time and temperature, and washing number were also evaluated. Optimal conditions for ferrate (VI) synthesis were established for both electrochemical and dry methods. Using the chitosan membrane, the best electrochemical conditions were 210 minutes of electrolysis at 30 °C, with a current density of 60 mA/cm² in 24 M NaOH and 0.12% C electrodes, yielding 0.19 M ferrate (VI).

For the dry method, the optimal process used iron sulfate particles sized 160–200 µm, pre-dried at 90 °C for 10 minutes, reacted at 30 °C for 60 minutes, followed by drying at 100 °C for 15 minutes and triple methanol washing. This achieved a maximum ferrate (VI) purity of 98.85%.

The resulting product was characterized quantitatively and qualitatively using UV–Vis, XRD, FTIR, SEM, TGA, CV and chromite titration. The characterization findings reveals that the synthesized product with both method is ferrate (VI). The UV–Vis analysis revealed characteristic absorption peaks within the typical range of 500–510 nm, the XRD pattern and SEM images confirms an orthorhombic structure, and the FTIR spectra show a distinct peak of Fe–O bond. The synthesized ferrate was subsequently applied in wastewater treatment, demonstrating significant and promising efficiency in the removal of key pollutants. Under optimal ferrate, concentrations rang of [0.08-0.12] %, the removal rates reached up to 94% for COD, 98% for BOD₅, 91% for nitrate, 97.22% for nitrite, 95.8% for ammonium, and 100% of bacterial removal.

Key words: chitosan, ferrate (VI), wastewater treatment, dry method, electrochemical synthesis.

TABLE OF CONTENTS

LISTE OF ABBREVIATION

LIST OF FIGURES

LIST OF TABLES

ABSTRACT

INTRODUCTION	1
CHAPTER 1 GENERAL OVERVIEW OF FERRATES	4
1.1 IRON AND IT'S COMPOUNDS	4
1.2 FERRATES (IV)	4
1.3 FERRATES (V)	5
1.4 ALKALI FERRATES (VI)	6
1.4.1. History of alkaline ferrate production	6
1.4.2. Ferrate properties	7
1.4.3. Characterization method of ferrate (VI)	10
1.4.4. Ferrate (VI) synthesis	13
1.4.4.1. Wet oxidation	13
1.4.4.2. Dry oxidation	14
1.4.4.3. Electrochemical synthesis	16
1. Electrochemical synthesis parameters	18
2. Types of separation in a two-compartment cell	22
1.5. CHITIN AND CHITOSAN	23
1.5.1 Definitions	23
1.5.2. Chitin and Chitosan production	24
1.5.3. Chitosan properties	24
1.5.4. Other applications of chitosan	26
1.6. FERRATE (VI) APPLICATION IN WASTEWATER TREATMENT	27
1.6.1. Water treatment	27
CHAPTER 2 WASTEWATER TREATMENT	30
2.1. WASTEWATER	30
2.1.1. Definition of wastewater	30
2.1.2. Origin and type of wastewater	30

2.1.3. wastewater characteristics	31
2.1.4. Wastewater pollution	31
2.1.5. Measurement parameters	33
2.1.6. Impact of wastewater	36
2.2. WASTEWATER TREATMENT	37
2.2.1. Pre-treatment	37
2.2.2. Primary treatment	37
2.2.3. Secondary treatment	38
2.2.4. Tertiary treatments	38
2.3. RE-USE OF WASTEWATER	39
CHAPTER 3 MATERIALS AND METHODS	40
3.1. CHEMICAL PRODUCTS	40
3.2. CHITOSAN CHEMICAL EXTRACTION	41
3.2.1. Pretreatment	41
3.2.2. Chitin extraction	41
3.2.3. Chitin deacetylation	41
3.3. MEMBRANE PREPARATION	42
3.4. PHYSICO-CHEMICAL ANALYSIS	42
3.4.1. Moisture content	42
3.4.2. Determination of solubility	42
3.4.3. Ash content	43
3.4.4. Fourier-Transform Infrared spectroscopy FTIR analysis	43
3.4.5. Deacetylation degree	43
3.4.6. X ray diffraction XRD analysis	44
3.4.7. Ion exchange capacity	44
3.4.8. Thermal analysis	44
3.4.9 Membrane thickness	44
3.5. FERRATE SYNTHESIS	45
3.5.1. Electrochemical synthesis	45
3.5.2. Ferrate (VI) dry synthesis	48
3.5.3. Ferrate (VI) characterization	50
3.6. FERRATE (VI) IN WASTEWATER TREATMENT	53
3.6.1. Beni Messous wastewater treatment plant (Algiers)	53

3.6.2. Beni Mered wastewater treatment plant (Blida)	54
3.6.3. Physico-chemical analysis	55
3.6.4. Analysis of bacteriological parameters	60
CHAPTER 4 RESULTS AND DISCUSSIONS	63
4.1. CHITOSAN EXTRACTION	63
4.2. CHITOSAN CHARACTERIZATION	63
4.3. FERRATE (VI) SYNTHESIS	67
4.3.1. Ferrate (VI) electro-generation with chitosan membrane	67
4.3.2. Dry synthesis of Ferrate (VI)	77
4.4. FERRATE (VI) CHARACTERIZATION	83
4.4.1. Characterization of potassium sulfate-ferrate (VI) (dry method)	83
4.4.2. Characterization of sodium ferrate (VI) (electrochemical method)	85
4.5. FERRATE (VI) IN WASTEWATER TREATMENT	91
4.5.1. Beni Messous (Algiers) wastewater treatment station	91
4.5.1.1. Chemical Oxygen Demand COD	91
4.5.1.2. Biochemical Oxygen Demand in 5 days BOD ₅	92
4.5.1.3. Nitrite (NO_2^-) removal by ferrate (VI)	93
4.5.1.4. Nitrate (NO_3^-) removal by ferrate (VI)	94
4.5.1.5. Ammonium (NH_4^+) elimination by ferrate (VI)	95
4.5.1.6. Analysis of bacteriological parameters	96
4.5.2. Beni Mered (Blida) wastewater treatment station	98
4.5.2.1. Chemical Oxygen Demand COD	98
4.5.2.2. Biochemical Oxygen Demand in 5 days BOD ₅	99
4.5.2.3. Nitrite (NO_2^-) removal by ferrate (VI)	100
4.5.2.4. Nitrate (NO_3^-) removal by ferrate (VI)	101
4.5.2.5. Ammonium (NH_4^+) elimination by ferrate (VI)	102
4.5.2.6. Analysis of bacteriological parameters	103
4.5.3. overall results	105
CONCLUSION	108
REFERENCES	111
APPENDIXES	122

INTRODUCTION

Water is essential for life and plays a vital role in economic progress and social well-being. It is considered an irreplaceable natural resource, essential to both ecosystems and human activity. However, the growing demand for water and the expansion of industrial, agricultural and domestic sectors have led to increasing pressure on water resources, particularly in terms of quality degradation. Many chemicals and pollutants are continuously released into the environment, threatening the fragile balance of aquatic ecosystems and posing serious risks to human health [1].

Wastewater from industrial and domestic activities should not be discharged directly into the natural environment, as if left untreated it can cause serious environmental and health problems. It is therefore essential that it be directed to treatment plants, where it is treated centrally to eliminate the pollutants it contains. This treatment, carried out using physicochemical and biological processes, allows the discharge of purified water that complies with current standards.

In recent years, several conventional treatment techniques have been proposed for the removal of pollutants in wastewater. These include biological processes and physicochemical processes such as coagulation, flocculation, and chemical oxidation by oxidizing agents such as chlorine, ozone, hydrogen peroxide, etc. However, the by-products of these treatment methods are often difficult to treat with these conventional treatment methods [2].

In response to this situation, the development of efficient and sustainable water treatment technologies has become a global priority. Among the many chemical agents explored to mitigate pollution, ferrate (VI) an iron compound in the +6 oxidation state. Ferrate (VI) is recognized for not only its strong oxidizing power and its multifunctionality capable of degrading a wide range of organic and inorganic contaminants, but also for its environmentally friendly by-products, such as iron oxides and hydroxides, which are non-toxic and even useful as coagulants in water treatment processes [2].

Ferrate chemistry dates back more than a century, recent environmental challenges have revived scientific interest in their applications. Currently, ferrates can be synthesized by three main methods: the wet method, the dry method, and electrochemical oxidation. Each method has advantages and limitations; although the dry method does not require the

use of water, which makes the ferrate more stable, it consumes a lot of energy due to the very high temperature synthesis, however, the electrochemical route is particularly attractive due to its cost-effectiveness, simplicity, and ability to produce high-purity ferrate in liquid and solid form [3].

Despite these advantages, widespread adoption of ferrates in industry remains limited, primarily due to production costs and instability over time, which require further optimization and innovation.

The objective of this research is to study the electrochemical synthesis of ferrate (VI) using a two-compartment electrochemical cell separated by chitosan membranes a natural and biodegradable polymer extracted from shrimp shells membranes, as well as dry ferrate synthesis using room-temperature processes, with the aim of improving yield, ferrate concentration, and stability over time. To this end, a parametric study was conducted for both synthesis methods to determine the optimal synthesis conditions for efficient ferrate (VI) production, with the ultimate goal of applying ferrate in wastewater treatment.

The outline of this manuscript is described briefly below:

The first part is composed of two chapters. The first chapter presents a state-of-the-art on ferrates, their properties, advantages, and production methods, as well as their application in water treatment. It also includes a section on chitosan, its physicochemical characteristics, and its suitability as a membrane material in electrochemical systems. Finally, general information on wastewater, its characteristics, and the stages of its treatment are detailed in the second chapter.

The second part is devoted to the experimental methodology, describing the chitosan extraction device, its characterization, and the preparation of the chitosan membrane, followed by an experimental protocol for the electrochemical and dry synthesis of ferrate (VI), the materials used, and the analytical techniques employed to characterize the synthesized ferrates. Finally, the source of the samples on which we conducted our study and the methods used to evaluate the quality parameters of wastewater after treatment with ferrate (VI) are presented.

The third part presents the overall results of our study. These were discussed and interpreted in order: chitosan extraction and characterization; the influence of different

synthesis conditions on the yield and stability of ferrate (VI) using the two synthesis methods and their characterization; and the effectiveness of the ferrate produced in degrading pollutants wastewater samples.

The study concludes with a summary of the main results, a general discussion on the influence of the originality brought by our study on ferrate synthesis, and suggestions for future work aimed at extending the process and improving the stability of ferrate for industrial use.

CHAPTER 1

GENERAL OVERVIEW OF FERRATES

1.1. IRON AND ITS COMPOUNDS

Iron is one of the most abundant elements in the earth's crust (around 5%), it is a malleable magnetic metal. It is found in various forms of minerals in nature. Mainly in the solid (Fe) state, with ferrous Fe (II) and ferric Fe (III) ions. There are also other exceptionally high oxidation states (+4, +5, +6), known as ferrates of which the most stable and easiest to synthesize is ferrate 6, first observed by Stahl in 1702 [1]. The different state of iron oxidation shown in table 1.1.

Table 1.1: The different state of iron oxidation.

compound	Name
FeO	Ferrous oxide
Fe ₂ O ₃	Ferric oxide
Fe ₃ O ₄	Ferrosoferric oxide
Fe ₂ O ₃ .H ₂ O	Ferric oxide monohydrate
FeOOH	Ferric oxyhydroxide
FeO_2^{2-}	Hypoferrite
FeO^{2-}	Ferrite
FeO_3^{2-}	Ferrate (IV)
FeO_4^{4-}	Ferrate (IV)
FeO_4^{3-}	Ferrate (V)
FeO_4^{2-}	Ferrate (VI)
FeO_5^{2-}	Ferrate (VIII)

Thanks to its excellent properties, iron has become one of the most widely used elements in the steel and cast-iron industries.

1.2. FERRATES (IV)

There are three types of iron compounds in oxidation state (IV): metaferrates, orthoferrates and pentaoferrates.

- Metaferrates: Characterized by an O/Fe ratio of 3. Their formula is: MFeO_3 where M is a divalent element (alkaline-earth, Pb^{2+}) [2].

- Orthoferrates: Characterized by an O/Fe ratio equal to 4, their corresponding formula is M_2FeO_4 where M is a divalent element (alkaline-earth elements such as Ba^{2+} and Sr^{2+}) [3].
- pentaoxoferrates: Characterized by an O/Fe ratio of 5. Their formula is of the M_3FeO_5 type, where M is a divalent element. Only barium pentaoxoferrate is described in the literature [4].

1.3. FERRATES (V)

The compound K_3FeO_4 is the only iron(V) salt cited in the literature. It was first synthesized in 1956 from mixtures of Fe_2O_3 and KO_x heated to 400-500°C under oxygen. However, the resulting compound is not pure, being polluted by $KFeO_2$ and KO_x obtained it by mixing the compounds Fe_2O_3 , $KFeO_2$ or K_2FeO_4 with anhydrous potash under oxygen at 600-700°C. Above 700°C and under oxygen, this compound becomes unstable [5].

Finally, ferrate (V) was obtained as a single crystal by intimately mixing K_2O_2 and $KFeO_2$ at a ratio of 1.78:1, and slowly heating it to 470°C at a rate of around 60-70°C per day in a silver vessel. It is then annealed for 18 days at this temperature, followed by 5 days at 350°C [6]. K_3FeO_4 single crystals are dark reddish-brown in color. They can be altered in air and must be preserved in dried kerosene. In solution, K_3FeO_4 breaks down into Fe(VI) and $Fe(OH)_3$.

The compound crystallizes in the orthorhombic Pnma space group system, with parameters: $a = 7.7016 \text{ \AA}$, $b = 9.092 \text{ \AA}$, $c = 7.837 \text{ \AA}$. The structure is characterized by isolated FeO_4 groups. The iron is in a deformed tetrahedral site; the O-O edge is highly elongated and the O-Fe-O angle has a value of 123°. Fe-O distances range from 1.71 to 1.72 Å.

The ferrate ion ($Fe^{VI}O_4^{2-}$) has received considerable attention due to its desirable chemical properties, such as its very high oxidizing capacity. In this context, it has been used as a green oxidant in various fields, such as synthetic organic transformations, water oxidation catalysis, waste remediation and high-capacity battery cathodes [5].

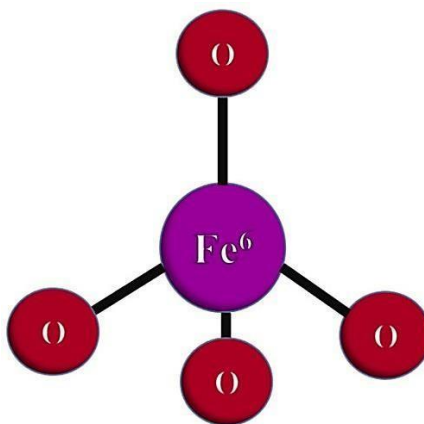


Figure 1.1: Presentation of the ferrate molecule $[\text{FeO}_4]^{2-}$.

1.4. ALKALI FERRATES (VI)

1.4.1. History of alkaline ferrate production

The first description of ferrate was given in 1702 [7]. In 1715, Stahl observed the appearance of a reddish-purple color when a molten salt resulting from a mixture of potassium nitrate and iron filings was dissolved in water [8]. More than a century later, in 1834, an identical compound was formed during the heating of a mixture of potash and various iron ores [9]. In 1841, Poggendorf observed the appearance of purple color in the anodic oxidation of an iron electrode in a strong alkaline solution [10]. In the same period, Fermy suggested a FeO_3 formula for this colored compound [11], although it was never isolated. The presence of the “+6” oxidation state of potassium barium ferrate was later demonstrated by various methods. Indeed, Moeser published his work in a journal on ferrates and their chemistry. The next period of notable interest in ferrate (VI) compounds came at the beginning of the twentieth century with the development of Ni-Fe alkaline battery technology. Haber and Pick examined the influence of various process parameters on the electrochemical synthesis of ferrate (VI) [12, 13].

From the 1950s onwards, there was once again a resurgence of interest in ferrates (VI) mainly because of their potential to oxidize relatively stable organic compounds. During this time, several researchers investigated the chemical production of ferrates (VI) by electrochemical techniques Tosěk and Helferich and later by Venkatadri et al [14-16]. These authors focused on optimizing the conditions that offer the highest current yields for the electrochemical synthesis of ferrate (VI). The results obtained showed a marked increase in the number of new applications for ferrate (VI), particularly for use in organic synthesis, corrosion protection and environmental improvement [17, 18].

More recent research into ferrates (VI) has also involved the development of new characterization techniques that provide a better understanding of the reaction mechanisms and properties of ferrate (VI) [19].

In recent years, much new data has been published on the preparation of ferrates (VI) and their application in the removal of various organo-inorganic compounds and radionuclides, as well as on the mechanism of their action [19].

1.4.2. Ferrate properties

1.4.2.1. Physical properties

- Structure

X-ray spectroscopy studies on solid crystals such as K_2FeO_4 show that ferrate (VI) is formed by four oxygen atoms, which are covalently bonded to the central iron atom with an oxidation index of +6. The tetrahedral structure of ferrate (VI) is described on the confirmed website. Isotopic studies of oxygen in an aqueous solvent show that there are four oxygen atoms around the iron atom. Other studies have shown that ferrate (VI) ions can have three hybrid resonance structures with oxygen atoms. Structures 2 and 3 are considered the main structure [20].

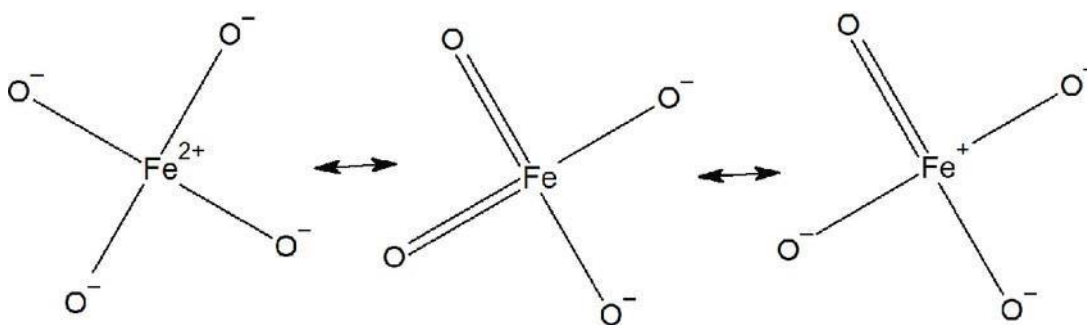


Figure 1.2: Hybrid resonance structure of the Fe (VI) ion.

1.4.2.2. Chemical properties

- Stabilities

Iron exists in two oxidation states: either ferrous (Fe (II)) or ferric (Fe (III)). However, under strong oxidation conditions, a higher oxidation state (+IV, +V and +VI) can be obtained, known as ferrate. Based on the $E = f(\text{pH})$ diagram, It's known as the Pourbaix diagram (Figure I.3), we can visualize the presence of various forms of iron at different pH and in an oxidative/reductive environment.

A reducing environment is generally represented by low Potential values, while high Potential values tend to represent an oxidizing environment. Ferrates predominate in the upper region of the E-pH diagram, while iron exists in the form Fe (0) at the bottom [4].

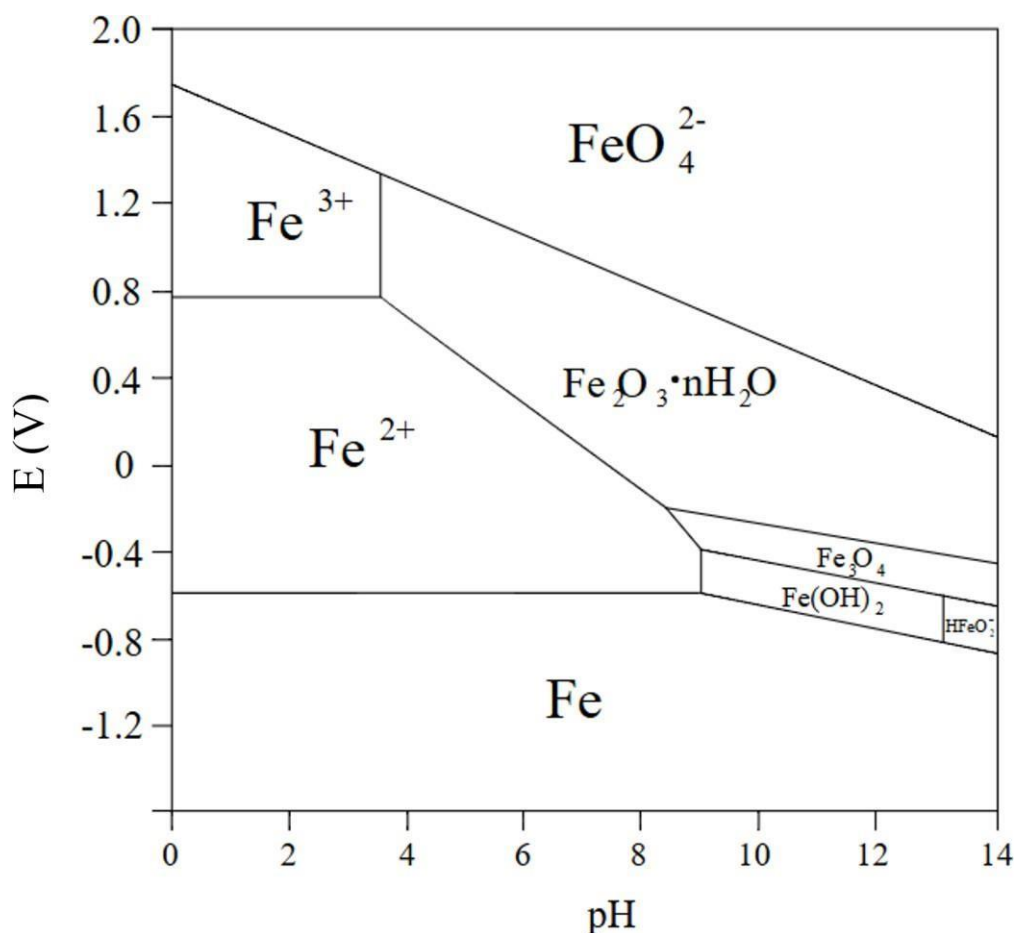
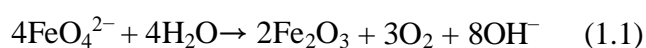


Figure 1.3: Approximate $E=f(\text{pH})$ diagram of the most common iron compounds at (1 atm ; 25°C) .

In the aqueous phase, ferrate stability depends on many factors such as pH, temperature and ferrate concentration. Ferrate ions and water molecules react to form ferric oxide (Fe_2O_3), oxygen gas and hydroxyl ions (Eq1.1). Due to the release of hydroxyl ions, the pH of the solution is highly alkaline. The product of ferric oxide is a coagulant.



The diluted ferrate solution would be more stable than a concentrated solution.

Ferrate stability improves with increasing pH. The temperature of the aqueous phase can also influence ferrate stability [21].

External factors such as light have no significant influence on ferrate stability [22].

- Oxidizing power:

Table 1.2. Displays the reduction potentials of numerous oxidants typically utilized in water treatment applications. According to studies, Fe (VI) has a reduction potential of 2.20 V at acidic concentrations and 0.57 V at alkaline pH levels. Table 1.2 shows that Fe (VI) is the greatest oxidizing agent in acidic solutions but becomes a minor oxidizing agent in alkaline solutions.

Table 1.2: Redox potential of oxidants/disinfectants used in water treatment.

Oxidant	Reaction	E° (V)
Hydroxyl radical	$\cdot\text{OH} + \text{H}^+ + \text{e}^- \leftrightarrow \text{H}_2\text{O}$	2.80
	$\cdot\text{OH} + \text{e}^- \leftrightarrow \text{OH}^-$	1.89
Ferrate	$\text{FeO}_4^{2-} + 8\text{H}^+ + 3\text{e}^- \leftrightarrow \text{Fe}^{3+} + 4\text{H}_2\text{O}$	2.20
	$\text{FeO}_4^{2-} + 4\text{H}_2\text{O} + 3\text{e}^- \leftrightarrow \text{Fe}(\text{OH})_3 + 5\text{OH}^-$	0.70
Ozone	$\text{O}_3 + 2\text{H}^+ + 2\text{e}^- \leftrightarrow \text{O}_2 + \text{H}_2\text{O}$	2.08
	$\text{O}_3 + \text{H}_2\text{O} + 2\text{e}^- \leftrightarrow \text{O}_2 + 2\text{OH}^-$	1.24
Hydrogen peroxide	$\text{H}_2\text{O}_2 + 2\text{H}^+ + 2\text{e}^- \leftrightarrow 2\text{H}_2\text{O}$	1.78
	$\text{H}_2\text{O}_2 + 2\text{e}^- \leftrightarrow 2\text{OH}^-$	0.88
Permanganate	$\text{MnO}_4^- + 4\text{H}^+ + 3\text{e}^- \leftrightarrow \text{MnO}_2 + 2\text{H}_2\text{O}$	1.68
	$\text{MnO}_4^- + 8\text{H}^+ + 5\text{e}^- \leftrightarrow \text{Mn}^{2+} + 4\text{H}_2\text{O}$	1.51
	$\text{MnO}_4^- + 2\text{H}_2\text{O} + 3\text{e}^- \leftrightarrow \text{MnO}_2 + 4\text{OH}^-$	0.59
Hypochlorite	$\text{HClO}^- + \text{H}^+ + 2\text{e}^- \leftrightarrow \text{Cl}^- + \text{H}_2\text{O}$	1.48
	$\text{ClO}^- + \text{H}_2\text{O} + 2\text{e}^- \leftrightarrow \text{Cl}^- + 2\text{OH}^-$	0.84
Perchlorate	$\text{ClO}_4^- + 8\text{H}^+ + 8\text{e}^- \leftrightarrow \text{Cl}^- + 4\text{H}_2\text{O}$	1.39
Chlorine	$\text{Cl}_{2(\text{g})} + 4\text{H}^+ + 4\text{e}^- \leftrightarrow 2\text{H}_2\text{O}$	1.36
Dissolved oxygen	$\text{O}_2 + 4\text{H}^+ + 4\text{e}^- \leftrightarrow 2\text{H}_2\text{O}$	1.23
Chlorine dioxide	$\text{ClO}_{2(\text{aq})} + \text{e}^- \leftrightarrow \text{ClO}_2^-$	0.95

1.4.2.3. Optical properties

- Color

The FeO_4^{2-} ion has the same color as the MnO_4^{2-} ion. However, a deep purple color was observed in strongly alkaline solutions [7].



Figure 1.4: Ferrate (VI) color in powder form and in aqueous solution.

- Visible absorption spectra

The UV-Vis technique known as the direct colorimetric method is suitable for quantifying liquid ferrate (VI) solutions. It is based on determining the concentration of a solution by the intensity of the absorbed color. In the case of ferrate (VI), the characteristic dark violet color corresponds to the visible spectrum between 500 and 510 nm. The molar absorptivity of ferrate (VI) salt has been estimated at between 1150 and $1170 \text{ M}^{-1} \text{ cm}^{-1}$, which can help to quantitatively determine the concentration of ferrate (VI) at equal pH 9.

As with other methods of analytical chemistry, this method faces certain disadvantages, as some salts such as barium (VI) ferrate are characterized by low solubility, especially in aqueous solution. In addition, most ferrate (VI) salts tend to decompose in aqueous solution into ferric hydroxides, which can cause some noise peaks during UV-Vis analysis. This can be avoided by mixing the phosphate buffer with a ferrate (VI) solution to form complexes with these ferric hydroxides.

This technique can also be applied to determine the rate constants of ferrate (VI) reactions [20].

1.4.3. Characterization method of ferrate (VI)

1.4.3.1. Infrared spectroscopy

IR spectroscopy is a quantitative approach for measuring iron (VI) in ferrous compounds. The form of the spectra relates to the symmetry of the molecule or the FeO_4^{2-} group (tetrahedral structure).

Iron ferrate FeO_4^{2-} has a tetrahedral structure, as in the case of chromate, with the hexavalent iron atom at the center of gravity of the tetrahedron. By infrared absorption spectroscopy, ferrate exhibits characteristic bands of XY_4 type molecules. This tetrahedral molecule has four vibration modes, as shown in Figure 1.5 below:

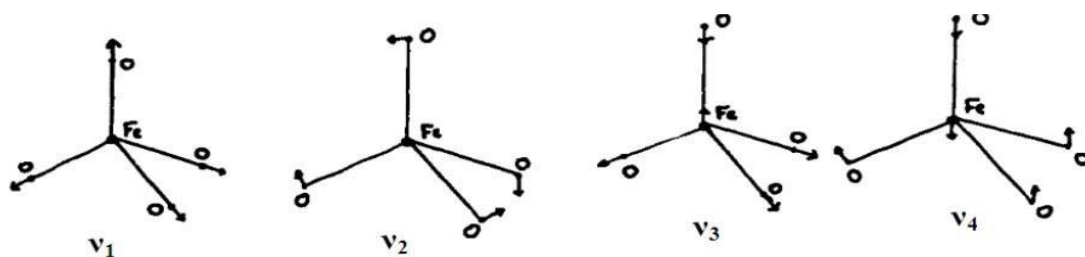


Figure 1.5: Vibration modes of the ferrate molecule.

The vibrations ν_1 and ν_4 represent valence vibrations; one ν_1 is simple, while ν_4 is triply degenerate (since there are three ways to vibrate a tetrahedron in this mode). The vibrations ν_2 and ν_3 correspond to deformations of the tetrahedron. ν_2 is doubly degenerate, ν_3 is triply degenerate. In fact, these considerations are valid for molecules that can vibrate freely, in particular those that are not part of a crystalline structure, where they are hindered by more or less marked coupling phenomena, but whose influence is difficult to separate from that of the molecular vibrations themselves. These remarks are probably more applicable to dilute solutions. The characteristic bands of ferrates in the IR range are around 300 and 800 cm^{-1} [4, 20].

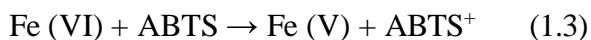
1.4.3.2. Volumetric titration method

A more appropriate method for determining the ferrate (VI) concentration is based on the oxidation of a chromite salt with ferrate (VI) and the chromate obtained is titrated with a standard ferrous salt solution in an acidic medium, and sodium diphenylamine sulfonate is used as an indicator [23]. This method is only applicable to the analysis of solutions containing low concentrations of ferrate (VI) ions.



1.4.3.3. Indirect method for determining ferrate (VI) using ABTS

In this method, colorless ABTS reacts with Fe (VI) to form the green radical cation ABTS^+ . The reaction of Fe (VI) with ABTS has a 1:1 stoichiometry in the presence of an excess of ABTS [24].



1.4.3.4. Electrochemical methods

a. Cyclic voltammetry

The cyclic voltammetry (CV) technique was presented earlier to quantify Fe (VI) [25]. CV curves in different mixtures of solutions were obtained and interpreted in order to elucidate the mechanism of the electrochemical synthesis of Fe (VI), in molten and aqueous solutions [9]. CV curves obtained in 15 M NaOH solutions at a Pt electrode for the reduction of K_2FeO_4 . A positive linearity between the cathodic current density and the square root of the scan rate, which suggests that the reduction of Fe (VI) is diffusion-limited.

b. potentiometric method

A novel potentiometric titration method has recently been developed for the determination of ferrate (VI) in millimolar concentrations within strongly alkaline solutions. This technique utilizes a platinum wire (Pt) as the indicator electrode and an Ag/AgCl electrode as the reference. The titration is carried out using a chromium(III) hydroxide solution as the titrant. Unlike traditional colorimetric methods, this approach minimizes human error in endpoint detection and enhances the accuracy and reliability of the results, making it a significant improvement for precise quantification of ferrate (VI) [26].

1.4.3.5. Mössbauer spectroscopy

Mössbauer spectroscopy can be used to detect the oxidation state of iron. It can therefore help to determine the rate of degradation of Fe (VI) in the ferrate (VI) ion over time. It can be used to verify the presence of magnetic order at low temperatures.

1.4.3.6. X-ray diffraction (XRD) method

X-ray diffraction (XRD) analysis is another method that goes hand in hand with FT-IR and SEM analyses to confirm the crystallinity, structures, and magnetic properties of ferrate (VI) salts. XRD analysis is one of the analytical techniques used to indicate the presence of ferrate (VI), demonstrating isomorphism with other ferrate salts obtained in the

literature. The study conducted by Lei et al showed, through their XRD results, an orthorhombic crystalline structure of the ferrate (VI) salt [27].

1.4.3.7. Scanning electron microscope study

Scanning electron microscopy (SEM) is currently used to characterize ferrate (VI) salts in powder form by providing micrographs or structural images of the product [27].

1.4.4. Ferrate (VI) synthesis

There are several methods for synthesizing potassium ferrate (VI) (K_2FeO_4), potassium ferrate (V) (K_3FeO_4) and sodium ferrate (IV) (Na_4FeO_4) using chemical (wet method), electrochemical and thermal (dry) methods [28].

When choosing a suitable synthesis method, it is necessary to take account of its experimental difficulty and trade-off between purity and the amount of ferrate prepared.

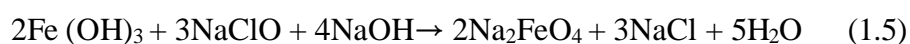
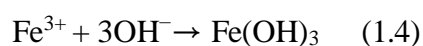
In general, wet chemical synthesis and electrochemical synthesis yield a high-purity ferrate sample, but the quantities of material synthesized are relatively small. For this reason, such an approach is not suitable for large-scale production, i.e. the application of ferrates in water treatment. On the other hand, thermal synthesis enables much higher quantities of ferrates to be prepared (up to kg per synthesis cycle), but their purities remain relatively low (around 30 to 50% of K_2FeO_4 in the sample), mainly due to the self-decomposition of ferrates at high temperatures.

1.4.4.1. Wet oxidation

Known since 1950, the method involves a reaction between ferric chloride and sodium hypochlorite in the presence of an alkali such as sodium hydroxide. Further recovery of potassium ferrate is achieved by precipitation with potassium hydroxide.

Although potassium ferrate recovery percentages as high as 96% have been achieved. The percentages of maximum yield obtained by continuous efforts and of recovery rate are 75% and 15% respectively [29].

The main reactions in this process are as follows.





The wet method considered the most practical, however, remains very expensive.

1.4.4.2. Dry oxidation

This is a high-risk method, as it can cause an explosion at high temperatures. Recent developments include the synthesis of ferrate salt by calcining a mixture of potassium peroxide and ferric oxide at a temperature ranging from 350 to 370°C.

Another method involves oxidizing iron oxide with sodium peroxide at a temperature of 370°C with a continuous flow of dry oxygen to obtain sodium ferrate.

The product obtained from this reaction gives a red-violet colored solution containing the tetrahedral ion FeO_4^{2-} [30]. The percentage recovery of ferrate using this method did not exceed 55% [31]. The equation for the reaction is given below:



Among the work on the dry synthesis of ferrates (VI), the investigation carried out by A. El Maghraoui et al and his colleagues in 2015. They showed that the Ba/Fe mass ratio of 3 is optimal for maximum barium ferrate concentration at a reaction temperature of 850°C, for better stability of synthesized ferrate (VI), with a high yield in the synthesis reaction and an optical density of around 2.635. The reaction time also had a significant impact on the synthesis of ferrate (VI). According to the experimental results, a duration of 12 hours was optimal in this study. In the same study, they showed that the storage period is up to 12 months with a degradation rate limited to 29.98% during the first six months [32].

In the same year and the same laboratory, A. El Maghraoui and his team conducted a study to optimize the key parameters influencing the performance of the iron (II) to iron (VI) using the dry reaction between Na_2O_2 and Fe_2O_3 and monitoring its degradation over time. These authors found that a Na/Fe mass ratio of 4 is optimal for this reaction, and that a temperature of 700°C ensures maximum reaction yield with high optical density and a more stable synthesized ferrate (VI). The reaction time is a very important parameter. A duration of 13 hours was optimal for this reaction to be complete and to synthesize more stable ferrates. They also showed that the degradation of ferrate (VI) is of the order of 20.53% in the first six months, and the degradation rate of iron (VI) remains variable over time

and varies differently from month to month during storage, which means that climate change has an impact on the degradation rate of ferrate (VI) due to variations in humidity [34].

For their part, N. Kanari et al (2000) studied the synthesis of alkali metal ferrates ($A_2Fe^{VI}O_4$) using a dry process, which is carried out in a rotary reactor at room temperature using chlorine as an oxidant. Overall, it has been shown that the Fe^{VI} yield from the synthesis of potassium ferrate reaches values close to 65%. The ferrate obtained is stable over time.

In the same line of research, N Kanari and his colleagues (2013) conducted a study on the synthesis of ferrate (VI) using the dry method by recovering residual iron sulfate as a waste product from the TiO_2 and steel surface treatment industries. The synthesis of $K_2Fe^{VI}O_4$ was achieved through a simultaneous reaction of two solids, iron sulfate and KOH in the form of pellets with a diameter of approximately 5 mm and approximately 15% H_2O (by weight), and a high-purity (99%) gaseous oxidant (chlorine). The synthesis process is carried out in a rotary reactor at room temperature. The effects of different experimental parameters on the synthesis of potassium ferrate are studied in order to determine the optimal conditions for the process. The results of this study show that ferrous sulfate must be dehydrated at a temperature of approximately $125^\circ C$, which allows the amount of water to be controlled during the synthesis of potassium ferrate, increases the reactivity of ferrous sulfate, and prevents its reaction with iron (VI), thereby reducing the yield of the latter [35].

In the same study, they observed an increase in reactor temperature between $45^\circ C$ and $175^\circ C$ due to the exothermic nature of the reactions, but a ferrate (VI) yield of over 60% was obtained at temperatures below $100^\circ C$. For the separation of the synthesis products from the unreacted ferrous sulfate, they found that sieving the synthesis product would allow their separation, which was facilitated by the difference in particle diameter between the ferrate (5 to 5 mm) and the iron sulfate (5 to 0.1 mm). They also showed that ferrate must be dried at temperatures below $70^\circ C$ and, in order not to compromise its stability; the drying temperature must be as low as possible and never exceed $100^\circ C$. This work demonstrates the possibility of transforming a waste product (iron sulfate) into a useful value-added product (potassium ferrate) [35].

The study by Bin Lei et al. focuses on the synthesis of potassium ferrate (K_2FeO_4) using a dry method, employing a mixture of ferric oxide (Fe_2O_3) and sodium peroxide (Na_2O_2) in a molar ratio of 6:1, calcined at $700^\circ C$ under dry oxygen.

The calcined product is then dissolved in a low-temperature KOH solution, filtered, and purified by washing with organic solvents. The ferrate obtained has a high purity (98.7%) and a yield of 26.7%. Analyses (ICP, XPS, FT-IR, XRD, SEM, UV-Vis) confirm its orthorhombic structure, iron valence VI, and the presence of tetrahedral FeO_4^{2-} ions. The product also exhibits high crystallinity and a columnar morphology, confirming its high structural and chemical quality [36].

In another work of A. El Maghraoui et al. (2023) introduces an optimized dry synthesis method for producing high-purity potassium ferrate (K_2FeO_4), achieving purity levels of 98.3–99.1% and stability for up to 12 months at $\sim 30^\circ\text{C}$. The process involves heating a mixture of K_2O_2 and Fe_2O_3 (molar ratio $\text{K}/\text{Fe} = 4$) at 560°C for 5 hours under an oxygen flow. Compared to other synthetic routes, this method significantly improves both yield and stability. Various experimental parameters (K/Fe ratios from 1–6, temperatures from 200 – 750°C , and durations from 6–17 hours) were tested to identify optimal conditions for industrial feasibility, cost reduction, and ease of storage and transport. The formation and purity of ferrate(VI) were confirmed using XRD, FTIR, UV-Vis spectroscopy, and volumetric titration, while its long-term stability was evaluated through Mössbauer spectroscopy, UV-Vis, and titration methods [37].

1.4.4.3. Electrochemical synthesis

The first electrochemical synthesis of ferrate (VI), by Poggendorf (1841) [19], remains one of simplest methods for obtaining pure ferrate in liquid form.

The principle of synthesis is to oxidize crude iron or ferric salts in concentrated alkaline solutions or mixtures thereof.

During electrochemical ferrate synthesis, the anodic dissolution of iron occurs in a strongly alkaline solution. The current applied during the synthesis process oxidizes the iron to ferrate in the alkaline solution (KOH or NaOH), as shown in Figure 1.6.

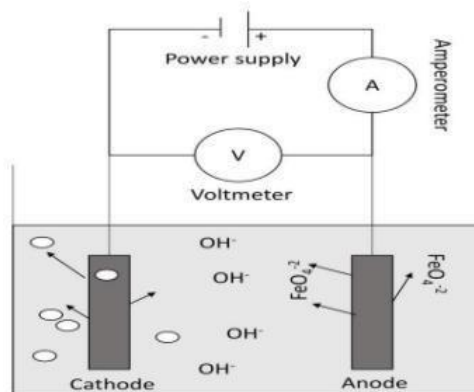


Figure 1.6: Electrochemical cell for ferrate production.

The electrochemical synthesis of FeO_4^{2-} in solution is usually performed using a two-compartment electrolysis cell separated by an anion-impermeable membrane.

High-surface iron (wire, foil, particles) is normally used as the anode. The electrolyte is usually a highly concentrated alkaline solution (NaOH or KOH).

Fe (VI) yield is strongly related to various synthesis parameters, including anode materials, separator, alkaline electrolyte, anode current density, electrolysis temperature and time, etc.).

NaOH electrolytes support higher solution Fe (VI) generation rates and efficiencies than KOH electrolyte at low temperatures. Consequently, in most studies of Fe (VI) generation in solution at low temperatures, NaOH base is generally used as the alkaline electrolyte [4].

The reaction at the anode: $\text{Fe} + 8\text{OH}^- \rightarrow \text{FeO}_4^{2-} + 4\text{H}_2\text{O} + 6\text{e}^-$ (1.8)

The reaction at the cathode: $2\text{H}_2\text{O} + 2\text{e}^- \rightarrow \text{H}_2 + 2\text{OH}^-$ (1.9)

The overall reaction: $\text{Fe} + 2\text{OH}^- + 2\text{H}_2\text{O} \rightarrow \text{FeO}_4^{2-} + 3\text{H}_2$ (1.10)

Several steps are required to ensure the formation of ferrates, which can be described as follows:

1. The formation of intermediate species.
2. Ferrate formation and electrode passivation.

3. Formation of a passivation layer that prevents further ferrate generation

This synthesis has been widely studied and remains an active area of research aimed at optimizing its parameters. Moreover, the electrochemical method may offer an industrially useful way of mass-producing Fe(VI) and could be suitable for in situ generation of Fe(VI) solution [4].

1. Electrochemical synthesis parameters

a. Electrolyte

Because of the stability of FeO_4^{2-} ions and the drop in the apparent normal potential of the Fe (VI)/Fe(III) redox couple at basic pH, synthesis requires highly concentrated alkali hydroxide solutions, typically 5M according to Denvir and Pletcher [38].

Numerous studies have shown that electrolysis yields are better with sodium hydroxide solutions than with potassium hydroxide solutions [4].

In fact, the nature of the hydroxide plays an important role in the synthesis yield, which can be explained on two levels. The main reason is the difference in solubility between sodium and potassium salts, at constant alkalinity. The other is the influence of the nature of the hydroxide on the oxide layer formed on the electrode surface.

b. Anode

Ferrate synthesis takes place in the iron transpassivation range. Thus, it takes place in a potential range where there is competition with solvent oxidation to oxygen and on a surface passivated by an oxy-hydroxide film. According to Denvir and Pletcher, ferrate (VI) concentration increases over time, but not linearly [38]. Whatever the nature of the anode (iron, cast iron, steel.), electrochemical synthesis is possible. However, numerous studies have shown that the yield of iron oxidation to ferrate (VI) is highly sensitive to the composition of the anode, and particularly to its carbon content. Thus, Denvir and Pletcher note that the characteristic violet coloration of the FeO_4^{2-} anion is more intense with carbon-rich alloys, unlike other elements such as manganese and silicon, which do not appear to influence synthesis yields [38]. Bouzek and Rousar studied more precisely the influence of carbon speciation in the iron electrode (graphite or carbide) and observed that it influences the nature of the oxide-hydroxide layers. It was shown that oxide layer properties (porosity, compactness) differ according to whether the carbon is in graphitic or carbide form [39].

Iron carbide suppresses the passive properties of the layer through local disintegration, allowing the anode to be continuously dissolved and oxidized. The oxide layer is more porous, more disordered and therefore more active. More recently, Bouzek et al have shown that Fe_3C cementite can react under anodic polarization with (OH^-) ions, causing local disruption of the protective passive layer and the formation of a thin, porous layer that facilitates ferrate synthesis [40]. In the case of pure iron, the oxide layer is compact and therefore less soluble: it protects the anode more effectively against dissolution. If the carbon is in the form of graphite, the competitive reaction (oxidation of the solvent to oxygen) is preferred. In addition, these authors believe that graphite can catalyze the decomposition of ferrate (VI) to Fe (III).

c. Cathode

It can be made of steel, nickel, iron or alloys such as Ni-Mo or Ni-V [13].

d. Duration of electrolysis

The Fe (VI) concentration increases with time, but follows a non-linear evolution, as the oxide layer at the origin of passivation thickens over time and protects the electrode from dissolution. As a result, the duration of electrolysis should not be too long.

It is also important to consider the stability of ferrate (VI) solutions in these environments.

e. Temperature

Temperature is an important operational parameter whose effect on the efficiency of ferrate (VI) synthesis was observed in the early stages of research. Temperature has two fundamental effects on ferrate (VI) production.

An increase in temperature produces depassivation of the electrode surface during anodic polarization. This is caused by an increase in the chemical interaction of the oxo-hydroxide layer with the hydroxyl anion during the formation of soluble products.

The fresh surface of the anode material is thus continuously exposed to electrolyte and anodic dissolution, and the full current yield of the electrolysis increases.

Bouzek et al, studied different iron anode materials and concluded that pure iron had the strongest tendency to form a compact and stable surface layer. A higher temperature, 30-50°C depending on electrolysis conditions, is required to overcome this problem. On the

other hand, the use of an anode material with a high iron carbide (Fe_3C) content (commonly known as white cast iron) makes it possible to achieve a relatively high current yield, during prolonged electrolysis, at a temperature as low as 20°C [1].

f. Other important synthesis parameters

The current density applied and the duration of electrolysis have significant effects on the efficiency of ferrate synthesis. The first parameter is related to the applied electrode potential and therefore to the reactions that will take place at the electrode surface.

Ferrate (VI) formation takes place in the trans-passivation (iron dissolution) region, where it competes with oxygen release. The high potential involves parasitic reactions, reducing the faradic yield of ferrate (VI). The reduced ferrate (VI) rate also formed at higher anode potentials is caused by accelerated deactivation of the anode surface. At insufficient anode potentials, the kinetics of ferrate (VI) formation is limited by the rate of formation of intermediates that can interfere with the ferrate formation process. Consequently, for a given set of conditions, such as electrode material, temperature and electrolyte, there is an optimum current density.

This method has been widely employed by numerous researchers for the synthesis of sodium and potassium ferrates. Over the past decades, ferrates have been the subject of extensive investigation by the scientific community.

Among the first works on the synthesis of ferrate (VI) carried out in 1901 by Haber and Pick was the proof that during electrolysis of a concentrated NaOH or KOH solution with an iron anode, the yield of alkaline ferrate depended on the current density employed (which must be low). The quality of the anode iron (better with cast iron), the temperature (higher at 70°C than at 0°C) and that it was independent of the starting salt (ferrous or ferric); This is hardly surprising, since iron in both cases undoubtedly passes partially into solution within an anion of the form FeO^- or FeO_2^{2-} [11,12].

As Grube and Gmelin (1920) confirm, the cathode compartment should be isolated, as the ferrate formed could be reduced at the cathode.

In Cécile Stanford et al (2010) study, they focused on synthesizing sodium ferrate electrochemically, using steel as anode and cathode (99% Fe and 0.1 to 0.12% C) with a 16 M NaOH electrolyte and a 25 minute reaction time. They showed that the Fe(VI) concentration was highest at the time of production (4 min: 84 mg/l), so they observed that

the Fe(VI) solution should be used within 40 to 50 minutes of production at a pH below 10 [41].

Sibel Barışçı et al (2014) focused on determining the optimum conditions for ferrate (VI) production and the effect of various parameters on electrochemical ferrate (VI) ion production were investigated for high-purity iron electrodes. Ferrate (VI) ion showed high stability at higher alkalinity, lower temperatures, increasing ferrate (VI) ion concentration and pH between 9.2 and 10. Current efficiency and energy consumption were used to determine optimum parameters for ferrate (VI) production. According to the experiments, the optimum conditions were a NaOH concentration of 20 M, a current density of 1.47 mA/cm² and a temperature of 30°C with an electrolysis time of 1.5 hours. Ferrate (VI) ion solutions with contents up to 2.0 Mm were produced in the electrochemical cell [42].

Anode passivation poses a significant challenge in the electrochemical synthesis of ferrate (VI) (FeO₄²⁻, Fe (VI)). In the study by Xuhui Suna and Kexin Zu (2017), it was demonstrated that using a sponge iron anode resulted in a higher Fe (VI) yield compared to a gray cast iron anode. The optimal conditions for Fe (VI) generation with the sponge iron anode were identified as a temperature range of 35–50 °C and a current density of 30 Ma/cm². Notably, under these conditions, the sponge iron anode maintained Fe (VI) production for over 10 hours. The study concluded that the most effective parameters for maximizing Fe (VI) production were a current density of 30 mA/cm², a temperature of 50 °C, and a hydroxide concentration of 10 M, achieving an Fe (VI) concentration of up to 0.16 mol/L [43].

Hernandez et al. (2016) synthesized ferrate (VI) using a two-compartment electrochemical glass cell and a Nafion NR- 112 cation exchange membrane as a separator with carbon steel anode and stainless steel cathode with a precise dimension of 1.50 cm × 5.0 cm for both electrodes. Each compartment of was filled with 80 mL of 14 M NaOH electrolyte and subjected to a current density of 10 mA/cm² for 24 h producing ferrate at a concentration 1.25 mM [24, 44].

Liu et al, (2018) optimized conditions to synthesize Fe (VI) efficiently. Using two different types of electrodes, to generate more Fe (VI), which showed that a maximal concentration of ferrates (0.4 mmol/L) was obtained with one cathode and one anode configuration , under optimal conditions of 6.2 M NaOH, current density of 31.2 mA/cm²,

100 g/L NaCl (sodium chloride) concentration, and 2 cm distance between cathode and anode [26].

Diaz et al. (2021) studied the influence of the passivity in the in-situ ferrate (VI) electro-production using three iron electrodes. The reaction took place in a plate-and-frame electrolytic cell under optimal conditions of 10 M NaOH, 50 mA/cm² current density, and 4h electrolysis using gray cast iron anode yielding a ferrate concentration of 37 Mm; the results show the composition of the alloy directly affects the type of substances formed within the passivation layer. It has been proven that the inclusion of silicon in grey cast iron electrodes has a detrimental influence on the electrode's stability [45].

Klein et al. (2023) explored the effect of different parameters of the electrochemical synthesis of ferrate (VI) in an H-cell batch reactor separated by a Nafion-N324 membrane. The results show that 14 M of NaOH with a current density of 100 mA/cm² gives a maximum concentration of sodium ferrate of 0.99 g/L after 2 h of electrolyze [46].

2. Types of separation in a two-compartment cell

According to several studies, researchers have used a two-compartment cell for electrochemical synthesis. Cell separation improves ferrate concentration and faradic efficiency, reduces power consumption, and solves problems encountered during synthesis (anode deposition, ferrate instability, ferrate solubility).

a. The salt bridge

Chemical isolation of the anodic and cathodic compartments, the salt bridge ensures ionic conductivity by allowing the current carried by the ions to pass through (figure 1.7) [47].

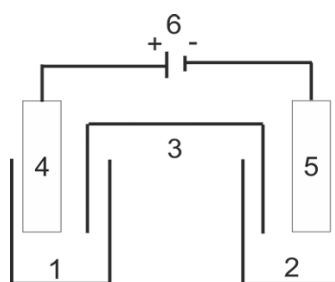


Figure 1.7: The electrochemical method for ferrate synthesis in a two-compartment cell with salt bridge separation.

1. anode compartment; 2. Cathode compartment; 3. Salt bridge; 4. Iron plate ; 5. Platinum plate; 6. Electricity generator.

b. Separation by fritted glass

No contact between the solutions of the two compartments, the passage of electricity is ensured by the fritted glass, which enables the synthesis to be carried out [31].

c. Separation by cation exchange membrane

This type of membrane ensures ion exchange and prevents contact between the two compartments. In propose of enhance ferrate (VI) yield, this study-utilized membrane elaborated from the biopolymer chitosan, a natural cationic polysaccharide derived from chitin, which is structurally similar to cellulose. Chitosan is one of the most promising candidate polymers. This natural, non-toxic polymer has unique properties and considerable application potential [39].

1.5. CHITIN AND CHITOSAN

1.5.1 Definitions

Chitin is a polymer naturally synthesized by living organisms, and is the main product derived from crustaceans [48]. This bio-polymer was discovered in 1811 by the French chemist Braconnot. It is the most abundant natural polysaccharide after cellulose [49].

It has been traditionally extracted from crustacean shells since the 1970s, for a wide range of applications including pharmaceuticals, cosmetics and water treatment [49].

This polymer consists of a linear chain of 2 acetamido-2-desoxy- β -D- glucose units linked by the β (1-4) glycosidic linkage (figure 1.8) [48].

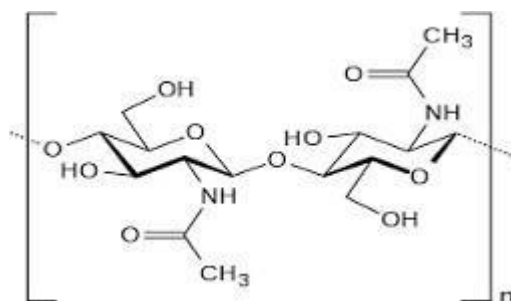


Figure 1.8: Chemical structure of chitin.

Unlike Chitin, Chitosan is rarely found in nature. Chitosan, according to Cheung et al, sometimes referred to as deacetylates Chitin, is a linear polysaccharide derived from the partial deacetylation of Chitin, its chemical structure similar to that of cellulose and aimed at a whole family of copolymers is composed of a random arrangement of D-glucosamine and N-acetyl-D-glucosamine units linked together by bonds [50]. The structures of Chitin and Chitosan differ only in the C-2 groups: acetamide for Chitin and amine for Chitosan (figure 1.9). Both Chitin and Chitosan are characterized by the fraction of residual N-acetamide groups known as the Degree of Acetylation (DA).

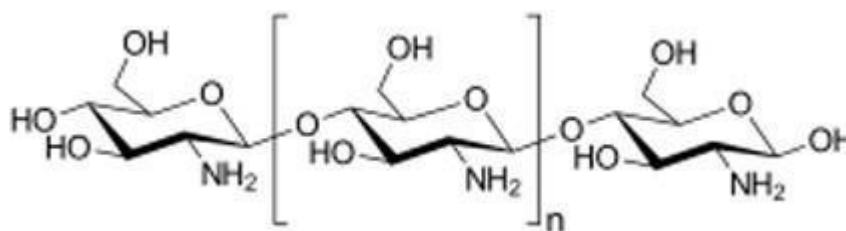


Figure 1.9: Chemical structure of chitosan.

In the case of Chitosan, we use the Deacetylation Degree Percentage (DD%), which corresponds to the relative quantity of acetylated groups removed from the Chitin macromolecule during the preparation of Chitosan. The structures of Chitin and Chitosan are thus characterized by the presence of amine and acetamide groups (figure 1.9), to which should be added the presence of numerous hydroxyl functions which confer a strong hydrophilic character, particularly to Chitosan [51].

1.5.2. Chitin and Chitosan production

Chitin is present in crustaceans in the form of a chitin-protein-mineral complex. It is therefore extracted in 3 stages:

- Demineralization with hydrochloric acid to remove minerals.
- Deproteinization with soda to remove proteins.
- Bleaching (or decoloration) with an oxidizing agent, an optional step to remove pigments.
- Finally, Chitin is deacetylated to obtain Chitosan [52].

1.5.3. Chitosan properties

1.5.3.1. Degree of Deacetylation (DDA)

The degree of deacetylation (DDA) is the molar percentage of removal of N-acetyl groups. Following the deacetylation process, Chitosan becomes rich in highly reactive amine

groups, making the degree of deacetylation an important parameter, influencing all the physico-chemical properties (molecular weight by weight, viscosity, solubility, etc.) of Chitosan and thus determining its applications. Deacetylation gives Chitosan an advantage that Chitin does not possess: to dissolve Chitin, highly toxic solvents such as

Lithium chloride must be used, whereas Chitosan dissolves in dilute acids such as acetic acid. The degree of deacetylation of Chitosan varies between 56 and 99%, with an average of 80%, depending on crustacean species and preparation methods [51].

Several methods are available, including potentiometric (or volumetric) titration, infrared (IR) spectrometry, ultraviolet-visible (UV) spectrophotometry, elemental analysis and nuclear magnetic resonance (NMR).

1.5.3.2. Molecular weight

Molecular weight is considered one of the most important characteristics affecting the functionality of the polymer in question. In general, high temperatures, dissolved oxygen and shear stress can cause Chitosan to degrade, with polymer chains breaking and molecular weight decreasing. Chromatography, viscometry and polydispersity are methods used to determine molecular weight [39].

1.5.3.3. Solubility

Although Chitin is insoluble in most organic solvents, Chitosan is readily soluble in dilute acid solutions, with a pH below 6.0 by protonation of the amine groups present on the macromolecule. Organic acids such as acetic acid, formic acid and lactic acid are used to dissolve Chitosan.

According to Kalut, the most commonly used solution is 1% acetic acid. The acidity constant pK_a of Chitosan is around 6.3. Consequently, when the DD% is low, i.e. when there are fewer amine groups; the solubility of Chitosan is poor. We use Chitosan with a DD% higher than 70% to have a high solubility [53].

1.5.3.4. Viscosity

The viscosity of Chitosan depends on the degree of deacetylation. The more deacetylates it is, the more free amine groups there are, the more soluble Chitosan is, and therefore the greater its viscosity [54]. Viscosity also depends on polymer concentration (it increases with concentration), temperature (it decreases with increasing temperature),

molecular weight (it increases with increasing molecular weight) and pH (the lower the pH, the higher the viscosity) [54].

1.5.4. Other applications of chitosan

Numerous studies by both academic and industrial researchers are exploring the applications of chitosan. Thanks to its physical, chemical, and biological properties, it has various applications in several industries. The following table gather the main chitosan applications.

Table 1.3: Fields of chitosan applications.

Field	Application
Wastewater treatment	Coagulant agent
	Sludge dewatering agent
	Recovery of reusable metals
	Reduction of toxic metals and radioisotopes
	Metal complexing agent
Drinking water treatment	Coagulant agent
	Removal of iron and magnesium from swimming pools
	Removal of toxic metals
Agriculture	Control of metals essential for plant growth
	Seed coating Poultry feed fertilizer
Food	Iron extraction
	Antibacterial agent
	Food additives (binding agent, emulsifier, stabilizer)
	Drink clarification
	Antioxidant
Biomedical and pharmaceutical	Lowering cholesterol levels
	Accelerating wound healing
	Antibacterial and anti-tumor agent
	Synthetic skin
Cosmetics	Moisturizing agent
	Antibacterial
	Anti-odor
	Hair treatment
Textiles	Water retention agent
Photography	Silver extraction

1.6. FERRATE (VI) APPLICATION IN WASTEWATER TREATMENT

Ferrate plays an important role in the purification of pollutants in water and industrial wastewater, due to its intended use as a non-toxic solid. Fe (VI) is a very powerful oxidant [42]. There is currently a great deal of interest in ferrate (VI) as a promising oxidizing agent for organic synthesis and as a material for rechargeable alkaline batteries.

1.6.1. Water treatment

Coagulation and oxidation/disinfection are two important processes in water treatment. Coagulation destabilizes colloidal impurities and converts small particles into large aggregates, enabling their removal by precipitation and filtration. Disinfection in water treatment aims to kill harmful organisms (bacteria and viruses) and control/eliminate odors [27].

Large quantities of coagulants and oxidants/disinfectants are used to treat water. The best-known and most commonly used coagulants are iron sulfate and aluminum sulfate and ferric chloride [55]. The most commonly used oxidants/disinfectants are chlorine, sodium hypochlorite, chlorine dioxide and ozone. At a time when water pollution is getting worse, we need chemical reagents capable of achieving the best water quality. Such reagents must destroy microorganisms, oxidize and partially degrade organic impurities, and enable the extraction of suspended colloids and heavy metals. The potential chemical reagent meeting these criteria may be ferrate (VI), its use as a multifunctional reagent will bring significant advantages in terms of simplicity and lower cost (single compound using a single dosing and mixing system, low cost stoichiometric and least sludge production) also it could avoid the formation of reaction producing toxic elements according to Jiang and Lloyd. It is a very powerful oxidant in acidic media. The redox potential of ferrate (VI) exceeds that of ozone, which is in fact the most powerful oxidizing agent.

The most powerful of all oxidizing disinfectants used to treat and dispose of wastewater [41]. Ferrate (VI) is a disinfectant, coagulant, deodorizer, bleach, desulfurizer and phosphorus remover [26].

1.6.1.1. Coagulation-flocculation

Coagulation involves introducing into the effluent to be treated a product capable of discharging the generally electronegative colloids and destabilizing the electrokinetic equilibrium of suspended particles. This is achieved by neutralizing or even reversing the charges of the suspended solids [25].

Flocculation is the agglomeration of discharged colloids. It results from successive collisions favored by mechanical agitation. A flocculent is therefore primarily an inter-particle bridging reagent that increases the rate of formation, cohesion and density of flocs. Given the negative charge of colloidal particles in water, the main coagulants are cations, generally added in the form of mineral products such as aluminum sulfate and chloride, ferric sulfate and chloride, ferrous sulfate or lime combined with aluminum sulfate.

Ferrate is better than ferrous and ferric salts because it destabilizes colloidal particles rapidly, making it a highly effective coagulant [25].

1.6.1.2. Disinfection

Disinfection is the process of killing harmful organisms (bacteria and viruses) and controlling odour precursors. Ferrate has been studied as a better alternative for water disinfection. Ferrate disinfection is influenced by several criteria such as ferrate dose, contact time and water pH [56].

1.6.1.3. Oxidation of organic and inorganic pollutants

High-valent bridging iron species have been used in many chemical, biological and environmental reactions. The role of bridging irons in the oxidation of organic molecules has been studied by mixing iron complexes with H_2O_2 . The study of these complexes may improve our understanding of the role of these high-valent irons in enzyme chemistry [57].

In the last decade, interest in ferrates (Ferrate (VI), FeO_4^{2-}) in aqueous solutions has grown due to their importance in green technologies for organic synthesis. The oxidation of several inorganic pollutants such as cyanide, ammonia and hydrogen sulfide has also been studied. Ferrate (VI) is a reliable oxidant for cyanide degradation at pH 8-12 and temperatures 15-30°C. More than 22% of ammonia can be removed, when the molar ratio

of ferrate (VI) to ammonia is greater than 1, and 99.9% of hydrogen sulfide has been removed by ferrate in water [57].

Among the works relating to the use of ferrate in wastewater treatment, the study of Bin lei et al continued their investigation by testing the effectiveness of ferrate (VI) in the removal of methyl orange at a concentration of 25mg/L with different ferrate (VI) doses (1 to 10 mg). The obtained results shows that the removal rate of methyl orange was accelerated with increasing pH up to an optimum value of pH 6 with a degradation rate of 58.11%. The decomposition of pollutant strongly increased with the increase of ferrate adding a mass of 9 mg was optimal to remove 99.2% of methyl orange, which proves that ferrate is a potential product in water treatment.

On their part, Zhengwei Zhou et al (2017) studied the performance of commercial potassium ferrate (VI) with a purity (>97%) in urban wastewater treatment in Wujin City, Changzhou, China. The samples were collected, processed and analyzed on the same day. Chemical oxygen demand (COD), total phosphorus, suspended solids (SS), ammonium, total nitrogen and pH were analyzed. The results shows an optimal a total phosphorus removal of 90% and a COD removal efficiency of 40% at a ferrate concentration of 25mg/L at a pH range 5-6 [43].

In 2023 jian-qian qiang describes the first pilot-scale experiment using ferrate (VI) for the removal of micro pollutants from Lake Constance's drinking water. Ferrate (VI) outperformed standard therapies (FeCl_3 , with or without ozonation), even at a low dosage of 0.1 mg/L. It effectively eliminated 10% of metformin, benzotriazole, and acesulfame, unlike FeCl_3 /ozone treatments failed to achieve the same. Among other micro pollutants, ferrate (VI) completely removed bisphenol-S, followed by considerable degradation of azithromycin and imidacloprid. The study identifies ferrate (VI) as a potential alternative method due to its combination oxidation and coagulation characteristics for improved micro pollutant removal in drinking water treatment [58].

CHAPTER 2

WASTEWATER TREATMENT

2.1. WASTEWATER

2.1.1. Definition of wastewater

Wastewater, is water loaded with pollutants, soluble or insoluble, originating mainly from human activity [59]. Wastewater is generally a mixture of pollutants meeting these categories, dispersed or dissolved in water used for domestic or industrial needs. Therefore, the term wastewater covers water of very diverse origins that have lost their purity; that is, their natural properties due to the effect of pollutants after being used in human activities (domestic, industrial or agricultural)

2.1.2. Origin and type of wastewater

Wastewater, as defined in the introduction, has three possible sources:

- Industrial sources: All discharges resulting from non-domestic water use are classified as industrial discharges. This definition covers discharges from factories, but also discharges from craft or commercial activities: laundries, restaurants, medical analysis laboratories [60].
- Domestic origin: Domestic wastewater includes household wastewater (toilet water, laundry water, kitchen water) and sewage (urine and feces) in the so-called “sewer system” [61].
- Agricultural origin: These are waters that have been contaminated by substances used in agriculture. In the context of efficient and intensive agriculture, farmers are required to use various industrial or agricultural products, some of which present or may present risks to the environment and, more specifically, to water quality. These are mainly fertilizers (commercial mineral fertilizers or animal manure produced on or off the farm) and plant protection products (herbicides, insecticides, fungicides, etc.) [62].
- Rainwater: Including rainwater, wash water, and drainage water that carries all kinds of mineral and organic waste.

2.1.3. wastewater characteristics

The following table shows the different characteristics of wastewater [63].

Table 2.1: Characteristics of wastewater.

physical characteristics	chemical characteristic	bacteriological characteristic	organoleptic characteristic
<ul style="list-style-type: none"> • Temperature • Suspended matter 	<ul style="list-style-type: none"> • BOD: biological oxygen demand • COD: chemical oxygen demand • Dissolved oxygen • Hydrogen potential • Conductivity • Nitrate nitrogen • Ammonium • Sulfate 	<ul style="list-style-type: none"> • Coliforms • Staphylococci • Fecal coliforms and Enterococcus • Sulfur-reducing bacteria 	<ul style="list-style-type: none"> • Color • Turbidity

2.1.4. Wastewater pollution

Water pollution or contamination can be defined as the degradation of water by altering its physical, chemical, and biological properties through spills discharges, foreign bodies or undesired substances, such as germs, hazardous compounds, and industrial waste, may be deposited directly or indirectly. Pollution may be classified into several forms based on its characteristics.

2.1.4.1. Mineral pollution

This consists mainly of heavy metals from the metallurgical and mineral processing industries, e.g. lead, copper, iron, zinc, and mercury, etc.

2.1.4.2. Microbiological pollution

Wastewater contains a variety of microorganisms excreted with feces, including both normal enteric flora and pathogenic organisms. These microorganisms are generally classified into four main groups, arranged in ascending order of size: viruses (Enterovirus), bacteria (*Salmonella shigella*), protozoa, and helminths [64, 65].

2.1.4.3. Chemical pollution

This results from chemical discharges, mainly from industrial sources. Chemical pollution of water is divided into two categories:

- Organic (hydrocarbons, pesticides, detergents, phenols, etc.).
- Mineral (heavy metals, cyanide, nitrogen, phosphorus, etc.).

2.1.4.4. Physical pollution

Resulting from the presence of particles or waste capable of clogging the bed of a watercourse (e.g., water from mines, wood pulp mills, tanneries).

2.1.4.5. Phosphorus Pollution

Phosphorus originates from the metal surface treatment industry, industrial laundering, and agri-food fertilizer manufacturing. Like nitrogen, phosphorus is a nutrient; it is the cause of eutrophication, i.e., the excessive proliferation of algae and plankton in aquatic environments.

2.1.4.6. Nitrogen Pollution

Industrial activities can be the source of discharges of varying amounts of nitrogen from fertilizer manufacturing, coking plants, and the chemical and food industries. Nitrogen exists in two forms: the reduced form, which includes ammoniacal nitrogen (NH_3 or NH_4^+) and organic nitrogen (protein, creatine, uric acid). Plus an oxidized form, which produces nitrite (NO_2^-) and nitrate (NO_3^-) ions [66].

2.1.4.7. Hydrocarbon pollution

Oil pollution results from several activities related to oil extraction, its transportation, and the downstream use of finished products (fuels and lubricants), as well as discharges from ships (oil spills). The effects of hydrocarbons in the marine environment are considerable. They depend largely on their composition. In fact, their activities can occur in several very different ways.

- Acute toxicity: It affects all living beings in the environment (plants, animals, or bacteria), causing immediate disappearance of fish by clogging bronchitis. Birds are also killed in large numbers by sticking their feathers.

- Long-term toxicity: Hydrocarbons or their degradation products can be accumulated by various marine organisms; after ingestion, their effects can last for very long periods. This danger is obviously more serious when it comes to carcinogenic polycyclic aromatic hydrocarbons (PAHs). They are absorbed by food chains and concentrated to very high levels. One can imagine the danger this phenomenon can pose for human consumers.

2.1.5. Measurement parameters

For a better assessment of the composition of wastewater, there are pollution assessment criteria, which are water temperature, water potential (pH), electrical conductivity, suspended solids (SS), biochemical oxygen demand (BOD), chemical oxygen demand (COD), nitrogen, phosphorus and other microbiological criteria such as fecal coliforms. There are also heavy metals, which can represent a potential nuisance.

2.1.5.1. Physicochemical Parameters

a. Temperature

This is an often-overlooked parameter in urban sewers, but it should be measured more frequently, especially in the case of industrial discharges into the network. The operation of some treatment plants is very sensitive to excessively high temperatures; therefore, all discharges must be below 30°C.

b. Hydrogen potential

pH is used to express the acidity level of wastewater. Its measurement is very important for assessing the proper functioning of a treatment stage.

c- Conductivity

This is a simple measurement performed with an electrode and provides a precise indication of the total dissolved salt concentration. By comparing it with the conductivity of drinking water, it is thus possible to quickly assess whether significant inputs, particularly industrial inputs, are occurring in the sewerage network.

d. Suspended Solids

Suspended solids represent materials that are neither soluble nor colloidal, and are therefore retained by a filter. Suspended solids, which include organic and mineral matter,

are an important parameter that clearly indicates the degree of pollution of an urban or even industrial effluent [16].

e. Chemical Oxygen Demand (COD)

Chemical oxygen demand is the amount of oxygen consumed by existing materials in the water that are oxidizable under well-defined operating conditions [17]. It is higher when there are oxidizable substances in the environment. Oxygen affects virtually all biodegradable and non-biodegradable organic matter. COD is measured in mg of O₂/L.

- COD = 1.5 to 2 times BOD for urban wastewater.
- COD = 1 to 10 times BOD for all wastewater.
- COD > 2.5 times BOD for industrial wastewater.

The empirical relationship between oxidizable matter and BOD₅ and COD is given by the following equation:

$$OM = \frac{(2 \times BOD_5 + COD)}{3} \quad (2.1)$$

f. Biochemical Oxygen Demand (BOD)

This corresponds to the amount of oxygen required to decompose organic matter in wastewater through oxidation using aerobic bacteria. This oxidation occurs in two stages:

- Oxidation of carbon compounds, a phenomenon that at 20°C is practically complete in 20 days;
- Oxidation of compounds containing nitrogen, a reaction that only begins after about ten days.

BOD₅ expresses the amount of oxygen consumed by bacteria, at 20°C and in the dark during 5 days of incubation of a previously inoculated sample, a time that ensures aerobic oxidation. For measurement, the amount of oxygen consumed after 5 days is taken as a reference; this is the BOD₅.

g. Biodegradability:

Biodegradability reflects an effluent's ability to be decomposed or oxidized by microorganisms involved in biological water treatment processes. It is expressed by a coefficient K, with $K = COD/BOD_5$ [62].

h. Total Organic Carbon (TOC):

Determines variable properties of dissolved and particulate organic carbon, organic carbon from volatile substances, and dissolved mineral carbon. It is measured using an infrared CO₂ analyzer after high-temperature catalytic combustion of the sample.

i. Nitrogen:

In domestic wastewater, nitrogen is in organic and ammoniacal forms. The forms of nitrogen in wastewater are:

- Total Kjeldahl nitrogen (TKN).
- Nitrates (NO₃⁻).
- And nitrites (NO₂⁻).

In addition to the toxicity of the ammoniacal and nitric forms, nitrogen is involved in the phenomenon of eutrophication. Therefore, its characterization and quantification are essential for liquid discharges into the natural environment [66].

- Kjeldahl nitrogen:

Kjeldahl nitrogen = Ammoniacal nitrogen + organic nitrogen.

- Organic nitrogen:

The nitrogen contained in animal waste, and more generally in dead organic matter, is gradually released by the activity of aerobic and anaerobic soil microflora, uric acids, and proteins.

- Ammoniacal nitrogen:

Ammoniacal nitrogen is present in two forms: ammonia NH₃ and ammonium NH₄⁺. In an oxidizing environment, ammonium transforms into nitrite and then nitrate.

k. Total phosphorus:

Phosphorus is found in wastewater in the following forms:

- Orthophosphate, soluble PO₄H₂.
- Polyphosphate, which tends to hydrolyze into orthophosphate.
- Undissolved phosphorus.

2.1.5.2. Biological parameters

a. Escherichia coli (E. coli)

E.coli is a type of bacteria commonly found in the intestines of humans and warm-blooded animals. In wastewater monitoring, E. coli is used as an indicator organism to assess fecal contamination and the microbiological quality of water. Its presence in treated or untreated wastewater suggests the possible presence of pathogenic microorganisms, making it a key parameter in evaluating water safety and treatment efficiency.

b. Enterococci

Enterococci are bacteria commonly present in the intestines of humans and warm-blooded animals. In wastewater treatment, they serve as important indicators of fecal contamination and help assess the microbiological safety of water. Because of their resilience to environmental conditions and disinfection processes, enterococci are considered reliable markers for the possible presence of harmful pathogens, particularly in coastal and recreational waters.

2.1.6. Impact of wastewater

2.1.6.1. Impact on the natural environment

a. Surface water:

Direct discharges into rivers or lakes promote eutrophication (algal blooms), which reduces oxygen in the water and threatens aquatic life. Heavy metals such as mercury or arsenic can accumulate in the food chain and pose a danger to species and humans.

b. Groundwater:

Groundwater can be polluted by wastewater in the event of leaks or malfunctioning sewage systems, which deteriorates the quality of groundwater.

c. The ocean:

When wastewater is discharged into the sea without adequate treatment, it contaminates bathing areas with bacteria, viruses, and parasites. In Algeria, several beaches, such as Bab El Oued (Algiers) and Chatt El Hillal (Boumerdès), have been temporarily closed to swimming due to the discharge of untreated wastewater. This pollution can cause illness in humans through simple contact or accidental ingestion.

2.1.6.2. On human health

Water, a natural resource essential to life, has also become, directly or indirectly, the leading cause of mortality and disease in the world. Inequality in the distribution of water resources, combined with deteriorating water quality, is causing major health problems.

2.2. WASTEWATER TREATMENT

2.2.1. Pre-treatment

Raw wastewater must generally undergo pretreatment before actual treatment pretreatment, which aims to extract as many elements as possible whose nature or size would interfere with subsequent treatment. These include the following three operations:

- Screening;
- Sand removal;
- Oil and grease removal.

a.Screening

Screening and sieving remove insoluble waste such as branches, plastics, sanitary napkins, etc. from water. Since this waste cannot be eliminated through biological or physicochemical treatment, it must be mechanically removed. To do this, the wastewater passes through one or more screens with increasingly fine meshes [67, 68].

b. Sand/Oil Removal

Its purpose is to extract sand, grease, and more or less fine suspended mineral particles from raw water. The sand deposited at the bottom of the structure is pumped or sucked up by crane-mounted pumps, while floating grease and oil are aerated using air bubbles, which increases the rate at which the grease particles rise. Recovery takes place in a stilling zone.

2.2.2. Primary treatment

2.2.2.1. Primary decantation

Decantation is a technique for separating suspended solids from colloids collected in floc. This technique is widely used in water treatment plants. Primary decantation aims to

improve the quality of pretreatments, particularly by capturing naturally decantable suspended solids and thoroughly removing floating solids (oils and greases).

During this stage, particles, whose density is higher than that of water, will tend to accumulate at the bottom of the decanter under the effect of gravity. The particles will be periodically removed from the bottom of the tank [8]. This treatment eliminates 30 to 40% of suspended solids and reduces BOD and COD by approximately 30% [67, 68].

2.2.3. Secondary treatment

It involves bringing wastewater into contact with a purifying biomass, which is in fact a simplified and selected ecosystem using only microorganisms. It is made up of small living organisms, less than a millimeter in size, including bacterial microflora and animal microfauna, protozoa [9].

In the case of urban wastewater, the development of aerobic bacteria, i.e., bacteria that use oxygen to grow, is encouraged.

- a. Biological treatment: It takes place at the aeration basin level and includes carbon elimination:
- b. Secondary settling (clarification): At the outlet of the aeration tanks, the biological liquor will be subjected to clarification in order to separate the activated sludge from the purified water and recycle it to the aeration tanks. The water, freed from 80 to 90% of its impurities, then undergoes analysis and controls before being released into the natural environment.
- c. Sludge treatment: Consists of concentrating organic matter by filtering liquid sludge to obtain solid sludge that is more easily transported and stored [69, 70].

2.2.4. Tertiary treatments

In the context of reuse of purified wastewater, wastewater requiring additional treatment, mainly to eliminate microorganisms that could pose health problems. This treatment is mainly disinfection Using calcium hypochlorite ($\text{Ca}(\text{ClO})_2$).

Calcium hypochlorite comes in powder form. The solution must be prepared on site by diluting the powder with water. This allows the active chlorine to be used [70].

2.3. RE-USE OF WASTEWATER

2.3.1. wastewater reuse in Algeria

The reuse of treated wastewater is a voluntary and planned action that aims to produce additional quantities of water for different uses. Today, the national strategy for sustainable development in Algeria is materialized particularly through a strategic plan that brings together three dimensions: Social, Economic and Environmental.

Algeria's national sewerage network currently extends over approximately 97,000 kilometers, with a connection rate reaching 93% of the non-dispersed population. By 2025, the total volume of wastewater collected and treated is estimated at nearly 600 million m³ per year, of which approximately 550 million m³ is generated by the major urban areas in the north of the country.

Faced with dwindling water resources, Algeria plans to increase this volume to more than 1.2 billion m³ per year by 2030, notably through the commissioning of new wastewater treatment plants and the expansion of tertiary treatment. The national objective is to reuse at least 60% of treated wastewater for agricultural, industrial, or environmental uses, compared to less than 10% currently.

To support this objective, 16 additional wastewater treatment plants are being equipped with tertiary treatment systems, which will add 140 million m³/year of reusable capacity. This strategy is part of a national framework led by the Ministry of Hydraulics and the National Sanitation Office (ONA), aimed at securing unconventional water supplies in the long term.

The national strategy for the reuse of treated wastewater for irrigation has three objectives:

- To conserve and preserve traditional water resources.
- To increase irrigated areas.
- To contribute to increasing agricultural production.

CHAPTER 3

MATERIALS AND METHODS

This chapter covers the experimental set-ups and protocols used for the ferrate electro-synthesis in a double compartment electrochemical cell and the elaboration of the chitosan membrane used as separator as well as the use of ferrate (VI) in wastewater treatment.

3.1. CHEMICAL PRODUCTS

All the chemicals and reagents used in this investigation are of analytical grade and are listed in Table 3.1.

Table 3.1: The chemical products used in this study.

Product	Source	Purity
Hydrochloric acid (HCl)	Sigma-Aldrich, USA	38%
Sodium hydroxide (NaOH)	Sigma-Aldrich, USA	100%
Potassium hydroxide (KOH)	Sigma-Aldrich, USA	100%
Acetic acid (CH ₃ COOH)	Sigma-Aldrich, USA	100%
Hydrogen peroxide (H ₂ O ₂)	PanReac AppliChem, Germany	/
Sulfuric acid (H ₂ SO ₄)	PanReac AppliChem, Germany	98%
Phosphoric acid (H ₃ PO ₄)	PanReac AppliChem, Germany	99%
Chromium chloride hexahydrate (CrCl ₃ .6H ₂ O)	BioChem, France	93%
Ammonium iron (II) sulfate ((NH ₄) ₂ SO ₄ ·Fe (SO ₄) ·6H ₂ O)	Bio Chem, France	98.5%
Sodium diphenylamine sulfonate	Bio Chem, France	98%
Sodium hypochlorite (NaClO)	BioChem, France	50 Cl°
iron sulfate heptahydrate(FeSO ₄ 7H ₂ O)	BioChem, France	100%
Potassium bromide (KBr)	Bio Chem, France	99.5%

3.2. CHITOSAN CHEMICAL EXTRACTION

3.2.1. Pretreatment

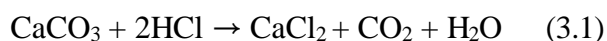
Shrimp shells collected from fishmongers, considered as the raw material for this study, undergo a pre-treatment process. The shells must be peeled, washed and placed in boiling water for 10 minutes, then air-dried for least 8 hours. They can then be frozen until the day of use. Once removed, they should be dried in an oven at 80°C for 24 hours, then ground [71;72].

3.2.2. Chitin extraction

Pure chitin was extracted following three main steps

a. Demineralization

This step is carried out with acid hydrolysis using a 5M HCl hydrochloric acid solution with a weight : volume (w:v) ratio of (1:10) the shrimp shell powder is gradually added so that the contents of the beaker do not overflow and the release of carbon dioxide produced during the reaction is controlled. The mixture is left stirring for 1 hour at room temperature, then filtered through a sieve and rinsed with distilled water until the pH of the filtrates is neutral [72, 73].



b. Deproteinisation

After stabilizing the pH, the material is then introduced into a beaker to which a 1.25 M NaOH solution (1:15) (w: v) is added and then placed in the oven at 90°C for 18 hours. This step is carried out in order to remove proteins and organic matter. The contents of the beaker are again filtered and rinsed with distilled water until the pH of the filtra is neutralized (pH = 7). The product is then placed back in the oven at 90°C for 20 hours. The product obtained in this step is chitin [71, 72, 74].

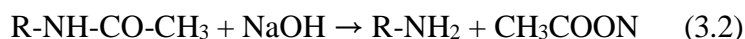
3.2.3. Chitin deacetylation

Chitosan was obtained by deacetylation of chitin extracted with a NaOH solution using the following steps [75-77]:

- Treatment of chitin with NaOH 50% using a (w : v) ratio of (1 : 15)

- The mixture stirred for 4h at a temperature of 100°C then placed in the oven for 18h at the same temperature
- Filtering the solution through a sieve then rinsing with distilled water at 45°C to remove residual soda until pH neutralization

The deacetylation of chitin is done according the following chemical reaction:



Chitin

Chitosan

- After the neutralization of the pH of the obtained chitosan it is placed in the oven for drying over 24h at 80°C.

3.3. MEMBRANE PREPARATION

Chitosan membranes are prepared by solubilizing 2g of chitosan in 100 mL of 1% acetic acid solution and stirring until a homogeneous gel is obtained. A volume of 15 mL and 20 mL gel is then poured into petri dishes and placed in an oven at 40°C for 24 hours [78].

3.4. PHYSICO-CHEMICAL ANALYSIS

3.4.1. Moisture content

To determine the moisture content in the extracted chitosan, 1g of sample was weighted in a dish of a known weight, and then it was placed in an oven at 100°C for 24 hours, and reweighed after 30 min of cooling. The moisture content was calculated according to the following formula (3.1) [79]:

$$\text{Moisture content}\% = \frac{\text{wet weight} - \text{dry weight}}{\text{wet weight}} \times 100 \quad (3.1)$$

3.4.2. Determination of solubility

The extracted chitosan is tested for its solubility in acidic, neutral and basic media. The solubility test was carried out in 3 different solutions by adding 0.05g of chitosan in 50 mL of each solution and leaving stirring for 24 hours at room temperature [80].

Solution 1: 1% acetic acid.

Solution 2: 0.5M NaOH.

Solution 3: distilled water.

3.4.3. Ash content

Ash content allows to determines the effectiveness of the crustacean shell demineralization process, which relies on heat resistance. 1g of chitosan is weighed into a crucible of a known weight, which is then placed in a calciner at 500°C for 5 hours. After cooling, it is reweighed. The ash content was evaluated according to the following formula (3.2) [81]:

$$\text{Ash content \%} = \frac{\text{Ash weight of the calcined sample (g)}}{\text{Weight of the dry sample (g)}} \times 100 \quad (3.2)$$

3.4.4. Fourier-Transform Infrared spectroscopy FTIR analysis

Fourier transform infrared spectroscopy (FTIR) can identify the presence of specific chemical groups. This analytical method allows rapid IR spectra of solid and liquid samples to be obtained without requiring much manipulation. In this study the FTIR spectra were undertaken in transmittance mode with SHIMADZU FTIR-8400S Spectrometer, in a wave number range of 400- 4000 cm^{-1} . IR spectra were obtained with an accuracy of 4 cm^{-1} [82].

3.4.5. Deacetylation degree

Chitosan is mainly characterized by DDA. Many methods are proposed to determine the degree of deacetylation of chitosan. However, FTIR is the most suitable method for easy and fast characterization that does not require many manipulations. The DDA of the sample determines the amount of acetyl groups removed from the chitosan structure. The DDA was calculated according to the following formulas (3.3) and (3.4) [83].

$$DD\% = \frac{A_{1320}/A_{1420} - 0.3822}{0.03133} \quad (3.3)$$

$$DDA\% = 100 - DD\% \quad (3.4)$$

While $DD\%$ is the acetylation degree, A_{1320} and A_{1420} are the absorptions at wavelengths 1320 and 1420 cm^{-1} , and $DDA\%$ is the deacetylation degree.

3.4.6. X ray diffraction XRD analysis

The generated chitosan was characterized using an X-ray diffractometer (Shimadzu XRD-6100) with a Cu K α radiation source and a 50 kV applied voltage. To determine its crystallinity, the scanning range was maintained at 5° to 80° (2 θ) with a scan rate of 0.01 °/s. This analysis allows the calculation of the crystallinity index (Cr %) according the following equation (3.5), [84]:

$$CrI\% = \frac{(I_{max} - I_{min})}{I_{max}} \times 100 \quad (3.5)$$

Where I_{max} is the intensity value 2 θ of 20° and I_{min} intensity value at 2 θ of 10°.

3.4.7. Ion exchange capacity

The ion exchange capacity of the chitosan membrane (IEC) was evaluated using back titration. an amount of 0.2 g Membrane was immersed in 1.0 M KOH for 24 h, rinsed with deionized water, and equilibrated with 40 mL of 0.01 M HCl standard solution for 24 h before being potentiometrically titrated with 0.01 M NaOH standard solution. The blank sample consisted of 40 mL of 0.01 M HCl standard solution. The ion exchange capacity value was obtained using the following equation (3.6); [85]:

$$IEC = \frac{(V_{blank} - V_{membrane})C_{HCl}}{m_{membrane}} \times 1000 \quad (3.6)$$

Where, V_{blank} and $V_{membrane}$ are the consumed volumes [mL] of the NaOH solution for the blank sample and the chitosane membrane sample, respectively, C_{HCl} is the concentration of the HCl solution, and $m_{membrane}$ is the dry membrane sample's mass [85].

3.4.8. Thermal analysis

To evaluate the thermal behavior and stability of the chitosan membrane, differential scanning calorimetry (DSC) and thermal gravimetric analyzer (TGA) were used in conjunction with NETZSCH STA 409 PG/PC to conduct a linked thermal study. The thermal scans were done from room temperature to 650 °C, at a 10 °C min⁻¹ heating rate and 25 mLmin⁻¹ nitrogen atmospheres. The tested sample weighed 8 mg [86].

3.4.9 Membrane thickness

Chitosan membrane thickness was measured with an electronic micrometer (MAHR militant 1101) in five different spots of the film sample, and then the median values were computed [86].

3.5. FERRATE SYNTHESIS

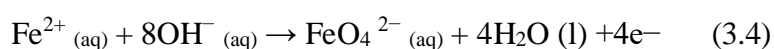
3.5.1. Electrochemical synthesis

The electro-generation ferrate of (VI) is the most straightforward approach for generating impurity-free sodium ferrate solution by the oxidation of iron (II) anode in an electrolysis cell carrying a high-concentration alkaline solution [61]. The chemical equations below illustrate the primary cathodic and anodic processes used in this technique [61].

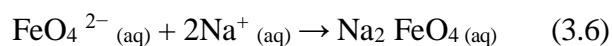
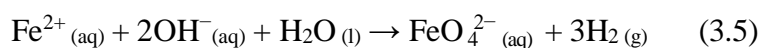
Cathodic reaction:



Anodic reaction:



Overall reaction:



The figure below represents the experimental setup used for the electrochemical production of ferrates (VI). It consists of:

- A current generator to control the current.
- An electrolytic cell with two compartments separated by a membrane chitosan to separate the oxidation and reduction reactions.
- Two metal plates representing the electrodes (anode and cathode) made of steel placed in parallel at a set distance from each other.
- A stirrer to maintain agitation of the electrolyte during the reaction.

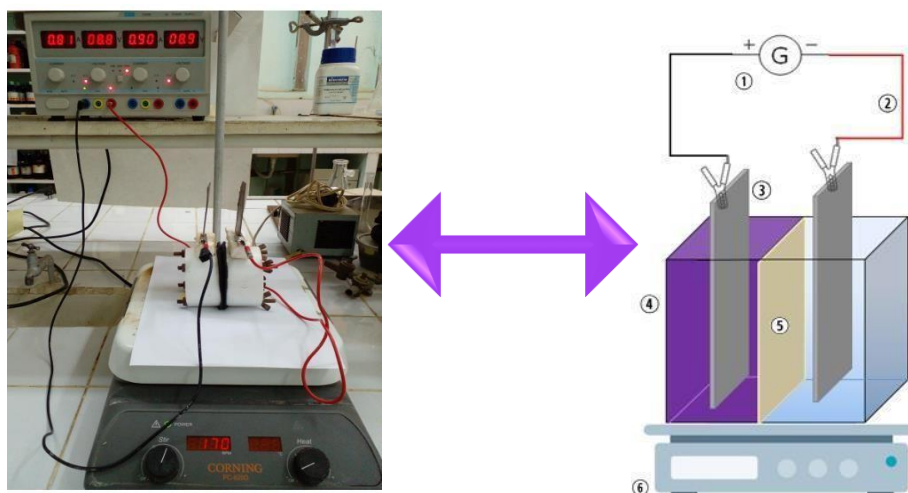


Figure 3.1: The process of electro-generation of ferrate (VI). (1) DC power supply, (2) electrical wire, (3) iron electrodes, (4) double compartment electrochemical cell, (5) chitosan membrane, (6) magnetic stirrer.

The following table gathers the ranges of the studied parameters for both membrane used:

Table 3.2: The range of parameters studied.

Parameters	range
NaOH concentration (M)	16-26
Current density (mA/cm^2)	40-90
Temperature ($^{\circ}\text{C}$)	25-45
Reaction time (h)	0.5-4

Table. 3.3: The different electrodes used for the synthesis.

Electrode nature
0.12% Carbon steel
0.087% Carbon steel
0.087 % Carbon steel with 3 mm holes
0.087% Carbon steel with 6 mm holes
Grey Cast Iron
White Cast Iron

After each use, the electrodes are oxidized, so it is necessary for them to be polished using abrasive paper of decreasing grit size (280, 200, 400, 600, 1200 mesh) to remove oxide films and passivation layers.

3.5.1.1. Ferrate (VI) powder

The solubility of the ferrate (VI) salt reveals how quickly it may be transported from solution to solid state. Moisture has a detrimental impact on the stability of ferrate (VI). Hence, the solid-state is required for long-term storage [60]. Ferrate (VI) powder was obtained using vacuum filtration of liquid-synthesized ferrate (VI) with a Whatman filter of 0.5 μm pore size. Then, placed in the oven at 80 $^{\circ}\text{C}$ until total dries.

3.5.1.2. Current efficiency

The current efficiency of the electrochemical synthesis of ferrate (VI) was determined for all the parameters studied, it was calculated as the ratio of the experimentally measured Ferrate yield to the theoretically predicted ferrate production based on Faraday's law, as expressed in Equation (3.7) :

$$\text{current efficiency}\% = \frac{\text{Ferrate experimental}}{\text{Ferrate faradaic}} \times 100 \quad (3.7)$$

The theoretical amount of ferrate produced (in grams) was calculated using Faraday's law, as described in Equation (3.8):

$$\text{Ferrate faradaic} = \frac{M I t}{n F} \quad (3.8)$$

Where I is the applied current (A), t is the electrolysis time (s), M is the molecular weight of ferrate (VI) Na_2FeO_4 (g/mol), F is the Faraday constant (96,485 C/mol), and n represents the number of electrons involved in the reaction (6 e^-) [45].

3.5.1.3. Consumed energy

The consumed energy (W) is an important parameter to take into consideration in the production of ferrate by electrochemical method. This energy is determined by the equation below (3.9):

$$w = \frac{V I t}{m} \quad (3.9)$$

With:

W: Energy consumed in kWh/kg, V: Voltage across terminals, I: Current intensity (A), t: Electrolysis time (h), m: mass of ferrate produced in kg.

3.5.2. Ferrate (VI) dry synthesis

The experimental setup used for the dry production of ferrates is shown in Figure 3.1. It consists of a water bath, a double-walled Pyrex glass electrolytic cell, and a mechanical propeller stirrer. The dry synthesis of ferrates was carried out in an electrolytic cell under stirring. To maintain a constant temperature during the reaction, a water bath was used.

The ferrate synthesis reaction was carried out mixing 3 g of iron sulfate heptahydrate ($\text{FeSO}_4 \cdot 7\text{H}_2\text{O}$) powder, 3 g of potassium hydroxide (KOH) in pellet form (K/Fe ratio = 1), and 1.55 g of calcium hypochlorite powder ($\text{Ca}(\text{ClO})_2$) these values were fixed for all the experiments.

Once the powders are in contact with KOH pellets the synthesis, reaction of potassium sulfate-ferrate begins instantly (reaction 3.7) due to the amount of water in potassium hydroxide and iron sulfate heptahydrate, that allows better diffusion powder/pellets. The oxidation of Fe (II) to Fe (VI) can be seen through the color change of KOH from white to dark purple.



After a certain time of reaction, the dark ferrate (VI) pellets are separated from the powder. In this stage the ferrate (VI) have an important amount of impurities due to the excess powder during the reaction for that a purification is necessary.

Ferrate (VI) purification was done using organic solvent: in small beaker, 20 mL of methanol was poured on the obtained ferrate (VI) and stirred for few minutes then filtered. The resulting product dried at studied temperature and duration.

The final product is stored in dark flasks away from light and moisture to ensure its stability over time.



Figure 3.2: Experimental setup used for the synthesis of ferrates by the dry route. 1- Mechanical stirrer, 2-Double-walled electrochemical cell, 3-Water bath.

3.5.2.1. Studied parameters

In order to improve the purity and yield of ferrate synthesized by dry process A parametric study was carried out on the effect of the different parameters cited below on the synthesis of ferrate (VI) by dry process:

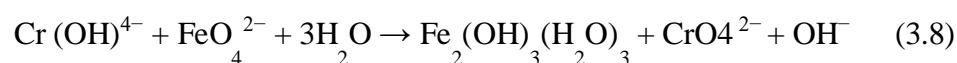
Table 3.4: Studied range of ferrate (VI) dry synthesis parameters.

Parameters	Studied range
Particle diameters	$75 < \phi < 250 \mu\text{m}$
Drying time of iron sulfate heptahydrate	[0-25] min
Drying Temperature of iron sulfate heptahydrate.	[60-110] °C
Reaction time	[30-120] min
Reaction temperature.	[20-40] °C
Drying time of ferrate (VI)	[5-30] min
Drying temperature of ferrate (VI)	[70-130] °C
Number of washes with methanol	[1-5]

3.5.3. Ferrate (VI) characterization

3.5.3.1. Chromite analysis

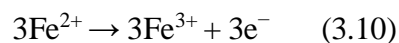
The concentration was determined to evaluate the effectiveness of the used method. The generated ferrate (VI) concentration was determined using the chromite titrimetric method. The reactions involved in the titration process are [87, 88]. When ferrates are dissolved, they can oxidize chromite from Cr^{3+} to Cr^{6+} according to the following chemical equation (3.8) [40].



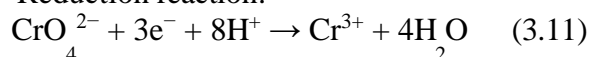
After that, a few drops of sodium diphenylamine sulfonate ($\text{C}_{12}\text{H}_{10}\text{NNaO}_3\text{S}$) were used as an indicator when the chromate was titrated with ferrous ammonium sulphate solution [24].



Oxidation reaction:



Reduction reaction:



To carry out this titration, the following steps are applied:

Step 1: Preparation of Ferrate (VI) solution sample

A 400 mL glass beaker was filled with 20 mL of 72% NaOH solution, 5 mL of a $\text{CrCl}_3 \cdot 6\text{H}_2\text{O}$ solution with a concentration of 16.66%, and 5 mL of water, the mixture was set aside to cool to ambient temperature. 5 mL of freshly synthesized ferrate (VI) was added to this solution and then stirred until a total dissolution of ferrate (VI) (Na_2FeO_4).

Step 2: Preparation of the titration solution

Preparing for titration, the Na_2FeO_4 solution (or 25 mL of a known concentration Cr (VI) solution) was mixed with 150 mL of water, and then 65 mL of 20% H_2SO_4 solution (produced by dilution of 95% H_2SO_4) was added. After introducing 15 mL of the $\text{H}_2\text{SO}_4/\text{H}_3\text{PO}_4$ solution (prepared with 240 mL of water, 65 mL of 95 % H_2SO_4 , and 150 mL

of H_3PO_4 in a 500 mL flask) then putting in 7 or 8 drops of the indicator sodium diphenylamine sulfonate [24;89].

Step 3: Preparation of the indicator

Dissolving 0.5 g of the sodium diphenylamine sulfonate in H_2SO_4 in a 100 mL flask [9].

Step 4: Preparing the titrating solution

Ferrous ammonium sulfate solution (3.34% w/v) is prepared to provide a concentration of 0.085N $\text{Fe}(\text{NH}_4)_2(\text{SO}_4)_2 \cdot 6\text{H}_2\text{O}$. To precisely determine the normality of ferrous ammonium solution, it was used to titrate a sample of Cr (VI) solution with a known concentration, 25 mL of 0.085 N $\text{K}_2\text{Cr}_2\text{O}_7$ (potassium dichromate) was used to prepare the Cr (VI) sample (prepared as 0.417 g of $\text{K}_2\text{Cr}_2\text{O}_7$ per 100 mL solution) and is treated as explained above before titration. The volume (mL) of $(\text{NH}_4)_2(\text{SO}_4)_2 \cdot 6\text{H}_2\text{O}$ produced a color shift from dark purple to yellowish green [24,88,89].

$$N = \frac{0.085 \times 25}{V} \quad (3.10)$$

Step 5: Determination of Na_2FeO_4 concentration

The ferrate (VI) concentration is estimated with formula (3.8) using the volume (mL) of $\text{Fe}(\text{NH}_4)_2(\text{SO}_4)_2 \cdot 6\text{H}_2\text{O}$ titrant required in the titration to achieve a color shift from dark purple to green [24,88,89]:

$$[\text{Fe(VI)}] = \frac{0.085 \times V}{3 \times V_{\text{Ferrate sample}}} \quad (3.11)$$

Ferrate sample (mL) is the volume of synthesized ferrate (VI) sample, whereas 0.085 is the concentration of ferrous ammonium sulfate, V (mL) is the poured volume of $(\text{NH}_4)_2(\text{SO}_4)_2 \cdot 6\text{H}_2\text{O}$ during titration, and 3 is the number of equivalents (number of electrons to convert Cr^{6+} to Cr^{3+}) per Fe^{6+} [24, 89].

For the ferrate synthesized with dry method, the purity is calculated with the following formula:

$$F(\text{VI})\% = \frac{0.085 \times V \times M_{\text{Fe(VI)}}}{3 \times m_{\text{Ferrate sample}}} \times 100 \quad (3.12)$$

While m Ferrate sample (0.175 g) is the weight of synthesized ferrate (VI) sample, whereas 0.085 is the concentration of ferrous ammonium sulfate, V (L) is the poured volume of $(\text{NH}_4)_2(\text{SO}_4)_2 \cdot 6\text{H}_2\text{O}$ during titration, 3 is the number of equivalents (number of electrons to convert Cr^{6+} to Cr^{3+}) per Fe^{6+} , and $M_{\text{Fe(VI)}} (\text{K}_2\text{FeSO}_4)$ is the molar weight of ferrate.

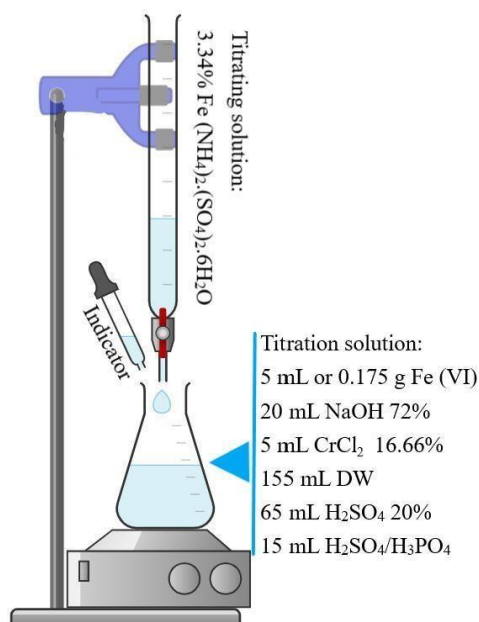


Figure 3.3: experimental setup of the chromite method.

3.5.3.2. UV-Visible spectroscopy

The visible spectra of the synthesized Ferrates were recorded in the 400-600 nm range using a UV-visible spectrophotometer SHIMADZU UV-1280 to determine the characteristic peak of Na_2FeO_4 using 1 mL of synthesized ferrate (VI) diluted in 50 mL of NaOH.

3.5.3.3. Fourier-transform infrared spectroscopy

The FTIR method was applied to analyze the sodium ferrate (VI) using the Shimadzu FTIR-8400S spectrometer. A thin KBr/ferrate (VI) powder pellet was prepared and scanned in a $400\text{--}4000\text{ cm}^{-1}$ wave number range.

3.5.3.4. Scanning electronic microscopy

Scanning electronic microscopy detects the structure of Ferrate (VI) powder by delivering some micrographs or structural pictures using ZEISS EVO 15. The instrument was operated at an accelerating voltage of 20 kV, and the magnification was 2500X and 10000X [90].

3.5.3.5. X-Ray Diffraction

XRD is a technique used with FTIR and SEM to investigate crystallinity [48]. XRD analysis was carried out using Shimadzu XRD-6100, a small amount of synthesized Ferrate (VI) powder was scanned in the 2θ range of 5° - 80° with a scan rate of $2^\circ/\text{min}$.

3.5.3.6. Cyclic voltammetry

Cyclic voltammetry was used to characterize Ferrate and to explain the reactional mechanism involved in its production using the determined optimal conditions and electrode materials. The cyclic voltammogram was recorded at a scan rate of 50 mV/s ranging from -1.6 V to $+0.2 \text{ V}$. The voltametric analysis was carried out using a Metro lab potentiostat/Galvano stat with a platinum counter electrode and a reference electrode of 3 M KCl Ag/AgCl , which was positioned in the anodic chamber approximately 10 mm from the working electrode [45].

3.5.3.7. Thermogravimetric Analysis

Thermogravimetric (TGA) of synthesized ferrate (VI) powder was performed with NETZSCH STA 409 PG/PC thermal analyzer using 10 mg of ferrate (VI) powder from 25°C to 650°C (10°C/min) in the N_2 flow of 25 mL/min .

3.6. FERRATE (VI) IN WASTEWATER TREATMENT

3.6.1. Beni Messous wastewater treatment plant (Algiers)

The Beni Messous wastewater treatment station is one of four wastewater treatment stations in the wilaya of Algiers. it receives effluent from the western part of Algiers.



Figure 3.4: Beni Messous station from above (Algiers, 2025).

3.6.1.1. Geographical location

The beni messous wastewater treatment plant, located at the coordinates (36°46'59" N) (02°53'53" E) in the town of Aine El Beniane, Algiers province, at the end of Oued Beni Messous, extends over sloping terrain, with an altitude of 12.46 m upstream to 3.32 m downstream. This WWTP covers a total area of approximately 12.7 hectares.

3.6.1.2. Characteristics of the beni Messous wastewater treatment plan

Initially commissioned in June 2007 with a capacity of 50,400 m³/d. The plant serves approximately 250,000 population equivalents, and the second phase has doubled this capacity to around 100,000 to 110,000 population equivalents. It treats wastewater from six municipalities in western Algiers (Aïn Benian, Beni Messous, Chéraga, Staouéli, Ouled Fayet, and Dely Ibrahim).

- Treatment Process

- Medium-load activated sludge technology (0.25–0.3 kg BOD/kg SS/day)
- 4 parallel aeration tanks: dimensions 55.5 x 15.5 x 4.58 m, total volume 188,000 m³, with 12 turbines for oxygenation.
- Pretreatment: screening, grit removal, and oil removal according to ONA standards.

- Challenges

- Several anomalies reported : sand deposits, rising sludge in the clarifiers, and high nitrogen and phosphorus concentrations at the outlet.
- No tertiary treatment or disinfection to date, which poses a risk to the receiving environment.

3.6.2. Beni Mered wastewater treatment plant (Blida)

The Beni Mered wastewater treatment plant (WWTP) was Inaugurated in the 1980s, in service before 2015, it is designed to treat wastewater from the urban area of Blida-Beni Mered, as well as from industries connected to this area.

3.6.2.1. Geographical location

Located east of National Road No. 1, at the coordinates (36°31'40" N), (2°52'13" E), near Oued Béni Azaa, which crosses the towns of Blida, Ouled Aiche and Beni Mered over a distance of approximately 30 km. It is also close to other rivers such as Oued Lekhel, Oued Ftiss, Oued El Harrach, Oued Bouroumi, and others.

3.6.2.2. Characteristics of the Beni Mered WWTP

Located on a plot of approximately 6 hectares

Nominal flow rate at planned restart (October 2016): 450,000 m³ population equivalent/day, increasing from 70,000 to 450,000 m³ population equivalent/day. This capacity covers a population of nearly 400,000 to 500,000 inhabitants (municipalities of BéniMered, OuledYaïch, Bouarfa, Blida)

- Treatment Process

Activated sludge filtration, comprising several aeration tanks (typical dimensions: 55.5×15.5×4.6m) and pretreatment (grits, sand removal, oil removal).

- Challenges

Recommendation of a tertiary phase / disinfection (UV/chlorination) to improve output quality and potentially reuse water for irrigation.



Figure 3.5: Beni Mered WWTP view from above (Blida, 2025).

3.6.3. Physico-chemical analysis

To evaluate and compare the efficiency of the synthesized ferrate (VI) with both electrochemical and dry method, an amount of ferrate powder in range of [0.06- 0.16] g with a step of 0.02 g was injected into wastewater samples of 200 mL.

The samples were freshly collected, at the exit of the second clarifier (purified water without chlorination) for both Beni Messous (Algiers) and Beni Mered (Blida) WWTP.

The samples were stirred for 90 minutes at room temperature, then filtered and analyzed. The physico-chemical parameters COD, nitrite, and nitrate were measured using micro-methods. BOD₅ was determined using the dilution method with the SP50 Skalar robotic system while the bacteriological analysis was based on the detection and enumeration of bacteria. All analyses were carried out at the central laboratory of SEAAL in Kouba, Algiers.

3.6.3.1 Chemical Oxygen Demand COD analysis

The COD analysis was carried out using the COD cuvette test LCI500 according ISO 15705 standards as follow:

- Invert 2–3 times the reagent tube until homogenization.
- A 2 mL aliquot of the wastewater sample was transferred into a reagent tube, which was then securely closed. The tube was gently inverted 2–3 times to ensure proper mixing of the contents. Subsequently, the tube was placed in a CR 3200 dry block thermostat and heated at 148 °C for 2 hours to facilitate digestion.
- After the heating period, the tube was again gently inverted several times and allowed to cool to room temperature (approximately 18–20 °C). The exterior of the vial was thoroughly cleaned to remove any residues that could interfere with the optical measurement.
- The prepared vial was then inserted into the spectrophotometer's cell holder. After selecting the appropriate analysis program, the measurement was initiated. The resulting concentration values were recorded in (mg/L).

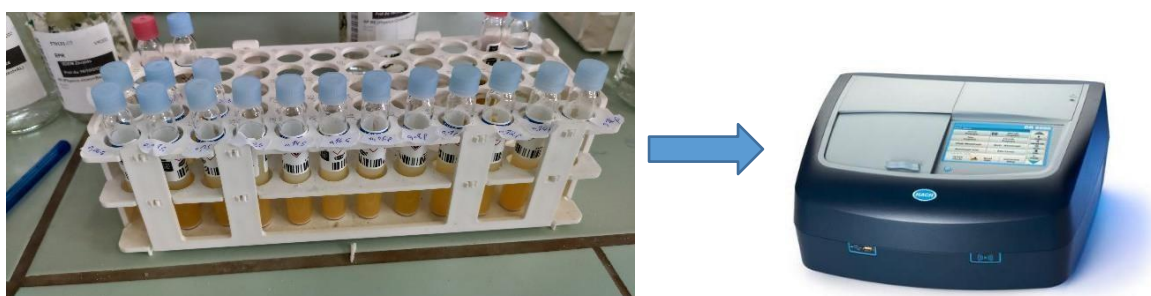


Figure 3.6 : Reagent tube LCI500 of COD (left) and the spectrophotometer used (right).

3.6.3.2. Biological Oxygen Demand BOD₅ analysis

The biochemical oxygen demand after 5 days (BOD₅) is determined by dilution and seeding using the SP50 SKALAR robot, coupled with an oximeter, according to ISO 5815-1, second edition 2019.

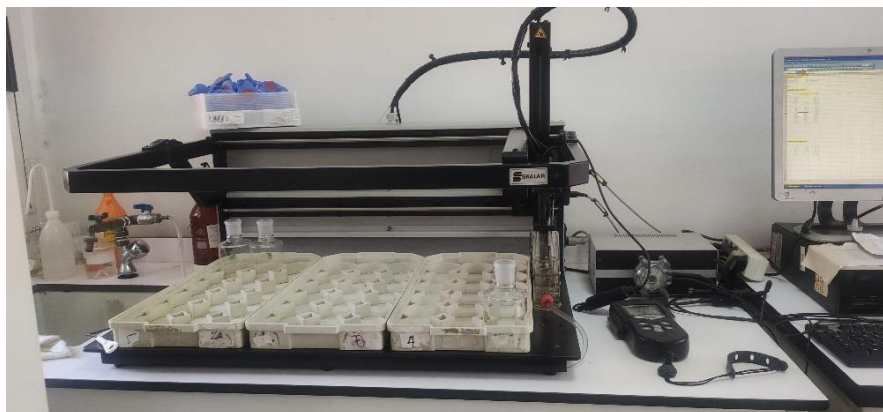


Figure 3.7: The SP50 SKALAR robot for BOD₅ analysis (central laboratory SEAAL, Algiers)

The determination of BOD with nitrification inhibition is performed using the dilution method. A series of preparations consisting of different dilutions of a sample is prepared and tested.

The dilutions are determined using the R factors (between 0.35 and 0.65 for untreated wastewater and between 0.10 and 0.35 for treated wastewater) of the COD in mg/L. According to the latter, the expected BOD₅ value is calculated using the formula (the lower and upper values of R are used respectively):

$$\text{BOD}_{\text{expected}} = R \times \text{COD} \quad (3.13)$$

Based on the calculated concentrations of the expected BOD, we found the possible sample volumes per liter of test solution and the corresponding dilution factors in Table (3.5).

Table 3.5: Dilution factors for BOD₅ analysis.

Expected BOD ₅ (mg/L)	Dilution factor	Sample volume (mL)
3 to 6	1.1 to 2	200
4 to 12	2	146
10 to 30	5	58.4
20 to 60	10	29.2
40 to 120	20	14.6
100 to 300	50	5.84
200 to 600	100	2.92
400 to 1200	200	1.46
1000 to 3000	500	0.584
2000 to 6000	1000	0.292

The dilution water is enriched with oxygen and inoculated with suitable aerobic microorganisms. The sample is incubated (20±1) °C for a specified period of 5 days, in the dark, in a fully filled and sealed bottle. The dissolved oxygen concentration is determined before and after incubation. The mass of oxygen consumed per liter of sample is calculated.

3.6.3.3. Nitrite (NO₂⁻) analysis with molecular adsorption spectrophotometry

50 mL of water to be analyzed is introduced into a volumetric flask. The nitrites react in an acidic medium with sulfanilamide (1 mL), forming a diazonium salt. The latter then reacts with 1 mL of N-(1-naphthyl) ethylenediamine (NEDA) to form a pink dye after 10 minutes of reaction, indicating the presence of NO₂⁻. The resulting color exhibits an absorbance maximum at a wavelength of 543 nm, and its intensity is proportional to the nitrite concentration in the sample.

Absorbance is measured by UV-Visible spectrophotometry, and the concentration is determined using a calibration curve prepared from standard nitrite solutions. The result is given directly in milligrams per liter of water (mg.L⁻¹).

3.6.3.4. Ammonium (NH₄⁺) analysis

Ammoniacal nitrogen (N-NH₄) is determined by the continuous flow analysis method, according to ISO 11732:2005 standard. In continuous flow, the principle of the

method: a gas-segmented carrier stream, the ammonium present in the sample reacts in the alkaline solution with hypochlorite (ClO^-) which has previously been released by dichloroisocyanurate. The chloramine formed reacts under nitroprusside catalysis with salicylate at a temperature between 37 °C and 50 °C, to form a blue-green indophenol coloration, which is quantitatively measured by a flow spectrometer from 640 nm to 660 nm.

After launching the Flow Access software, activate analyzer control, fluidic circuit cleaning, and select the parameters to be analyzed.

Fill the glass tubes with standards, samples, and quality controls solution. Create the worktable in the software by assigning a position to each glass tube in the auto sampler. Place the calibration range and the samples to be analyzed in the sampler. Match each item (tubes) with the worktable. Add a Drift and a Wash every 10 to 15 analyses. Enter the total number of tubes passed through the sampler counter and ensure that the aspiration and rinse times are each set to 60 seconds. Then press Start to begin the analysis.



Figure 3.8: Continuous flow analyzer (central laboratory SEAAL, Algiers).

3.6.3.5. Nitrate (NO_3^-) analysis with continuous flow

Nitrates are determined with the continuous flow method according to the ISO 13395-1996 standard. After preparing the equipment and the reagents to be used during the manipulation (buffer solution, colored reagent, quality control solution, distilled water, sample and calibration solution), we place our samples to be analyzed in the sampler table.

We start the equipment with passage of the reagents and recording of the data (Date and name of the element to be analyzed). We run the Flow Access software which is in direct contact with the sampler and the interface and finally. We select the element to be analyzed (nitrates as in our case) to allow the execution of the results. For a higher precision a cuvette teste spectrophotometer LCK 339 was used



Figure 3.9: LCK 339 reagent for nitrate analysis.

3.6.4. Analysis of bacteriological parameters

Bacteriological analysis of wastewater is essential. For this reason the efficiency of synthesized ferrate (VI) was evaluated in the range of [0.06-0.14] % (w: v) of ferrate (VI) in a volume of diluted wastewater sample of 100 mL. This analysis is based on the detection and enumeration of bacteria present in very low concentrations in wastewater samples by membrane filtration method, for intestinal Enterococci the analysis is carried out according to the standard NA ISO 7899-2 NA 766:2010, while the analysis of Escherichia coli follows the standard ISO 9308-1:2014.

These bacteria are specific to culture media in which they grow at a suitable incubation temperature for a favorable period. The presence of bacteria is revealed by colony types, which are characteristic of each group of bacteria.

3.6.4.1. Analysis method

The filtration unit consists of a cylindrical funnel that receives the sample to be analyzed, a filter holder on which the membrane is placed, a receiving flask that collects the filtrate, and a pump that creates a vacuum. Figure 3.9 shows the membrane filtration system.



Figure 3.10: bacterial filtration system (microbiology laboratory, SEAAL).

The system must be placed near a Bunsen burner to create a sterile work area (within a radius of approximately 20 cm) and to be able to sterilize the equipment with the flame. Flame sterilize the filter holders and cylindrical funnels. Once the filter holders and funnels have cooled, place the filter membranes sterily using sterilized forceps and place the funnels on the holders without damaging the membranes.

Remove the membranes using sterilized forceps; place them on the chosen media without creating bubbles and without turning them over. Incubate at the appropriate temperatures; this manipulation should be quick to avoid any kind of contamination. For another use, flame the funnel and support assembly: it is ready to be used again.

After incubation, the Petri dishes are removed from the incubation oven for characteristic colony counts.

3.6.4.2. Searching and counting intestinal enterococci bacteria

The enumeration of enterococci is based on filtering the sample to be analyzed through a sterilized membrane with a porosity of $0.45\ \mu\text{m}$. The filter is placed on a Slanetz selective medium, and then incubated at 36°C for 44 hours ± 4 hours. After incubation, the enterococci (if present) produce red or brown colonies. In this case, a confirmation test may be necessary by transferring the filter thus deposited in the first medium to the Petri dish containing BEA agar. Incubation is carried out again at 44°C for 20 minutes, the Petri dishes are removed after incubation, and the black colonies are counted.

3.6.4.3. Searching and counting Escherichia coli (E.coli) and coliforms bacteria

The E. coli bacteria were counted by membrane filtration using a sterilized filter membrane with a porosity of 0.45 μm . The retained bacteria were deposited on CCA culture medium and then incubated at $36^{\circ}\text{C} \pm 2^{\circ}\text{C}$. After 24 hours, their characteristic blue to purple color counts the E.coli colonies.

The pink to purple coloration generally recognizes coliforms. To confirm that colonies with this color are indeed coliforms, an oxidase test is performed. To do this, 2 to 3 drops of distilled water are placed on an oxidase disc using a sterilized Pasteur pipette, and then a colony is placed on it using another Pasteur pipette. If a dark purple, coloration appears following the reaction, the test is considered positive, indicating that the strain is not a coliform. In the absence of this coloration, the colony is confirmed as a coliforms.

CHAPTER 4

RESULTS AND DISCUSSIONS

4.1. CHITOSAN EXTRACTION

The chemical extraction of Chitosan was carried out in 3 main stages; demineralization, and deproteinization to obtain Chitin and finally deacetylation to obtain Chitosan then the membrane was prepared (figure 4.1).



Figure 4.1: From red shrimp shells to chitosan membrane.

4.2. CHITOSAN CHARACTERIZATION

4.2.1. Solubility, ash and moisture content Chitosan is insoluble in water

Concentrated or diluted alkaline solvents, and in many organic solvents, which is explained by the high molecular weight of each polymer chain. On the other hand, it dissolves in most aqueous acid solutions, including lactic, citric, acetic, and formic acids. Because of the protonation of its amine functions, acetic acid is the best solvent. The literature highlights several parameters that influence chitosan's solubility, most notably the temperature, ionic strength, pH solution, and degree of polymer deacetylation [72]. To ensure the extraction was successful, the chitosan powder was characterized quantitatively and qualitatively to define its properties.

The extracted chitosan has a low moisture content of 0.05% w/w due to its rigid structure, which provides exceptional stability and a long shelf life. Allowing it to be stored at room temperature for an extended period [91]; the same result was found by Heras et al. [66]. Alishahi et al, (2011) reported that chitosan must have less than 10% moisture content. Approximately, 0.2% of ash content was obtained due to seasonal changes [92, 93].

Table 4.1: Physico-Chemical properties of extracted chitosan.

Properties	Values
Moisture content	0.05%
Ash content	0.2%
Acid solubility	Soluble
Alkaline solubility	Insoluble
Neutral solubility	Insoluble

4.2.2. Fourier-transform infrared spectroscopy FTIR

The overlapping O-H, N-H, and C-H stretching modes explain the vast absorption band between 3500 and 2800 cm^{-1} seen in the infrared spectra of the chitosan membrane presented in Figure 4.1. The bending adsorption band at 1573 cm^{-1} corresponds to N=H in amide II. In amide I, the carbonyl group (C=O) stretching vibration displays an absorption band at 1640 cm^{-1} , a characteristic chitosan peak. The absorption peak at 1334 cm^{-1} corresponds to the stretching of C-N in amide III. The anti-symmetric stretching of the C—O—C bridge appears at 1153 cm^{-1} , and the peak at 1542 cm^{-1} is ascribed to the ammonium (NH_4^+) that is produced when the amine group is protonated in an acidic environment [66;82;83]. According to the formula (3), a deacetylation degree of a value of 96.85% was found, which indicates the excellent quality and the high solubility of extracted chitosan. Similarly, Kasongo et al. (2020) found a lower DDA value 69.50% [94], while Dhanashree et al. (2018) obtained a 72.51% DDA value in their research [95].

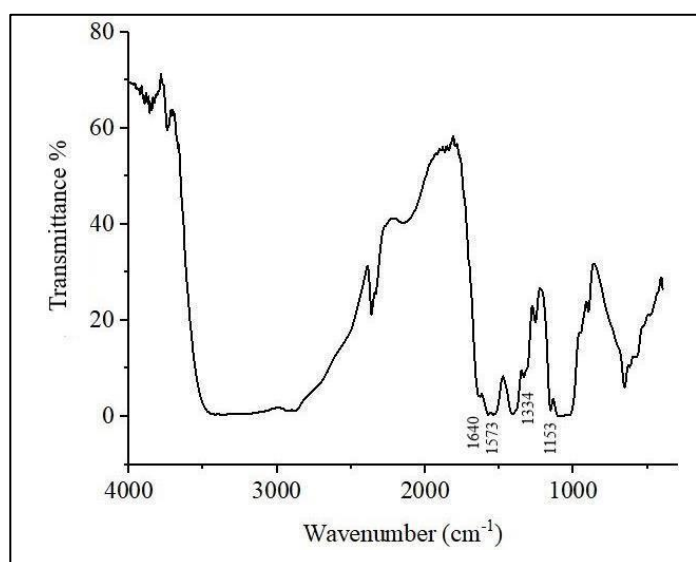


Figure 4.2: FTIR spectra of the extracted chitosan membrane.

4.2.3. Chitosan membrane thickness

An average thickness value of 0.07 ± 0.001 mm for the chitosan membrane was calculated after several measurements at different spots. The exact thickness is set for all trials to ensure a high cation exchange during ferrate production.

4.2.4 Chitosan structure and crystallinity

Figure 4.3 shows the diffractogram of raw chitosan powder and the chitosan membrane. The XRD method was used to examine modifications of the chitosan crystalline structure during membrane production [96]. Figure 4.3 shows characteristic high-intensity diffraction peaks at 10° and 20° for chitosan powder, which correspond to the (0 2 0) and (1 0 0) crystallographic planes [96], respectively, and low-intensity characteristics peaks at 11.5° and 18.5° for the chitosan membrane. These results suggest that during the dissolution of chitosan, the solvent systems fractured the crystal regions in it, and its crystal structure was restored throughout the film-forming process, leading to a loss in crystallinity, which appears in the calculated value of the crystallinity index [86]. Based on the intensity of those peaks, the crystallinity index of chitosan powder and membrane was calculated according to the following formula (4.1) [84]:

$$CrI\% = \frac{(I_{110} - I_{am})}{I_{max}} \times 100 \quad (4.1)$$

While $CrI\%$ is the crystallinity index, I_{110} is the intensity value at 2θ equal to 20° and 18.5° , and I_{am} is the intensity value at 2θ equal to 10° and 11.5° for chitosan powder and membrane, respectively [97]. The obtained values were 58.97% and 18.95%, respectively, typical fingerprints of a semi-crystalline structure for chitosan powder and amorphous for the chitosan membrane.

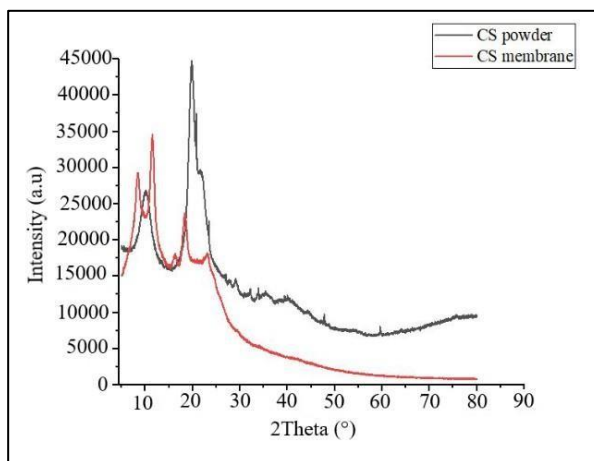


Figure 4.3: XRD spectra of the chitosan powder and membrane.

4.2.5 Thermal analysis of chitosan membrane

4.2.5.1. Thermogravimetric analysis

The TGA thermogram of the chitosan membrane is shown in Figure 4.4. The thermogravimetric method was used to define the thermal resistance of the chitosan membrane, which shows progressive weight loss in three major stages. The first weight loss of 26% was due to water evaporation at 25 °C to 150 °C, while thermal degradation starts at 150 °C to 290 °C with a weight loss of 50%. The second range might be related to carbohydrate molecule decomposition. The undegraded portion of the chitosan membrane, called ash content, was recorded as 27.15% [98,99].

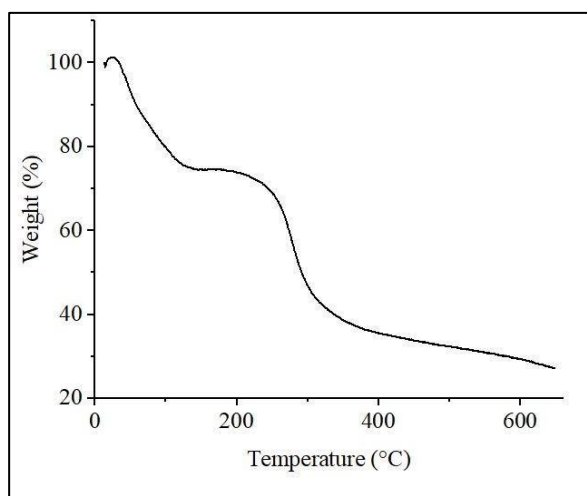


Figure 4.4: Thermogravimetric analysis (TGA) of chitosan membrane.

4.2.5.2. Differential scanning calorimetry (DSC)

Two peaks can be seen in the chitosan film DSC thermograms shown in Figure 4.5. A 51 °C endothermic peak may be related to the combined water loss. An exothermic peak at 290 °C correlates to the biopolymer's degradation [44]. According to the characterization results, the chitosan membrane has suitable properties for ferrate synthesis. Before using the chitosan membrane, it was evaluated in various electrolyte concentrations. The results show that the chitosan membrane is perfectly stable at high alkalinity.

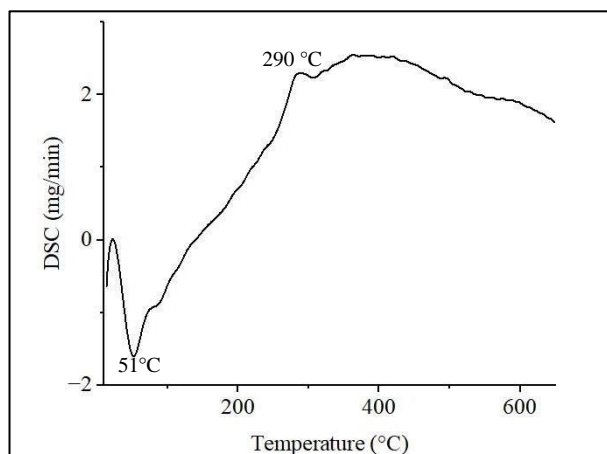


Figure 4.5: Differential scanning calorimetry (DSC) of the chitosan membrane.

4.2.6. Ion exchange capacity

The ion-exchange properties of chitosan mainly stem from its amino groups ($-\text{NH}_2$), which can protonate in acidic environments while producing the membrane to form $-\text{NH}_3^+$ groups. These protonated amino groups are primarily responsible for the ion-exchange capacity, according formula (3.6) the chitosan membrane has an ion exchange capacity of 1.75 meq/g This suggests that the membrane has a high degree of deacetylation, strong hydration capacity, and a large number of exposed amino groups, which all contribute to its high ion-exchange capacity [100]. This makes it potentially beneficial in ferrate production.

4.3 FERRATE (VI) SYNTHESIS

4.3.1. Ferrate (VI) electro-generation with chitosan membrane

4.3.1.1. Electrolyte concentration

The content and concentration of the electrolyte have a significant influence on ferrate (VI) synthesis. Numerous investigations have shown that NaOH is a more effective electrolyte than KOH. NaOH was utilized as an alkaline medium in this investigation [101]. The concentration of an electrolyte is as crucial as its type. As a result, several NaOH concentrations were investigated.

As shown in Figure 4.6, a maximum concentration of 0.08 mol/L of ferrate (VI) along with an optimal current efficiency of 54.92% was obtained in 24 M NaOH media using chitosan membrane.. The high alkalinity of the electrolyte enhances the solubility of lower-valence iron species, which slows down the formation process of the

oxyhydroxide layer that typically covers the anode. Moreover, generated Fe (VI) decomposition decreases with increased alkalinity [26]. The high concentration of NaOH showed an advantageous impact on the stability of ferrate (VI) [101,102].

Additionally, the chitosan membrane exhibits a strong cation exchange mechanism, At the same time, they are not involved in the primary reaction of ferrate synthesis. The OH^- ions that enters the anode chamber replaces the OH^- ions consumed during FeO_4^{2-} generation and contribute to ionic conductivity between the cathode and anode. Furthermore, the chitosan Proton exchange membrane blocks FeO_4^{2-} diffusion to the cathode, which explains ferrate (VI) high yield [23]. When the concentration of sodium hydroxide exceeds the optimal values, the electrolyte solution becomes viscous, resulting in a considerable reduction in solution conductivity. This decrease in conductivity reduces the electron transfer rate at the anode surface, reducing the efficiency of ferrate (VI) formation [103].the difference in optimal concentration of the electrolyte could be explained by the ion exchange capacity of each membrane.

Figure 4.7 also illustrates that the electrolyte concentration and the consumed energy of ferrate electrochemical synthesis have an inverse relationship. A remarkable drop in the consumed energy at the optimal concentration of NaOH, which decrease to value of 18.53 kWh/kg for chitosan which demonstrate that the electrochemical process becomes most efficient at these conditions [32].

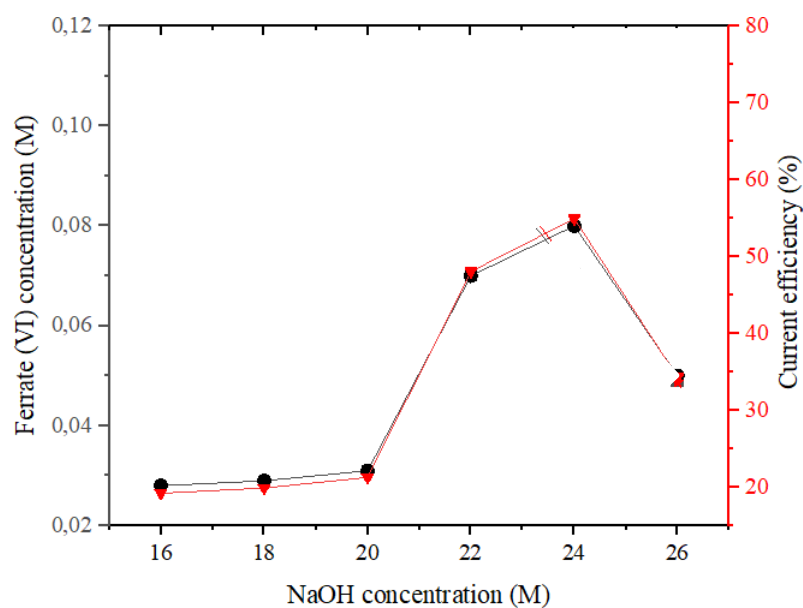


Figure 4.6: Ferrate (VI) concentration and current efficiency in different NaOH concentrations at 60 mA/cm^2 over 1 h of electrolysis at $25 \text{ }^\circ\text{C} \pm 0.5$ synthesized with chitosan (CS) membrane.

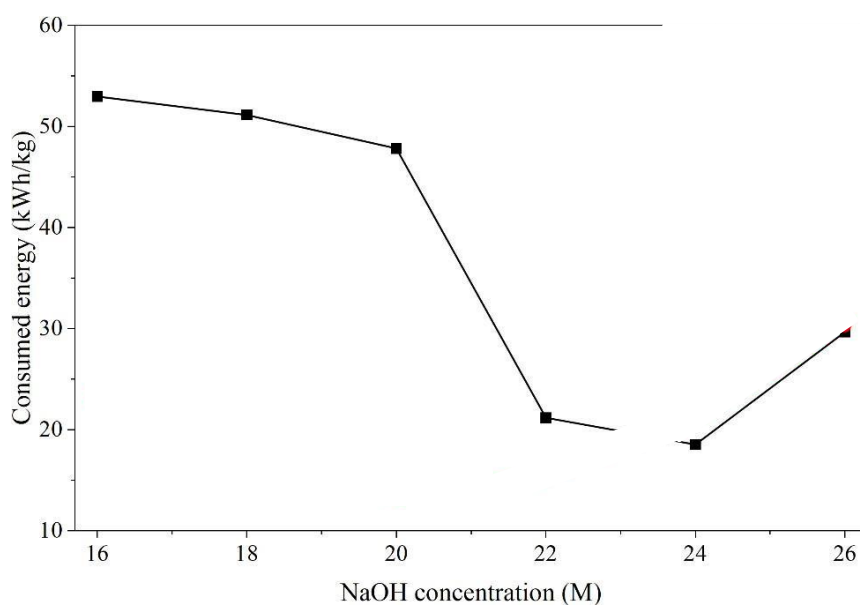


Fig4.7: Evolution of the consumed energy (kWh/kg) in different NaOH concentration for chitosan membranes.

4.3.1.2. Current density effect on ferrate (VI) synthesis

The current density influences the production of ferrate. As shown in Figure 4.8, a maximum concentration of ferrate of 0.031 mol/L and the highest current efficiency of

23.28% were attained at 60 mA/cm² using chitosan membrane. were obtained at the same current density, below this value, the Na₂FeO₄ concentration decreases. Accordingly, ferrate (VI) production is influenced by current density in three different ways. Initially, ferrate (VI) production at the anode surface (−0.96 V vs Ag/AgCl) competes with oxygen evolution. The participation of this parasitic process is enhanced by the higher current density, ultimately lowering the ferrate (VI) yield.

Secondly, the current efficiency was reduced while increasing current density, which provides more electrons at the cathode, accelerating the hydrogen gas generation. Additionally, the increased current density may drive a greater migration of hydroxide ions (OH[−]) through the membranes from the anode compartment toward the cathode where they are consumed during the reduction process;

This reduces the concentration of hydroxide ions at the anode that are necessary to Ferrate formation. With fewer OH[−] ions available at the anode, the ferrate formation reaction becomes less efficient, potentially reducing ferrate (VI) production. Finally, when the current density increases, the cell potential rises, increasing the rate of ohmic heating [26,45,101,104].

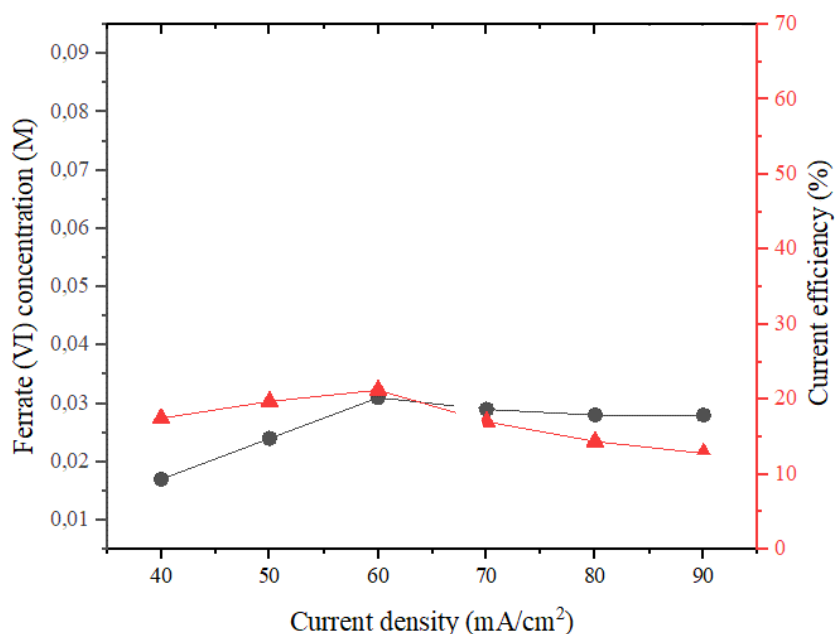


Figure 4.8: Ferrate (VI) concentration and current efficiency as a function of different current density (mA/cm²) in 20 M NaOH over 1h electrolysis at 25 °C ± 0.5, synthesized with chitosan membrane.

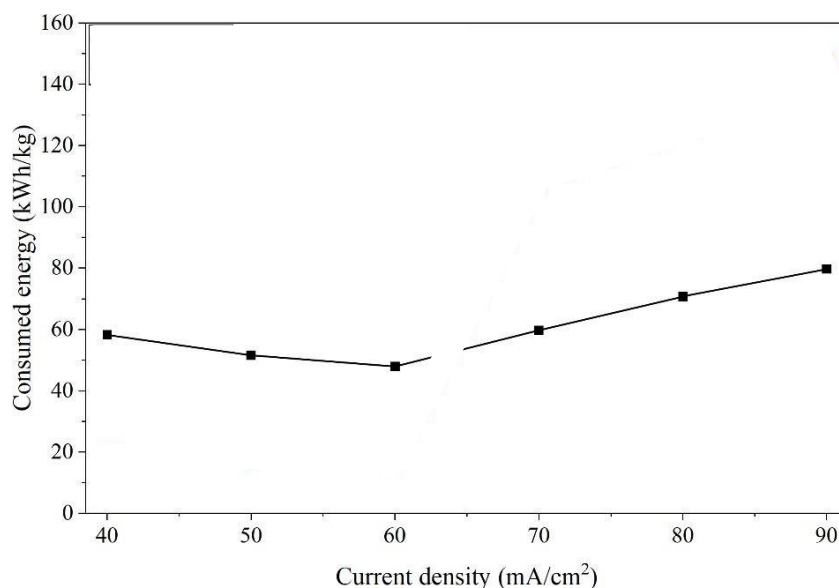


Figure 4.9: Evolution of the consumed energy (kWh/kg) in function of current density for chitosan membranes.

Figure 4.9 shows the evolution of the consumed energy at different current efficiency studied at the optimal value the consumed energy reach its lowest values of 47.95 kWh/kg for chitosan membrane which shows the electrochemical system achieves the optimal balance reaction rate, Faradaic efficiency, and minimal side reactions.

4.3.1.3. Influence of temperature on ferrate (VI) electro generation

Temperature plays a significant role in ferrate (VI) production. As the temperature increases, it reduces the passivation of the anode surface and accelerates the mechanism of iron oxidation into ferrate (VI). This process continues until an optimal temperature of 30 °C is reached. At which the Maximum ferrate (VI) concentration are achieved with a value of 0.115 mol/L the highest current efficiency of 78.95% for chitosan membrane respectively (Figure 4.10); this could be justified by the higher activity of OH^- anions at high temperature, which facilitates the ferrate (VI) formation process [105]. at elevated temperatures, the thermal energy becomes sufficient to overcome the energetic barrier that stabilizes the FeO^{2-} ion, a highly reactive species.

This results in the reduction of ferrate (VI) to the more thermodynamically stable Fe (III) in aqueous solutions. Furthermore, ferrate (VI) is susceptible to hydrolysis, a process facilitated by its interaction with water, leading to the formation of ferric hydroxide ($\text{Fe}(\text{OH})_3$) and the release of oxygen. The rate of hydrolysis increases with temperature, thereby

accelerating the decomposition of ferrate (VI) and causing a decrease in its concentration and current efficiency.

According Figure 4.11 the lowest values of the consumed energy corresponds to the optimal reaction temperature for both membranes with a value of 12.89 kWh/kg for chitosan membrane.

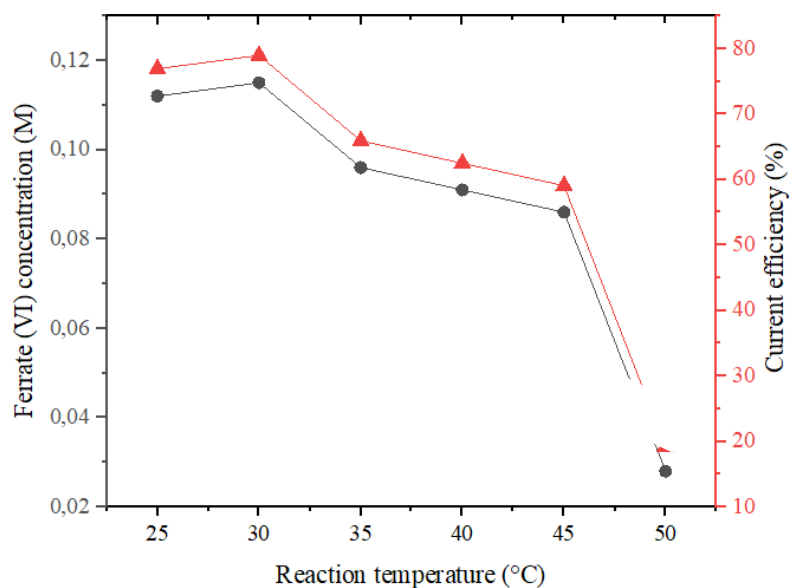


Figure 4.10: Ferrate (VI) concentration and current efficiency at different temperature in 20 M NaOH at 60 mA/cm² for 1h electrolysis synthesized with chitosan (CS) membrane.

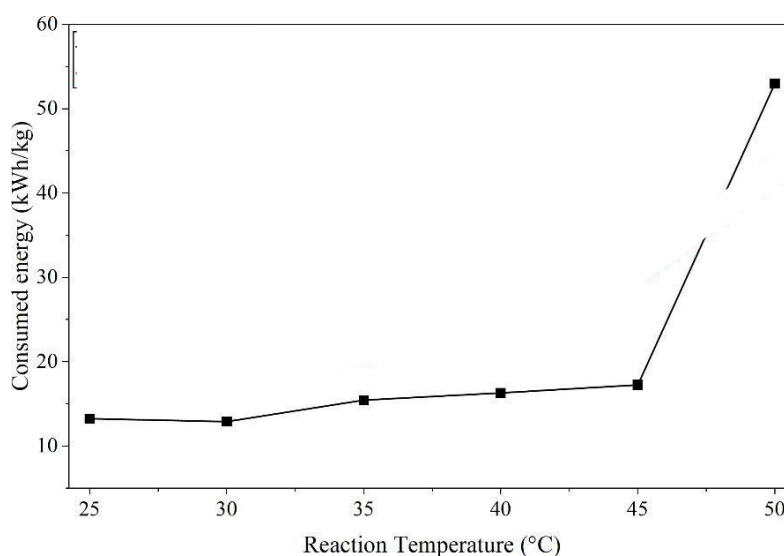


Figure 4.11: Evolution of the consumed energy (kWh/kg) in function of different reaction temperature for chitosan membranes.

4.3.1.4. Effect of the nature of the electrodes on the synthesis of ferrates (VI)

The comparison between the different types of electrodes used is shown in Figure 4.12. The study of the various types of electrodes employed reveals that ordinary steel OS (0.12% C) produces the best results of ferrate concentration of 0.112 mol/L along with a highest current efficiency of 76.89% and the lowest energy consumption of 13.24 kWh/kg (figure 4.13), the presence of carbon positively affects the disintegration of the anode, enhancing ferrate production. In contrast, Ordinary steel OS (0.087%C) results in a significantly lower ferrate (VI) concentration of 0.031 mol/L with the lowest current efficiency of 21.25%; this is explained by the high percentage of iron (99%), which accelerates the passivation of the anode more quickly compared to other materials [106].

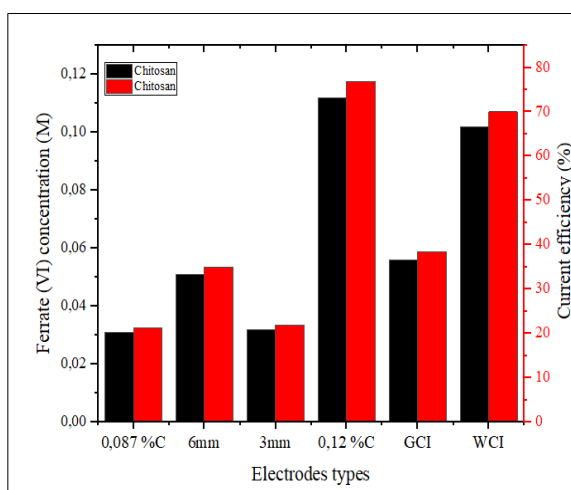


Figure 4.12: Impact of electrode composition on the concentration of generated ferrate (VI), and current efficiency using chitosan membrane.

However, the results acquired using perforated steel OS ($\varnothing=6$ mm and $\varnothing=3$ mm) demonstrate that the synthesis efficiency increases with the diameter of the holes submerged in the anode surface. This phenomenon may be attributed to a potential rise in the active specific surface area.

White cast iron WCI produced an average concentration compared to the other electrodes because it offers iron molecules in an oxidation state lower than Fe^{+6} , promoting ferrate (VI) breakdown. In grey cast iron GCI, carbon occurs in the form of graphite, which accelerates the competition reaction (solvent oxidation to oxygen). Graphite can catalyze the reduction of Fe^{+6} to Fe^{+3} [107]. While other studies suggest that a high carbon content in

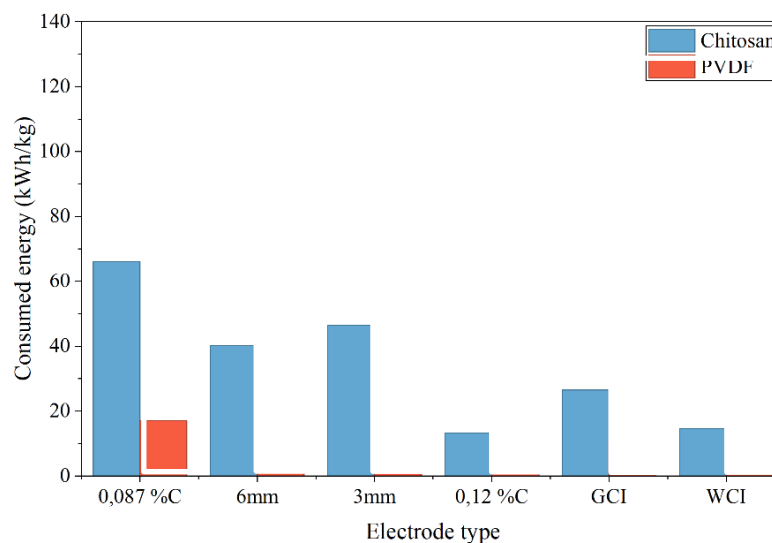


Figure 4.13: Evolution of the consumed energy (kWh/kg) for different electrodes types for chitosan membranes.

4.3.1.5. The impact of electrolysis time on ferrate (VI) production

A high concentration of 0.17 mol/L of Na_2FeO_4 with a maximum current efficiency of 35.34% and a low energy consumption of 30.53 kWh/kg was recorded within 210 min of electrolysis (Figure 4.14 and 4.15). above the optimal duration, ferrate (VI) generation is stopped due to the thickness of the oxide layer, which protects the electrode from dissolution because of the anode passivation. After ferrate (VI) generation is stopped, their concentration decreases due to its decomposition into ferric hydroxyl precipitate, based on the equation (4.1) [108].

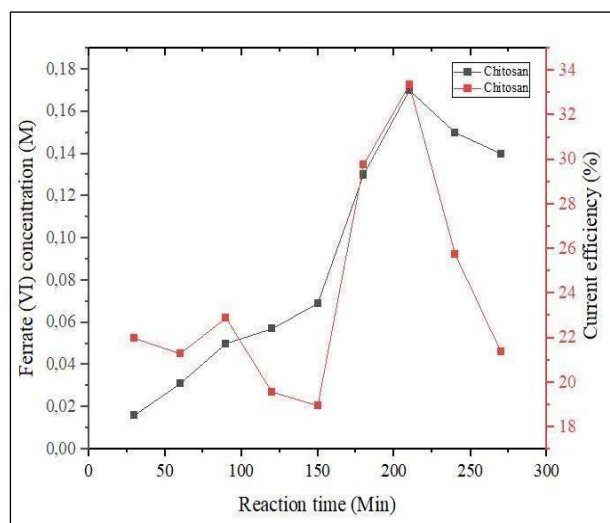
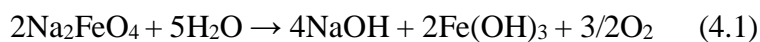


Figure 4.14: Ferrate (VI) concentration and current efficiency by electrolysis duration (min) in 20 M NaOH at 60 mA/cm² in 25 °C ± 0.5 for chitosan membrane.

Previous studies found different ferrate (VI) concentrations; Hernandez et al. obtained a ferrate maximum value of 1.25 mM after 24 h of electrolysis using nafion membrane [24, 44]. Due to the high cation exchange capacity of 1.75 meq/g of chitosan membrane between the cathodic and anodic compartment a notable ferrate (VI) yield of 0.17 mol/L was obtained with a maximum current efficiency of 35.34%, this result highlights the effectiveness of the chitosan membrane in enhancing ferrate (VI) production. In addition, chitosan membranes are more hydrophilic than nafion, which enhances their water retention capacity that facilitates hydroxide ions transport; furthermore, the ability to swell in alkaline conditions improves the effective ionic conductivity that prevents self-decomposition of ferrate (VI) at the anode. Moreover, the chitosan membrane maintains the anode chamber electrolyte in a strongly alkaline state during the electrolysis time to obtain a high yield of generated ferrate (VI) [23]. According to Zhong et al., the chitosan membrane is more effective in ferrate (VI) synthesis. The electro-synthesizing of the ferrate (VI) system has a lower cost than that of the nafion membrane [23].

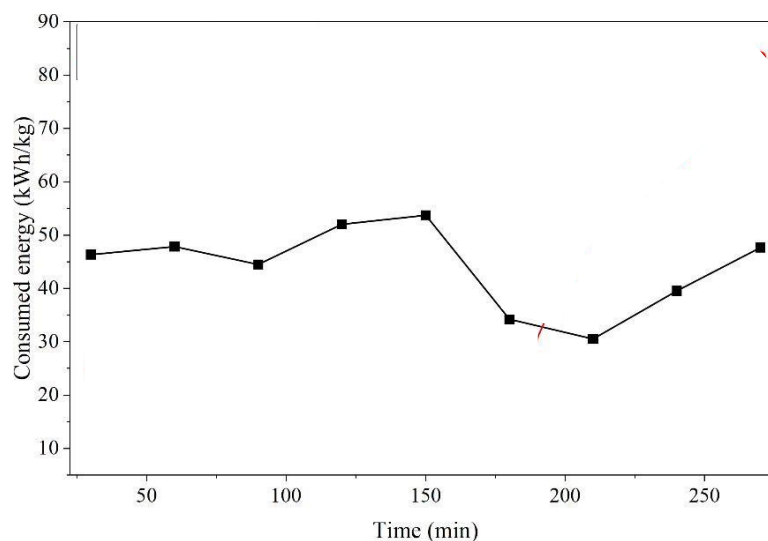


Figure 4.15: Evolution of the consumed energy (kWh/kg) at different electrolysis times for chitosan membranes.

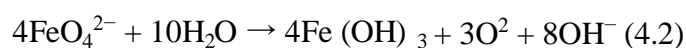
To evaluate the effectiveness of the chitosan membrane in ferrate (VI) synthesis in comparison to the nafion membrane, a comparative study was conducted. The experiment involved the use of a nafion NR-117 membrane with an ion exchange capacity of 0.9 meq/g and a chitosan membrane with an ion exchange capacity of 1.75 meq/g. Both membranes were evaluated under optimized experimental conditions, including a 24 M NaOH electrolyte, a current density of 60 mA/cm², and a temperature of 30 °C, an iron electrode containing 0.12% carbon, and an electrolysis duration of 210 minutes. Using a double-compartment electrochemical cell. The results indicated that the nafion membrane yielded a ferrate (VI) concentration of 0.02 mol/L whereas the chitosan membrane achieved a significantly higher concentration of 0.19 mol/L. These findings highlight the superior performance of the chitosan membrane in ferrate (VI) synthesis under the same identical experimental conditions, this due to the difference in the ion exchange capacity of the two membranes and the structure and hydrophilicity of chitosan membrane which gives it more permeability to hydroxide ions in compare to the perfluoro sulfonic structure of nafion [109].

4.3.2. Dry synthesis of Ferrate (VI)

4.3.2.1. Drying time of iron sulfate heptahydrate ($\text{FeSO}_4 \cdot 7\text{H}_2\text{O}$) and particle diameter (hypochlorite/sulfate)

Dehydration allows the moisture content to be controlled during the synthesis of ferrates and improves the reactivity of ferrous sulfate. It also weakens the particles by reducing their size and increasing their surface area.

Due to its strong oxidizing properties, ferrate (VI) is relatively unstable in the presence of water and decomposes according to the following equation:



Given that the iron sulfates used to prepare the ferrates are seven times hydrated, the presence of this moisture can influence our synthesis. For this reason, we decided to dry this reagent at a temperature of 90°C . The reactions are carried out under the following operating conditions: K/Fe ratio equal to 1, $m(\text{Ca}(\text{ClO})_2) = 1.55\text{g}$, $R(\text{K/Fe}) = 1$, $R_t = 30\text{ min}$, different drying times (0-25 min) and different particle diameters. The results obtained are presented in the figure 4.16.

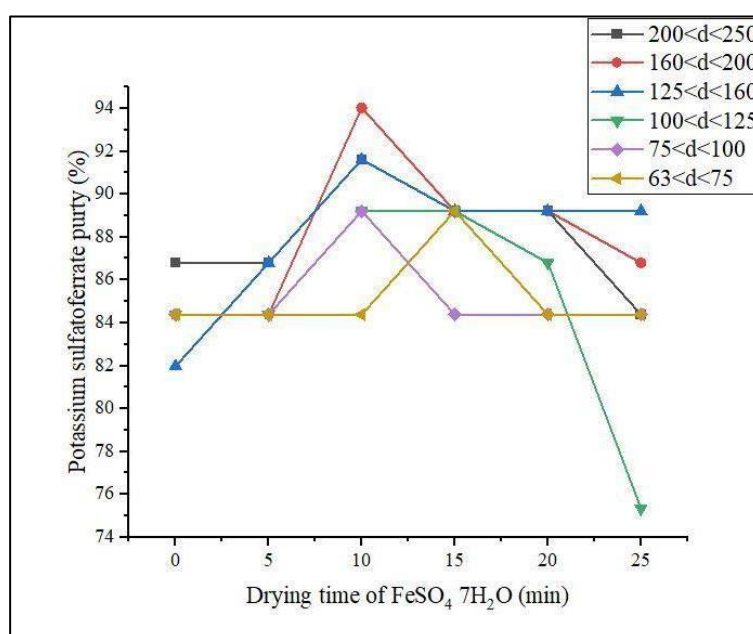


Figure 4.16: Variation of ferrate purity (VI) (%) as a function of drying time for iron sulfate heptahydrate and particle diameter of iron sulfate heptahydrate/calcium hypochlorite.

Analysis of Figure 4.16 indicates that the optimal purity of the synthesized ferrate (VI) reaches a maximum value of 94% after a 10 minute drying period of iron heptahydrate. Beyond this duration, the purity decreases, likely due to excessive water removal, which is essential for the reaction to proceed effectively. The same figure also shows that the optimal particle size of iron (II) sulfate heptahydrate and calcium hypochlorite for improved powder/pellet diffusion and thus higher ferrate concentration falls within the range of $160 < d < 200 \mu\text{m}$ [33].

4.3.2.2. Drying temperature of iron sulfate heptahydrate

Examination of the data presented in Figure 4.17 clearly indicates that the highest ferrate(VI) purity, reaching 94 %, is achieved when iron(II) sulfate heptahydrate is subjected to drying at 90 °C. This observation suggests that at this temperature, the majority of coordinated and crystallization water molecules associated with the heptahydrate structure are effectively removed. The elimination of these water molecules likely facilitates structural changes in the precursor that enhance its reactivity during the subsequent oxidation process. Therefore, 90 °C appears to be the optimal thermal condition for partial dehydration, ensuring sufficient removal of water without compromising the integrity of the iron (II) sulfate necessary for efficient ferrate (VI) synthesis [33].

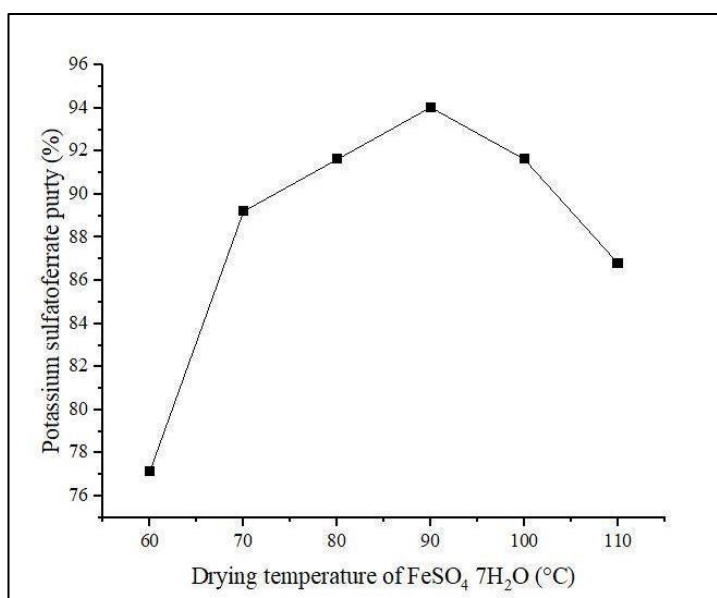


Figure 4.17: Variation of ferrate (VI) purity (%) as a function of drying temperature of iron sulfate heptahydrate.

4.3.2.3. Effect of reaction time (rt) on ferrate synthesis

Reaction time is an important factor in the synthesis of ferrates, the disappearance of the white color of the KOH pellets can be followed over time. The reactions are carried out under the following operating conditions: $T_d=90\text{ }^{\circ}\text{C}$, $160<d<200\text{ }\mu\text{m}$, K/Fe ratio equal to 1, $m(\text{Ca}(\text{ClO})_2)=1.55\text{ g}$, $t_r=30\text{--}120\text{ min}$. The results found are illustrated in Figure 4.18.

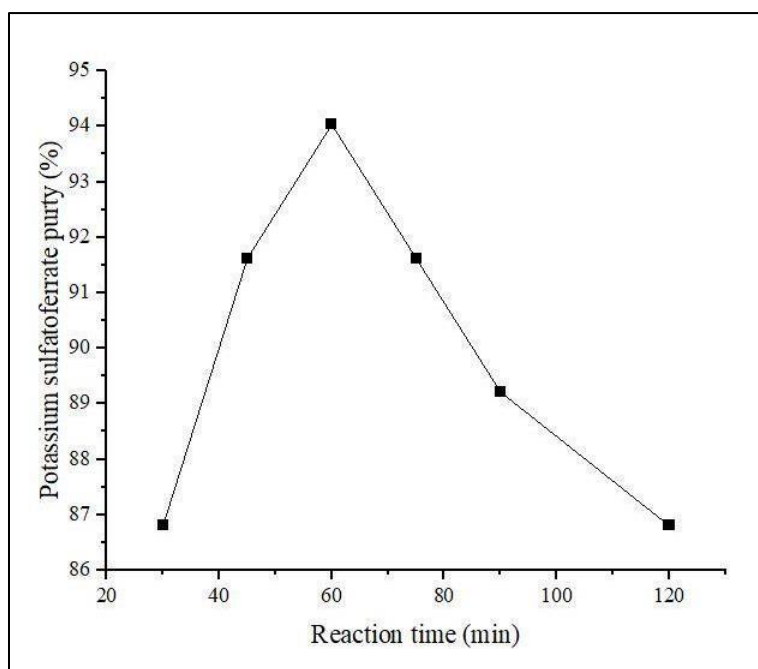


Figure 4.18: Variation of ferrate (VI) purity (%) as a function of reaction time (min).

Figure 4.18 suggests the increase in ferrate concentration obtained as a function of reaction time until reaching a maximum value at 60 min. The maximum ferrate purity read is 94%. After 60 minutes, the purity gradually decreases. This drop can be explained by the formation of secondary by-products by reduction or decomposition over long periods.

4.3.2.4. Effect of reaction temperature (Tr) on ferrate synthesis

Temperature is a key parameter in a chemical process, therefore it must be studied. The reactions occur under the following operational conditions: $T_s = 90^{\circ}\text{C}$, $160<d<200\text{ }\mu\text{m}$, $m(\text{FeSO}_4, 7\text{H}_2\text{O}) = 3\text{ g}$, $m(\text{KOH}) = 3\text{ g}$, $m(\text{Ca}(\text{ClO})_2) = 1.55\text{ g}$, $t_r = 60\text{ min}$.

From Figure 4.19, it can be deduced that the optimal synthesis temperature is 30°C , with a purity of the order of 98%. This temperature seems ideal to promote the oxidation of iron (II) and the formation of ferrate (VI), without initiating thermal decomposition or secondary reactions. Beyond 30°C , the purity drops rapidly, which can be explained by the

thermal decomposition of ferrate (VI), which is unstable at high temperature and the decrease in the selectivity of the reaction with increasing temperature [110].

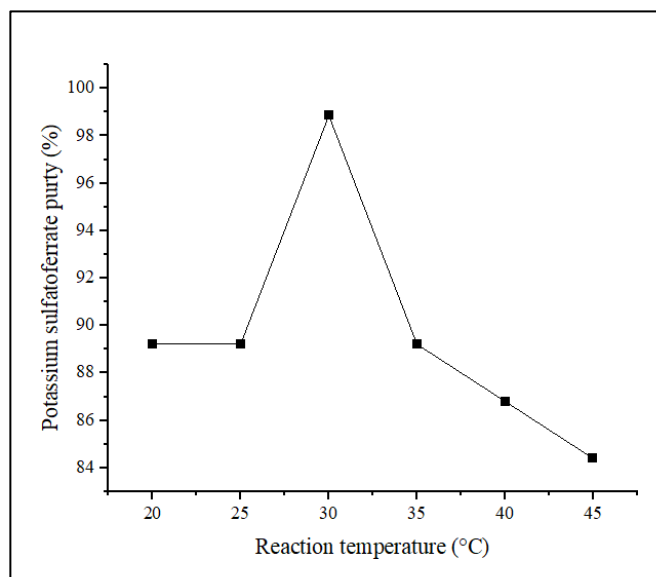


Figure 4.19: Variation of ferrate (VI) purity (%) as a function of reaction temperature (C°).

4.3.2.5. Ferrate (VI) drying time

The reactions are carried out under the following operating conditions: $T_s=90\text{ }^{\circ}\text{C}$, $160 < d < 200\text{ }\mu\text{m}$, $m(\text{FeSO}_4, 7\text{H}_2\text{O}) = 3\text{g}$, $m(\text{KOH}) = 3\text{g}$, $m(\text{Ca}(\text{ClO})_2) = 1.55\text{g}$, $t_r = 60\text{ min}$, $T_r = 30\text{ }^{\circ}\text{C}$.

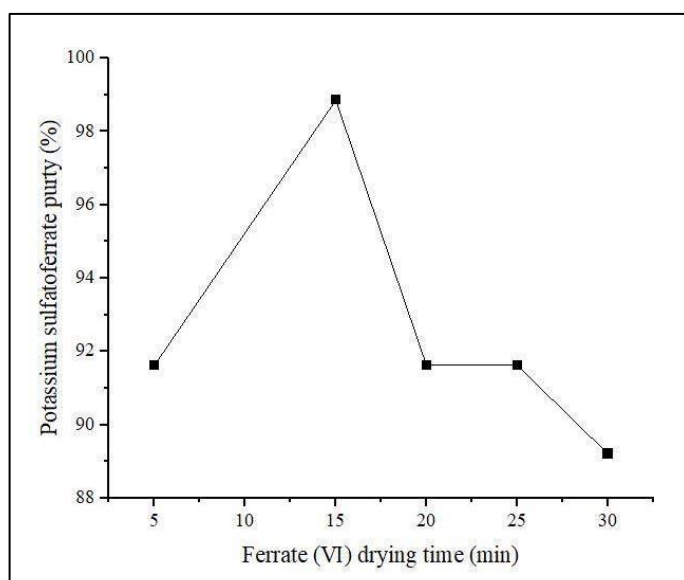


Figure 4.20: Variation of ferrate (VI) purity (%) as a function of Fe (VI) drying time (min).

The results presented in Figure 4.20 clearly indicate that a drying time of 15 minutes is sufficient to achieve a maximum ferrate (VI) purity of 98.85%. Beyond this duration, the purity decreases, likely due to the thermal decomposition of ferrate compounds caused by extended exposure to drying conditions.

4.3.2.6. Ferrate (VI) drying temperature

The figure 4.21 illustrates the synthesized ferrate by dry method after drying, through the obtained color the presence of the ferrate molecule can be preliminary identified.



Figure 4.21: Potassium sulfate ferrate (VI) after drying

Figure 4.22 shows that a high purity of ferrate (VI) of the order of 98 % can be achieved at a temperature of 100°C, which allows efficient evaporation without degradation of the compound. However, at very high temperatures above 100°C, the thermal degradation of ferrate becomes significant, which leads to a drop in purity.

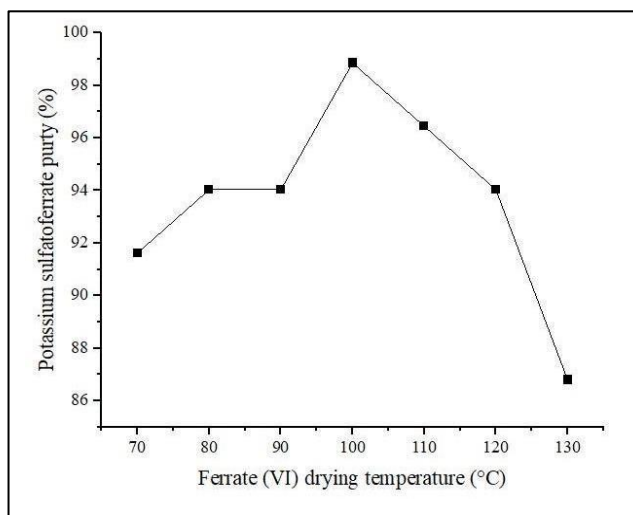


Figure 4.22: Variation of ferrate (VI) purity (%) as a function of Fe (VI) drying temperature.

4.3.2.7. Number of washes of ferrate (VI)

Figure 4.23 shows an optimal wash number of 3 with a purity of 94% which means that methanol effectively removes soluble impurities so the product becomes purer beyond 3 washes the purity decreases which can be explained by the slight solubility of ferrate in methanol (polar solvent).

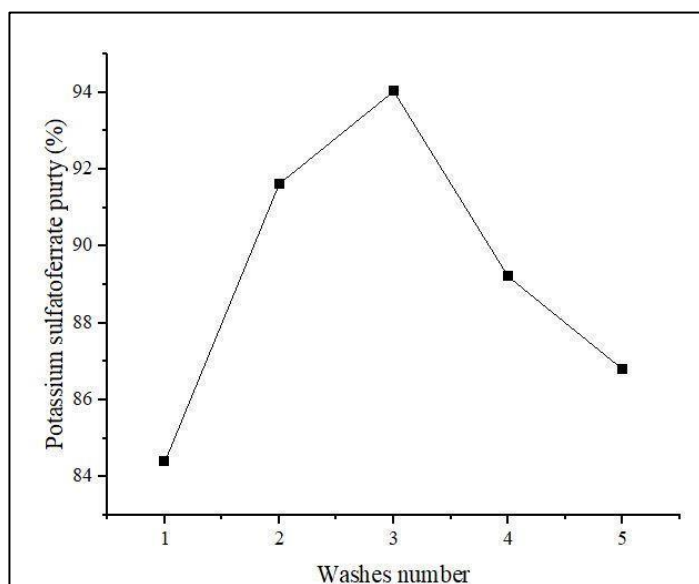


Figure 4.23: Variation of ferrate (VI) purity (%) as a function of Fe (VI) number of washes.

4.4. FERRATE (VI) CHARACTERIZATION

4.4.1. Characterization of potassium sulfate-ferrate (VI) (dry method)

4.4.1.1. UV-Visible spectroscopy

Figure 4.24 shows the final product of potassium sulfate ferrate (VI) ready to be characterized.



Figure 4.24: Potassium sulfate ferrate (VI) for characterization.

Due to their violet color, ferrates can be detected in the visible (near infrared) range between 500 and 800nm. The maximum absorption band of our product is 506.9 nm according figure 4.25, which is located in the characteristic interval of tetrahedral ferrate (VI), FeO_4^{2-} [500 -510 nm] [87].

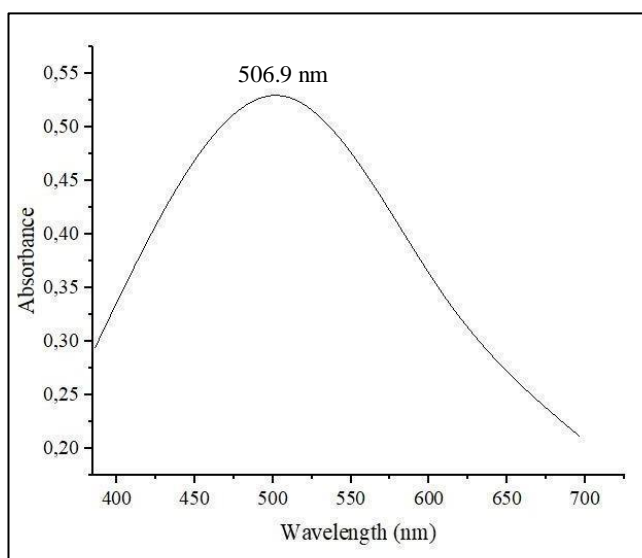


Figure 4.25: UV-Visible spectrum of synthesized potassium sulfate-ferrate (VI)

4.4.1.2. Fourier-transform infrared spectroscopy FTIR

The appearance of an infrared spectrum is related to the symmetry of the molecule or group studied. The spectrum analysis obtained (Figure 4.26) shows the appearance of an absorption band of 815.83 cm^{-1} corresponding to vibration frequencies of four equivalent symmetrical Fe-O bonds, the absorption band at 3419.56 cm^{-1} is attributed to the elongation in water. The bands 1109 cm^{-1} and 619.11 cm^{-1} are characteristic of the SO_4^{2-} group, while those at 993.27 cm^{-1} can be attributed to an intermediate compound between the K_2SO_4 and K_2FeO_4 forms [88].

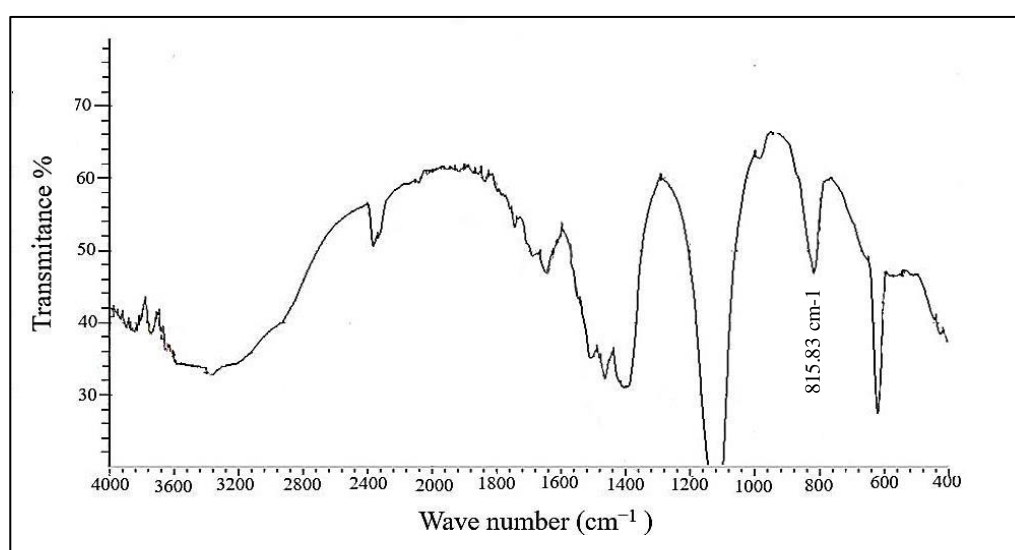


Figure 4.26: IR spectrum of potassium sulfate ferrate (VI) obtained.

4.4.1.3. X ray diffraction XRD

The DRX diffractogram of synthesized ferrate is shown in Figure 4.27. The XRD spectra reveals a Sharp characteristic peak of crystalline K_2FeSO_4 at 2θ value of 28° . It can be seen that the high purity ferrate sample shows sharper peaks in the DRX spectra. Several other characteristic diffraction peaks also appear at 2θ values of 30° , 33° , 40° that could be attributed to compounds of the K_2FeO_4 type, or secondary iron oxides (Fe_2O_3 , Fe_3O_4). The DRX results also indicate that the prepared ferrate sample has a tetrahedral geometric structure [88].

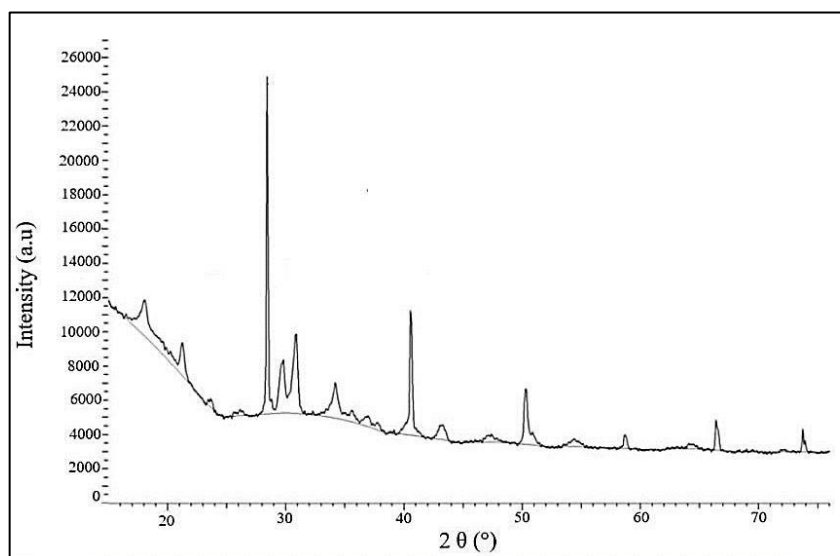


Figure 4.27: DRX spectrum of potassium sulfate ferrates (VI).

4.4.2. Characterization of sodium ferrate (VI) (electrochemical method)

The figure 4.28 shows sodium ferrate (VI) powder obtained from the electrochemical synthesis the high concentration of ferrate (VI) gives it the dark purple coloration.



Figure 4.28: Sodium ferrate (VI) powder synthesized with electrochemical method.

4.4.2.1. UV-Visible

As mentioned in Figure 4.29, the UV-VIS spectra of synthesized ferrate (VI). The most excellent absorption wavelength was 504.5 nm, within the range of ferrates typical wavelengths of 500 –510 nm. Other studies revealed similar results [111,112].

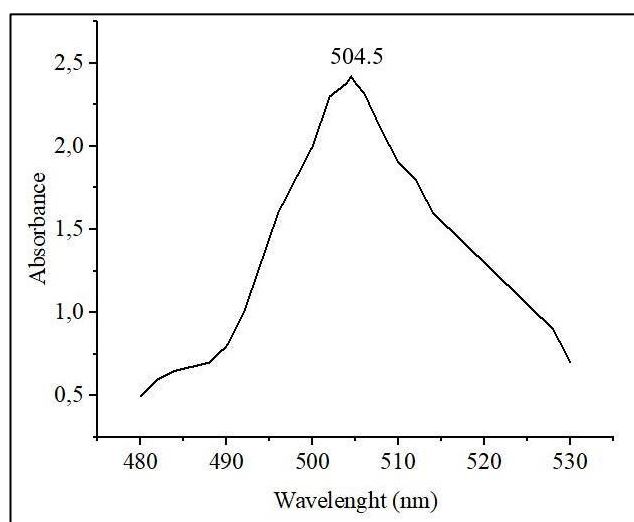


Figure 4.29: The UV–visible spectrum of the synthesized ferrate (VI).

4.4.2.2. Fourier-transform infrared spectroscopy FTIR

Figure 4.30 displays the IR spectra of sodium ferrate (VI), indicating the characteristic absorption peak of the elongation frequencies of four identical, symmetric Fe-O bonds in Ferrate obtained at 865.98 cm^{-1} [111,113]. According to the literature, there is a slight variation in the chemical positions of functional groups of the synthesized ferrate in this work, which generation parameters and crystallization could cause. The peaks identified in the range $1850 - 1050\text{ cm}^{-1}$ should be attributed to the distinctive peaks of the C-O bond stretching vibration, which might be caused by atmospheric carbon dioxide [104]. The $3600\text{-}2500\text{ cm}^{-1}$ peaks are related to the water H-O bond [114]. Furthermore, the visibility and the sharpness of peaks also confirmed the high purity of the product.

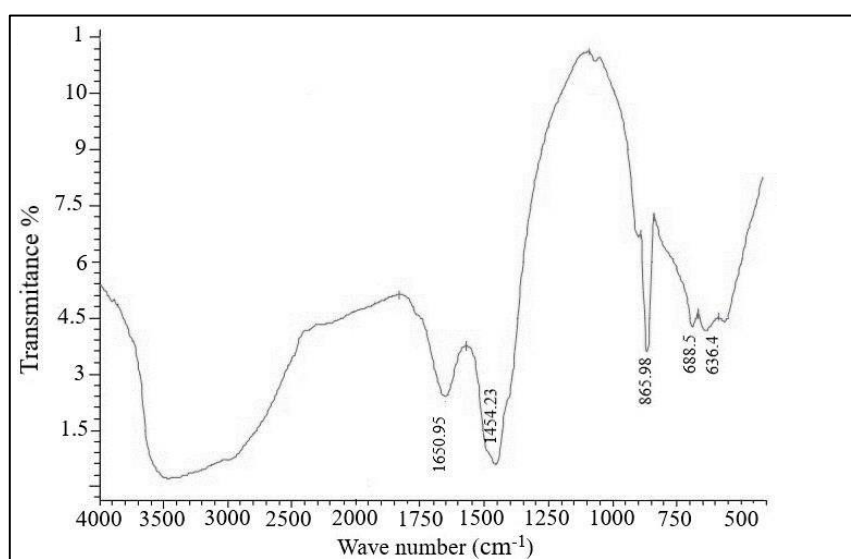


Figure 4.30: FTIR spectra of synthesized sodium ferrate powder in transmittance mode.

4.4.2.3. X ray diffraction XRD

Figure 4.31 shows Sharp characteristic peaks of crystalline Na_2FeO_4 at 2θ value of 30° . Several other characteristic diffraction peaks also appear at 2θ values of 27.5° , 33° , and 45° . Fig.3.11 shows a substantial similarity to the results reported by Xu et al. (2007) confirming that the generated ferrate (VI) is sodium ferrate with orthorhombic crystal structure [88, 111, 113, 114].

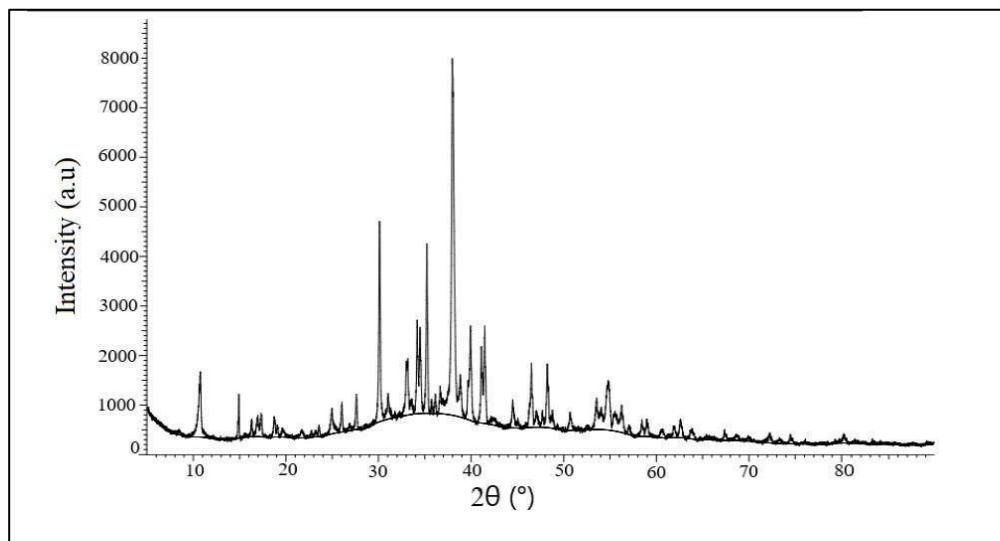
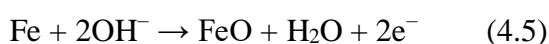
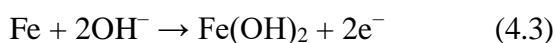


Figure 4.31: XRD patterns of synthesized sodium ferrate powder.

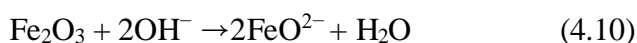
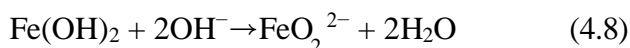
4.4.2.4. Cyclic voltammetry CV

The chemical activity on the anode surface was tracked through the CV curve with previously determined optimal ferrate (VI) synthesis conditions. Figure 4.32 shows four anodic peaks, A1 A2, A3 A4 located at -1.18 V, -0.96 V, -0.78 V, and -0.67 V respectively corresponded to the following oxidation reactions of the ferrate generation mechanism: A1 ($\text{Fe}^0 \rightarrow \text{Fe}^{2+}$) corresponds to the active iron dissolution to Fe^{2+} according to equation (10) Oxidation reactions, Equations (4.3, 4.5), may occur at the same time [45,103]

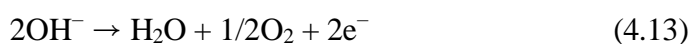
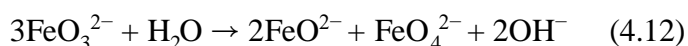
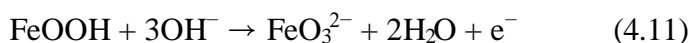


The peak A2 corresponds to a continuous oxidation of $\text{Fe}(\text{OH})_2$ to Fe_3O_4 , according to Equation (4.6). Parallel oxidation of Fe_3O_4 is possible, according to equation (4.7), it is

suggested that the interactions of the passive layer with OH^- ions, equations (4.8-4.10), cause the iron surface to degrade, allowing continual dissolution of the anode, which corresponds to the current peak A3.



Following the active dissolution zone, a large passivity plateau emerges. At a potential of -0.67 V (A4), oxygen evolution begins (equation 4.13). At the same time, the oxidation process (equation 4.11) occurs, followed by the disproportionation reaction (equation 4.12). Peak A4, which corresponds to the processes (equation 4.7-4.9), is not usually detected because a broad oxygen evolution overlaps the trans-passive iron dissolution, including ferrate (VI) formation [103].



in the negative potential scan the curve reveals three peaks, C1, C2, C3 and C4 at -0.38 V, -0.95 V, -1.23 V, and -1.3 V respectively associated with ferrate (VI) reduction according to the following mechanism [114]:

C1: is associated with the reduction of Fe(VI) to Fe(III). potentially including the hydrogen evolution reaction (HER):



C2: is associated with the reduction of Fe (III) to Fe_3O_4 .

C3: corresponds to the reduction of Fe_3O_4 back to Fe (II).

C4: the sharp intense peak relate to the Fe (II) to Fe transition (ferric hydroxide Precipitate)

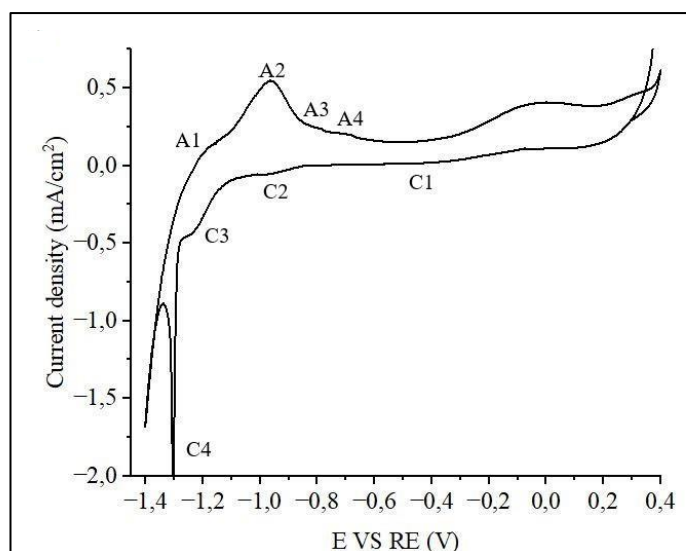


Figure 4.32: Cyclic voltammogram of ordinary steel 0.12%C in optimal conditions of ferrate (VI) synthesis at a scan rate 50 mv/s.

4.4.2.5. Thermogravimetric analysis

Ferrate (VI) in its powder form is stable at room temperature. However, it shows a different thermal behavior upon heating. Figure 4.33 revealed ferrate decomposes under high temperatures, releasing oxygen O_2 . This decomposition proceeds slowly with a total weight loss of 40%. Beginning around 45 °C and ending around 195 °C, two decomposition stages were observed in this range. The first one, from 45 °C to 155 °C, reflects the water evaporation of the sample absorbed [61]. In the second stage, between 155 °C and 195 °C, a decrease in weight of 2.3% was recorded, indicating that O_2 was liberated from the ferrate (VI) molecule [115].

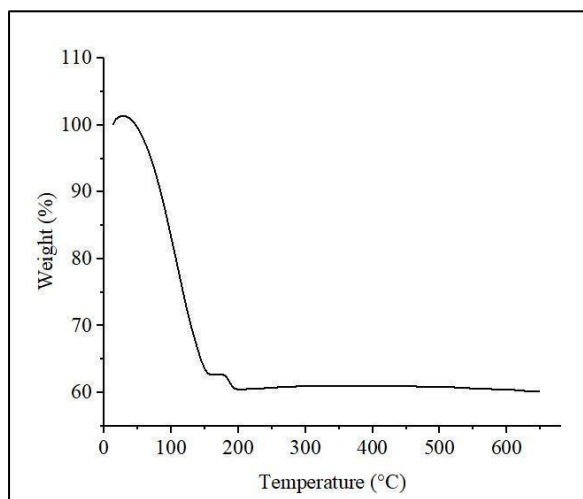


Figure 4.33: TGA spectrum of solid ferrate (VI).

4.4.2.6. Scanning electronic microscopy SEM

Scanning electron microscopy (SEM) was employed to offer more information regarding the ferrate (VI) structure. SEM observations (Figure 4.34) show plump crystals, columnar and have prominent cone spherical shape expanding the surface at the two ends of the crystalline grains [2, 48].

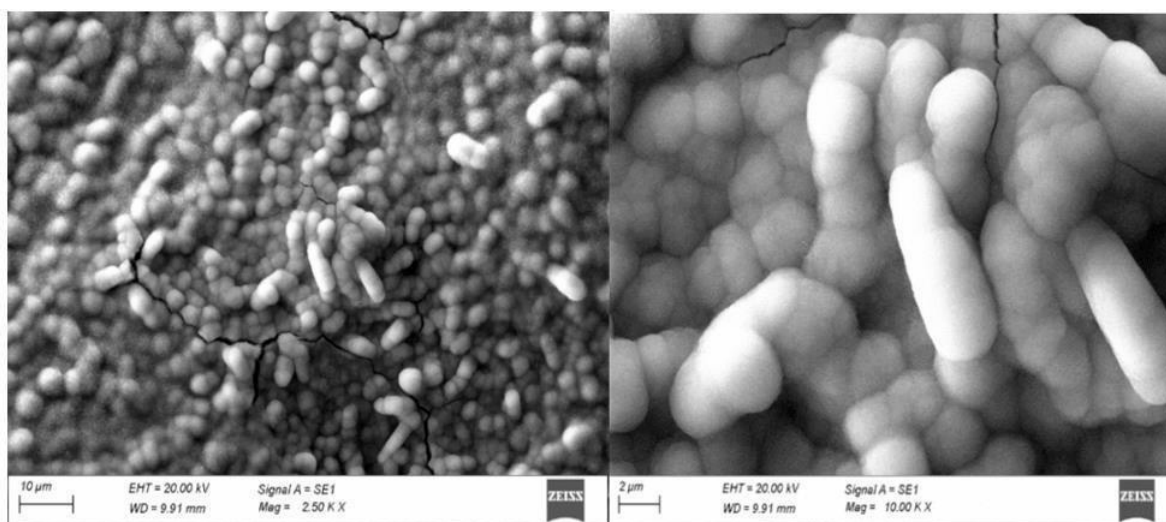


Figure 4.34: SEM photo of ferrate (VI) powder.

4.5. FERRATE (VI) IN WASTEWATER TREATMENT

Figure 4.30 shows the visual aspect of wastewater sample before and after ferrate treatment

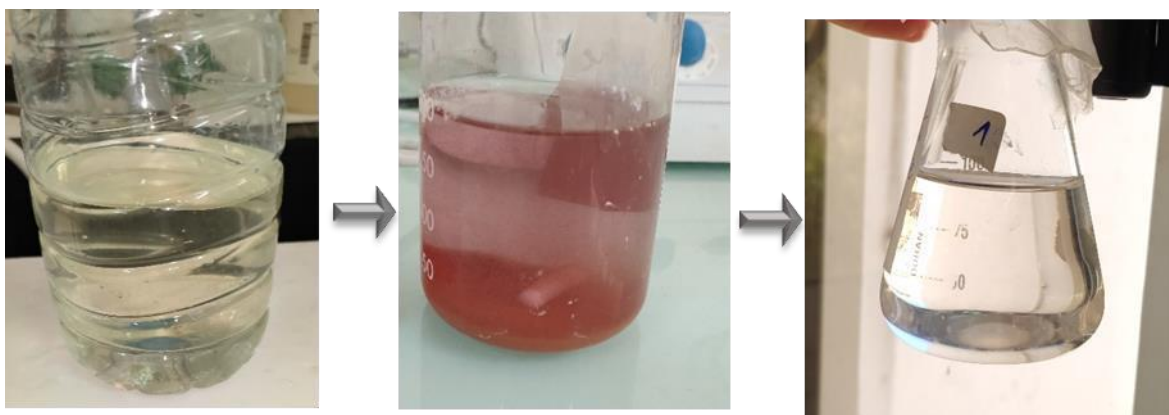


Figure 4.35: Wastewater sample before, during and after ferrate (VI) treatment.

4.5.1. Beni Messous (Algiers) wastewater treatment plant

4.5.1.1. Chemical Oxygen Demand COD

Figure 4.36 shows the variation of COD removal efficiency using ferrate powder obtained from electrochemical and dry synthesis method. For both samples, COD removal increases with ferrate concentration up to 0.10%, with high COD removal peaks of 92.2% and 92.87% for ferrate (VI) synthesized with electrochemical method and dry method respectively due to its high oxidation capacity of organic pollutants and the strong coagulating power of the by-product of ferrate reduction ferric hydroxide.

The efficiency declines beyond this point. The sharp drop in COD removal beyond 0.10% of ferrate (VI) may be due to Ferrate decomposition at higher concentrations, Formation of byproducts or radical scavenging. Overdosing effects leading to reduced oxidation efficiency [31,117].

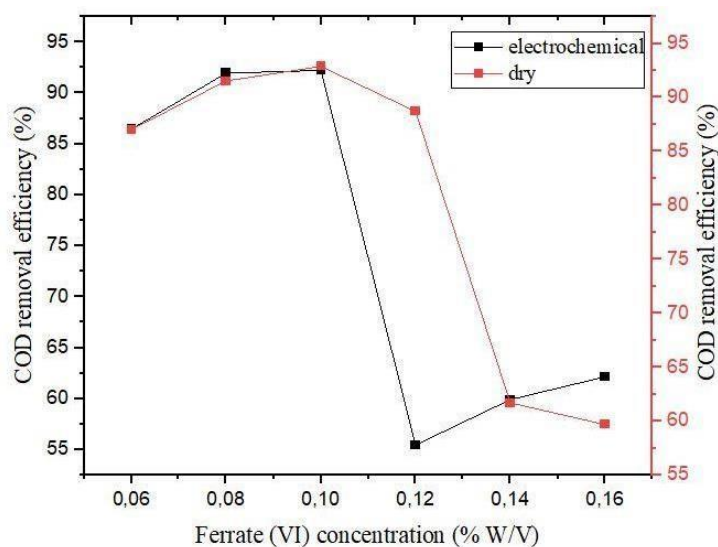


Figure 4.36: COD removal efficiency with both ferrate (VI) synthesized with electrochemical and dry method for Beni Messous WWTP.

4.5.1.2. Biochemical Oxygen Demand in 5 days BOD_5

Figure 4.37 illustrates the variation in BOD_5 removal efficiency using ferrate (VI) powders synthesized via electrochemical and dry methods. For both samples, BOD_5 removal efficiency increases with ferrate concentration, reaching a maximum at 0.10%. At this optimal concentration, peak removal efficiencies of 98.31% and 97.19% were observed for the electrochemically and dry-synthesized ferrate (VI), respectively. This high performance is attributed to the strong oxidative capacity of ferrate (VI) (high redox potential up to +2.2 V) which allows it to efficiently degrade a wide range of organic pollutants, commonly found in wastewater, as well as the effective coagulating-flocculating action of ferric hydroxide produced during the reduction of ferrate [31, 117].

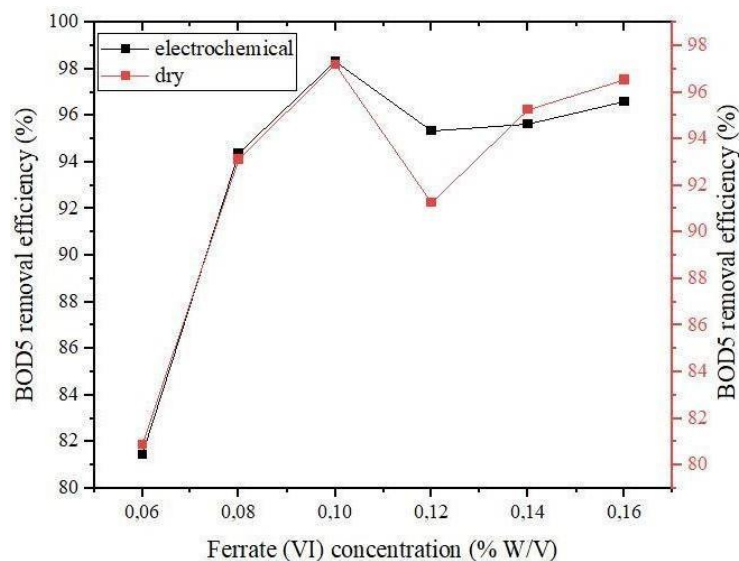


Figure 4.37: BOD₅ removal efficiency with both ferrate (VI) synthesized with electrochemical and dry method for Beni Messous WWTP.

Beyond the 0.10% concentration threshold, a decline in BOD₅ removal efficiency is noted. This reduction may be due to several factors, including the decomposition of ferrate(VI) at higher concentrations, may lead to side reactions that produce unwanted byproducts, neutralize reactive oxidative species, and ultimately reduce the treatment process's effectiveness [116].

4.5.1.3. Nitrite (NO₂⁻) removal by ferrate (VI)

Figure 4.38 shows the influence of ferrate powder obtained from electrochemical and dry synthesis method on Nitrite (NO₂⁻) removal efficiency. The presented data indicate, that nitrite (NO₂⁻) removal increases with ferrate concentration up to 0.12% and 0.08%, with a maximal efficiency of 97.22% and 95% for ferrate (VI) synthesized with electrochemical method and dry method respectively due to the chemical oxidation of nitrite into nitrate, which is more stable [27].

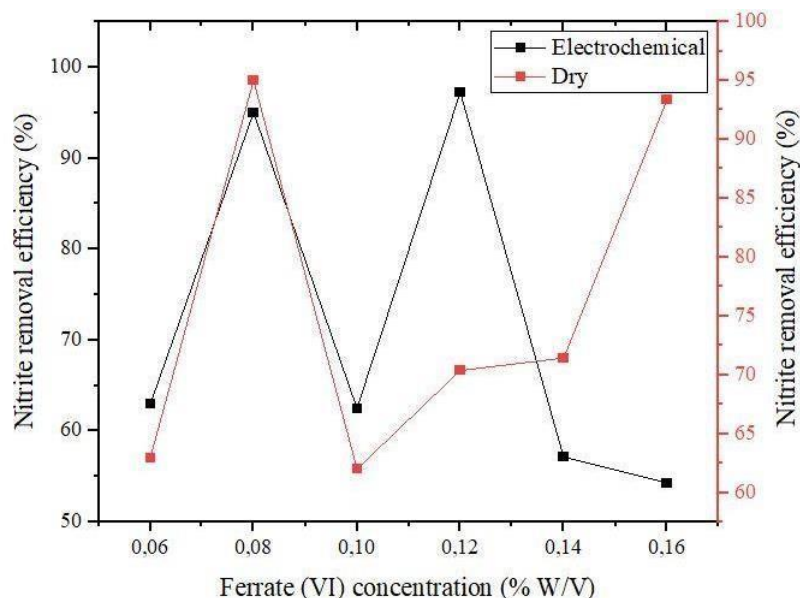


Figure 4.38: Nitrite (NO_2^-) elimination efficiency with both ferrate (VI) synthesized with electrochemical and dry method for Beni Messous WWTP.

4.5.1.4. Nitrate (NO_3^-) removal by ferrate (VI)

Nitrate themselves are difficult to remove directly for their stability. Figure 4.39 shows the variation of nitrate (NO_3^-) removal efficiency using ferrate powder of both electrochemical and dry synthesis method. For both samples, COD removal increases with ferrate concentration up to 0.08%, with high nitrate removal efficiency peaks of 86.34% and 86.15% for ferrate (VI) synthesized with electrochemical method and dry method respectively. These results can be explained by the multifunctionality of ferrate (VI) in wastewater treatment while it is hard to oxidize nitrate, ferrate (VI) eliminates it through adsorption mechanism with its reduced form ferric hydroxides.

The efficiency decrease beyond 0.08% ferrate concentration may be due to the excess Ferrate saturating the adsorption sites and generating unnecessary side reactions thus reducing overall efficiency [25, 45].

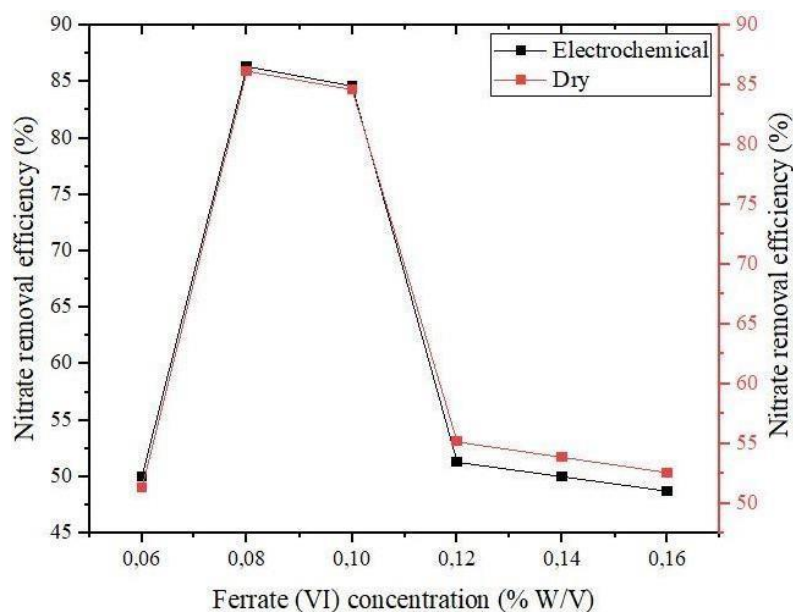


Figure 4.39: Nitrate (NO_3^-) elimination efficiency with both ferrate (VI) synthesized with electrochemical and dry method for Beni Messous WWTP.

4.5.1.5. Ammonium (NH_4^+) elimination by ferrate (VI)

Figure 4.40 shows the variation of ammonium removal efficiency as function of ferrate powder concentration. In the two samples, Ammonium removal increases with ferrate concentration up to 0.08%, with high NH_4^+ removal peaks of 95.8% and 94.5% for ferrate (VI) synthesized with electrochemical method and dry method respectively. Those results could be attributed to the oxidation of NH_4^+ into more oxidized nitrogen species such as nitrate (NO_3^-), nitrite (NO_2^-), The efficiency declines beyond this point.

The decrease in NH_4^+ removal beyond 0.08% of ferrate (VI) may be due to Ferrate decomposition at higher concentrations, Formation of byproducts or radical scavenging. Overdosing effects leading to reduced oxidation efficiency [105].

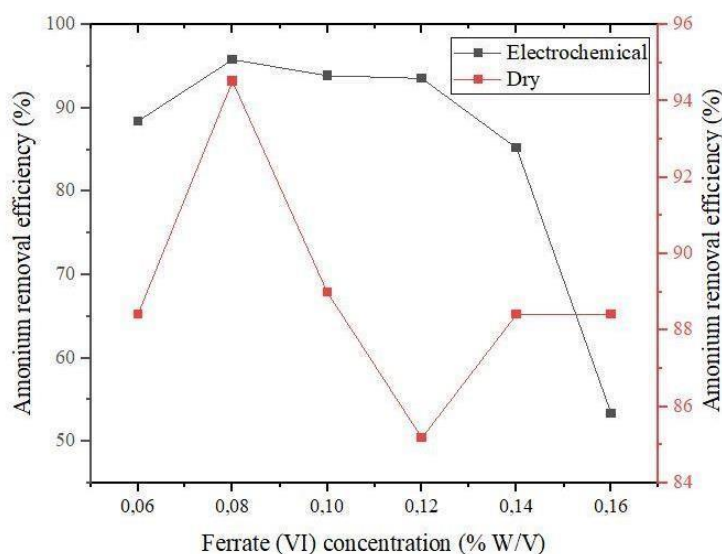


Figure 4.40: Ammonium (NH_4^+) elimination efficiency with both ferrate (VI) synthesized with electrochemical and dry method for Beni Messous (Algiers) WWTP.

4.5.1.6. Analysis of bacteriological parameters

The table below (4.2) shows the efficiency of ferrate synthesized with both methods in the elimination of different type of bacteria in wastewater sample. Several dilution are necessary to make the counting of colonies possible for this reason a 10^{-4} and 10^{-2} dilution was carried out for E. coli with total coliforms samples and intestinal enterococci samples respectively

Table 4.2: Ferrate efficiency in bacteria removal (beni messous WWTP).

Ferrate concentration (%)	E.coli (CFU/100mL)		total coliforms (CFU/100mL)		intestinal enterococci (CFU/100mL)	
Synthesis method	Electro	Dry	Electro	Dry	Electro	Dry
none (witness)	7×10^4	7×10^4	80×10^4	80×10^4	5×10^3	5×10^3
0.06	Abs	1.10^4	Abs	Abs	6×10^2	2×10^2
0.08	Abs	Abs	Abs	Abs	3×10^2	Abs
0.1	2×10^4	Abs	Abs	Abs	3×10^2	Abs
0.12	Abs	Abs	Abs	Abs	Abs	Abs
0.14	1×10^4	Abs	Abs	Abs	Abs	Abs

The obtained results demonstrate the high antimicrobial efficacy of ferrate against various bacterial indicators commonly found in wastewater. Electrochemically synthesized

ferrate begins to inactivate *Escherichia coli* at a concentration of 0.06%, achieving complete elimination at 0.08% and 0.12%. Interestingly, a slight reappearance of *E. coli* colonies at 0.10% and 0.14% may be attributed to measurement variability or possible interference during sampling.

In the case of total coliforms, ferrate exhibited complete removal across all tested concentrations, highlighting its strong bactericidal potential against this group. For intestinal enterococci, which are known to be more resistant to disinfectants, a gradual reduction in viable colonies was observed with increasing ferrate concentration. Total inactivation was achieved at 0.12% in the case of electro-synthesized ferrate, indicating the need for higher doses to overcome their resistance [34, 46].

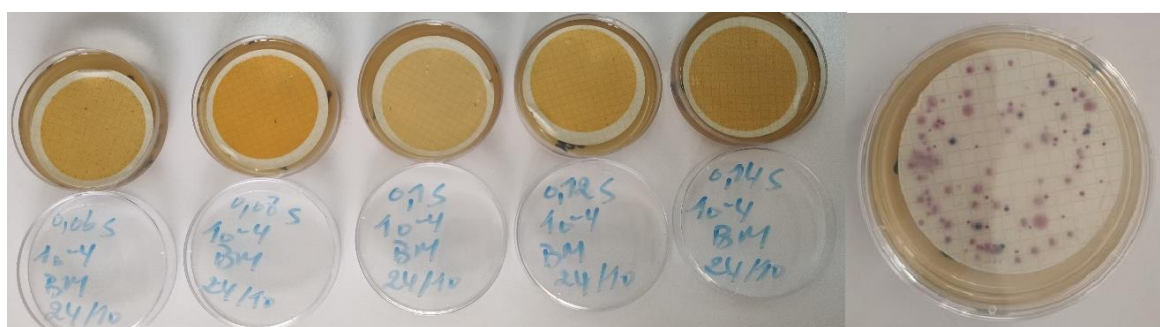


Figure 4.41: Treated samples and witness (case of *E. coli* and coliforms) using ferrate (VI) (Beni Messous WWTP).

On the other hand, ferrate synthesized by the dry method showed comparable results for total coliforms but demonstrated superior and more consistent performance against *E. coli*, with complete elimination observed from 0.08% onward. Moreover, for intestinal enterococci, the dry-synthesized ferrate achieved faster and more effective reduction, with total inactivation attained at just 0.08%.

These findings underscore the potent bactericidal action of ferrate, regardless of synthesis method, and particularly highlight the advantages of the dry synthesis route. The broad-spectrum antimicrobial activity of ferrate confirms its potential as a promising agent for advanced levels of wastewater disinfection and microbial risk reduction.

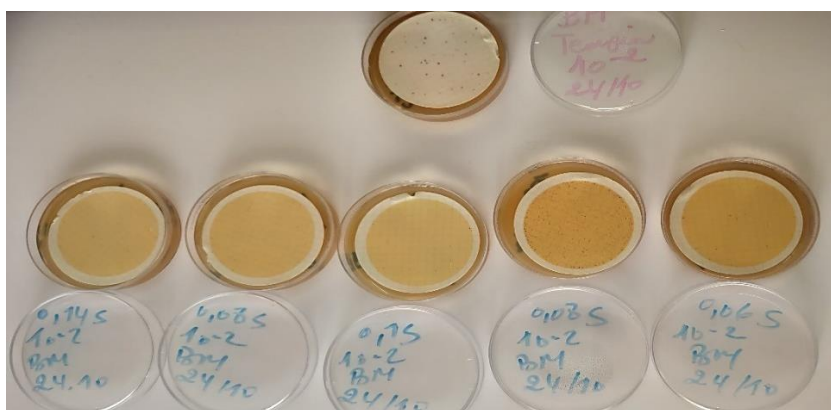


Figure 4.42: Treated samples and witness (case of intestinal enterococci) using ferrate (Beni Messous WWTP).

4.5.2. Beni Mered (Blida) wastewater treatment plan

4.5.2.1. Chemical Oxygen Demand COD

Figure 3.43 depicts the variation in chemical oxygen demand (COD) removal efficiency as a function of ferrate (VI) powder concentration, using materials synthesized via both electrochemical and dry methods. For both types of ferrate (VI), COD removal efficiency increases with rising concentration, peaking at 0.10%. Maximum removal efficiencies of 76.17% and 94.56% were achieved using ferrate (VI) produced by the electrochemical and dry synthesis methods, respectively. This performance is attributed to the dual functionality of ferrate (VI): its strong oxidative capability enables the degradation of a wide range of organic pollutants, while its reduction product, ferric hydroxide $[\text{Fe}(\text{OH})_3]$, acts as an effective coagulant aiding in the removal of suspended and colloidal organic matter [31].

Beyond the optimal concentration of 0.10%, COD removal efficiency declines sharply. This decrease may be attributed to several factors, including the self-decomposition of ferrate at higher concentrations, the formation of undesired by-products, or the scavenging of reactive radicals. Additionally, overdosing ferrate may lead to reduced oxidation efficiency due to the saturation of reactive sites and the interference of excess oxidant with ongoing oxidation reactions.

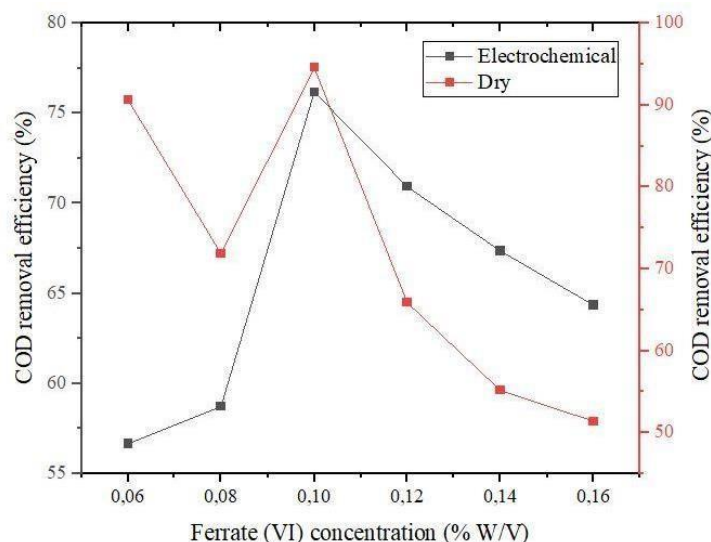


Figure 4.43: COD removal efficiency with both ferrate (VI) synthesized with electrochemical and dry method for Beni Mered WWTP (Blida).

4.5.2.2. Biochemical Oxygen Demand in 5 days BOD_5

Figure 4.44 compares BOD_5 removal effectiveness for ferrate (VI) powders generated using electrochemical and dry techniques. Both samples show a rise in BOD_5 removal effectiveness with ferrate concentration, peaking at 0.10%. At this ideal concentration, electrochemically and dry-synthesized ferrate (VI) had peak elimination efficiencies of 97.24% and 96.89%, respectively. This high performance is due to ferrate (VI)'s strong oxidative capacity (high redox potential up to +2.2 V), which allows it to efficiently degrade a wide range of organic pollutants commonly found in wastewater, as well as the effective coagulating-flocculating action of ferric hydroxide produced during ferrate reduction. Beyond the 0.10% concentration barrier, BOD_5 removal effectiveness decreases.

This drop might be attributed to a variety of processes, including ferrate (VI) breakdown at higher concentrations, the generation of undesired byproducts, the capture of reactive radicals, and overdose effects that reduce overall oxidation efficiency [116].

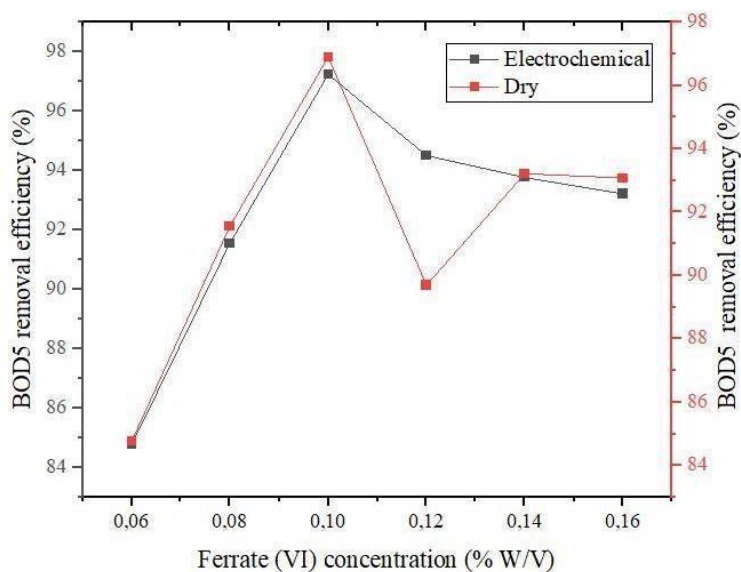


Figure 4.44: BOD₅ removal efficiency with both ferrate (VI) synthesized with electrochemical and dry method for Beni Mered WWTP (Blida).

4.5.2.3. Nitrite (NO₂⁻) removal by ferrate (VI)

Figure 4.45 illustrates the effect of ferrate (VI) powder, synthesized via both electrochemical and dry methods, on the removal efficiency of nitrite (NO₂⁻). The data reveal that nitrite removal efficiency increases with rising ferrate concentration, reaching maximum values of 90.47% and 84.76% at concentrations of 0.12% and 0.08% for electrochemically and dry-synthesized ferrate (VI), respectively.

This enhanced removal is primarily attributed to the strong oxidative potential of ferrate (VI), which facilitates the conversion of nitrite into nitrate (NO₃⁻), a more stable and less reactive nitrogen species. The reaction underscores ferrate (VI)'s capability as a powerful oxidizing agent in aqueous systems [27].

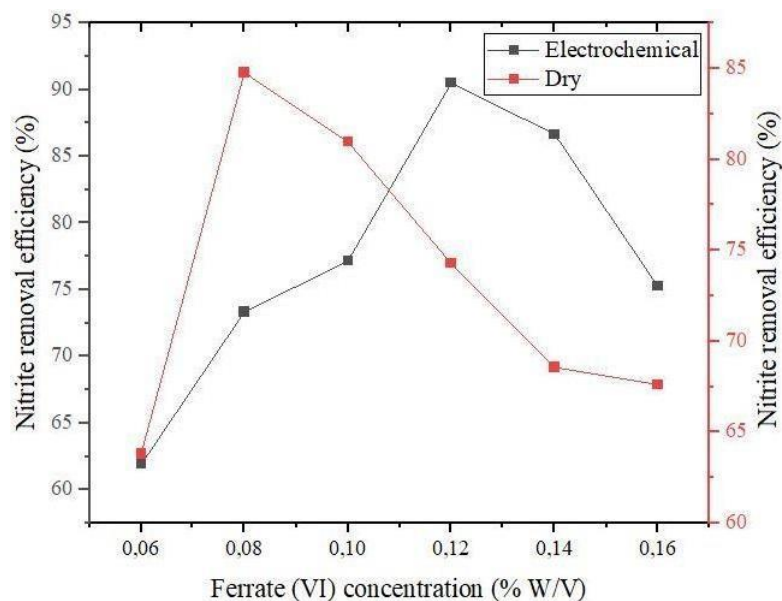


Figure 4.45: Nitrite (NO_2^-) elimination efficiency with both ferrate (VI) synthesized with electrochemical and dry method for Beni Mered WWTP (Blida).

4.5.2.4. Nitrate (NO_3^-) removal by ferrate (VI)

Figure 4.46 presents the variation in nitrate (NO_3^-) removal efficiency as a function of ferrate (VI) powder concentration, comparing both electrochemically and dry-synthesized ferrate. In both cases, nitrate removal efficiency increases with ferrate concentration, reaching a maximum at 0.08%, with peak efficiencies of 91.15% for electrochemically synthesized ferrate and 89.23% for the dry-synthesized counterpart. Although nitrate is a stable and highly soluble anion, making it difficult to remove by conventional oxidation, ferrate (VI) demonstrates multifunctional properties in wastewater treatment.

In this context, the observed removal is attributed not to direct oxidation, but rather to adsorption onto ferric hydroxide $[\text{Fe}(\text{OH})_3]$, the reduction product of ferrate (VI), which acts as a coagulant. The decline in efficiency beyond 0.08% ferrate concentration may result from oversaturation of adsorption sites and the onset of side reactions, which hinder nitrate, capture and reduce overall efficiency [25, 45].

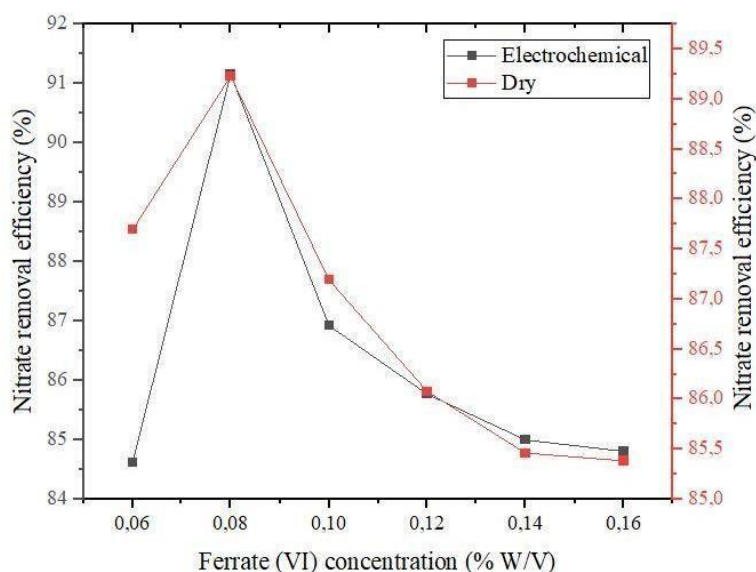


Figure 4.46: Nitrate (NO_3^-) elimination efficiency with both ferrate (VI) synthesized with electrochemical and dry method for Beni Mered WWTP (Blida).

4.5.2.5. Ammonium (NH_4^+) elimination by ferrate (VI)

Figure 4.47 illustrates the relationship between ammonium removal efficiency and ferrate (VI) powder concentration. In both samples, the ammonium removal efficiency increases with the ferrate concentration, reaching a maximum at 0.1%. At this optimal concentration, the highest removal efficiencies were observed: 89% for ferrate (VI) synthesized via the electrochemical method and 85.48% for that produced using the dry method.

These elevated removal rates are likely due to the strong oxidative properties of ferrate (VI), which facilitates the conversion of ammonium ions (NH_4^+) into more oxidized nitrogen species, such as nitrate (NO_3^-) and nitrite (NO_2^-) [105, 118].

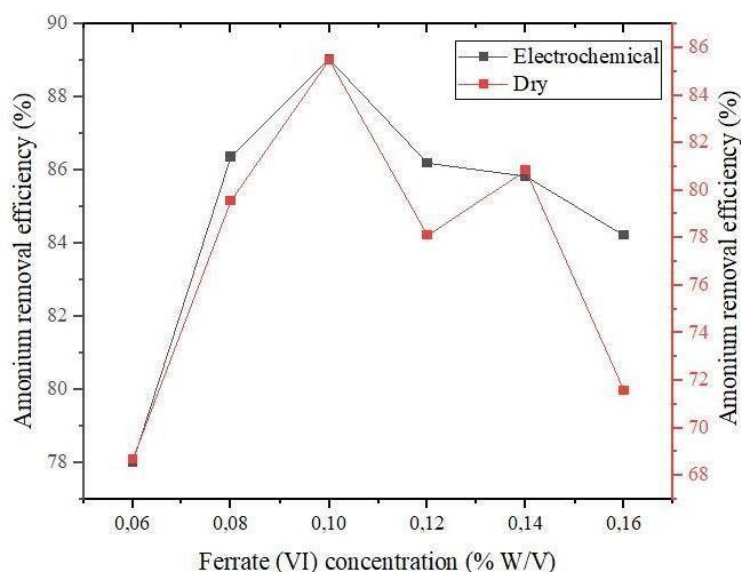


Figure 4.47: Ammonium (NH_4^+) elimination efficiency with both ferrate (VI) synthesized with electrochemical and dry method for Beni Mered WWTP (Blida).

4.5.2.6. Analysis of bacteriological parameters

The table below (4.3) presents the disinfection efficiency of ferrate (figures 4.48 and 4.49), synthesized by both electrochemical and dry methods, in eliminating various types of bacteria from a wastewater sample. To enable accurate enumeration of bacterial colonies, serial dilutions were necessary. Specifically, dilutions of 10^{-5} and 10^{-4} were applied to the *E. coli* and total coliform samples, and to the intestinal enterococci samples, respectively, in order to obtain countable colony-forming units (CFUs).

Table 4.3: Antimicrobial efficacy of ferrate (Beni Mered WWTP).

Ferrate concentration (%)	E.coli (CFU/100mL)		total coliforms (CFU/100mL)		intestinal enterococci (CFU/100mL)	
Synthesis method	Electro	Dry	Electro	Dry	Electro	Dry
none (witness)	18×10^5	18×10^5	95×10^5	95×10^5	9×10^4	9×10^4
0.06	Abs	1×10^4	Abs	Abs	3×10^4	Abs
0.08	Abs	Abs	Abs	Abs	3×10^2	Abs
0.1	Abs	Abs	Abs	Abs	Abs	Abs
0.12	Abs	Abs	Abs	Abs	Abs	Abs
0.14	Abs	Abs	Abs	1×10^5	Abs	Abs

For *E. coli*, electro-synthesized ferrate exhibited strong bactericidal activity, achieving complete inactivation at a concentration as low as 0.06%. In contrast, the dry-synthesized ferrate showed slightly lower performance at this concentration, with residual colonies measured at 1×10^4 CFU/100 mL. However, total elimination was observed at 0.08%, indicating that both synthesis methods are effective, with the electrochemical method offering more rapid disinfection at lower concentrations.

Regarding total coliforms, complete removal was achieved from 0.06% using electro-synthesized ferrate and from 0.08% with the dry-synthesized variant. An exception was noted at 0.14% with the dry method, where a resurgence of bacterial growth (1×10^5 CFU/100 mL) was observed, potentially due to experimental variability or cross-contamination. Despite this anomaly, both synthesis approaches demonstrated reliable efficacy at concentrations equal to or greater than 0.08%.



Figure 4.48: Treated samples and witness (case of *E. coli* and coliforms) using ferrate (VI) (Beni Mered WWTP).

Intestinal enterococci, known for their greater resistance to disinfectants, exhibited a gradual decline in CFU with increasing ferrate concentration. Electro-synthesized ferrate achieved complete inactivation at 0.10%, while the dry-synthesized ferrate achieved this outcome earlier, at 0.08%, suggesting a slightly higher efficiency of the dry method in eliminating more resistant bacterial strains. Notably, at 0.06%, electro-synthesized ferrate still led to a substantial reduction (3×10^4 CFU/100 mL), whereas the dry method resulted in full elimination.

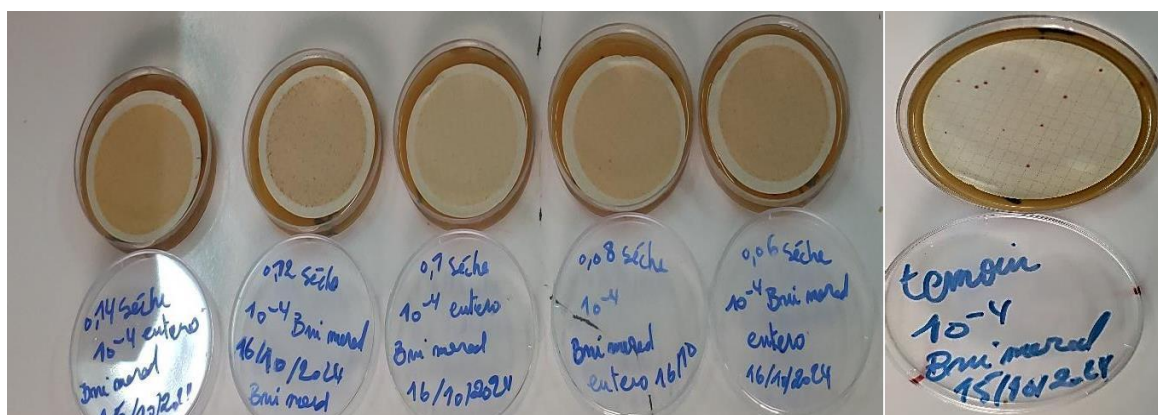


Figure 4.49: Treated samples and witness (case of intestinal enterococci)) using ferrate (VI) (Beni Mered WWTP).

These results confirm the strong antimicrobial capacity of ferrate, especially at concentrations of 0.08% and above, and highlight its potential as an effective agent for advanced wastewater disinfection.

4.5.3. overall results

The following table (4.4) shows the value of each parameter under the optimal concentration of ferrate (VI) synthesized with both dry and electrochemical method in compare with the Algerian discharges standards. It is clear through the data on the table that both ferrate have a high efficiency in wastewater treatment with the same mechanism to eliminate pollutants, due to the multifunctional effect of ferrate (VI) with the respect of the Algerian discharges standards according the WHO.

Table 4.4: Value of different parameter under the optimal concentration of ferrate (VI).

Parameters (mg/L)	COD	BOD ₅	NO ₂	NO ₃	NH ₄ ⁺
Beni Mered WWTP	53.3	5.8	5.25	26	31
After treatment with Electro-Fe(VI)	12.7	0.16	0.5	2.3	3.4
Optimal ferrate (VI) concentration (%)	0.1	0.1	0.12	0.08	0.1
Optimal ferrate (VI) removal (%)	76.17	97.24	90.47	91.15	89
After treatment with Dry –Fe(VI)	2.9	0.18	0.8	2.8	4.5
Optimal ferrate (VI) concentration (%)	0.1	0.1	0.08	0.08	0.1
Optimal ferrate (VI) removal (%)	94.56	96.86	84.76	89.23	85.48
Beni Messous WWTP	44.9	7.12	5.4	26	31
Electro-Fe(VI)	3.5	0.12	0.15	3.55	1.3
Optimal ferrate (VI) concentration (%)	0.1	0.1	0.12	0.08	0.8
Optimal ferrate (VI) removal (%)	92.2	98.3	97.22	86.34	95.8
Dry –Fe(VI)	3.2	0.2	0.2	3.6	1.7
Optimal ferrate (VI) concentration (%)	0.1	0.1	0.08	0.08	0.8
Optimal ferrate (VI) removal (%)	92.87	97.19	95	86.15	94.5
Algerian discharge standards (mg/L)	90	30		30	20-80

Table 4.5 presents the bacterial removal efficiency of ferrate synthesized via both electrochemical and dry methods across the two-wastewater treatment plants. In both cases, ferrate exhibited high effectiveness against *E. coli*, with both synthesis methods achieving complete removal at concentrations equal to or above 0.08%. Similarly, total coliforms were fully inactivated from 0.08% onward, indicating that ferrate is highly efficient even at relatively low doses. Notably, the dry-synthesized ferrate demonstrated superior initial performance against the more resistant intestinal enterococci, achieving complete removal at lower concentrations compared to the electro-synthesized variant. This could be explained by the combination of higher oxidizing strength, improved stability, and more favorable interaction with microbial cells, making it more effective in overcoming bacterial resistance mechanisms early in the treatment process.

Table 4.5: Ferrate removal efficiency (%) for both WWTP studied.

Ferrate concentration (%)	E. coli removal efficiency (%)		Total coliforms removal efficiency (%)		intestinal enterococci removal efficiency (%)	
Beni Mered WWTP						
Synthesis method	Electro	Dry	Electro	Dry	Electro	Dry
Witness(CFU/100mL)	18×10 ⁵	18×10 ⁵	95×10 ⁵	95×10 ⁵	9×10 ⁴	9×10 ⁴
0.06	100	94,44	100	100	66,66	100
0.08	100	100	100	100	44,44	100
0.1	100	100	100	100	100	100
0.12	100	100	100	100	100	100
0.14	100	100	100	98,94	100	100
Beni Messous WWTP						
none (witness)	7×10 ⁴	7×10 ⁴	80×10 ⁴	80×10 ⁴	5×10 ³	5×10 ³
0.06	100	85,71	100	100	88	96
0.08	100	100	100	100	94	100
0.1	71,42	100	100	100	94	100
0.12	100	100	100	100	100	100
0.14	85,71	100	100	100	100	100

CONCLUSION

This research focuses primarily on the chemical extraction of chitin and chitosan from shrimp shells. The extracted chitosan was analyzed using infrared (IR) spectroscopy and X-ray diffraction (XRD), and then characterized based on its physicochemical properties.

Membranes were then prepared from the extracted chitosan and characterized by X-ray diffraction (XRD), thermogravimetric analysis (TGA), and differential scanning calorimetry (DSC), as well as their ion exchange capacity.

The chemical extraction of chitosan and membrane preparation were successfully carried out according to the physico-chemical characterization results; the FTIR shows a characteristic peak of amide I and amide II at a wavelength of 1573 and 1640 cm^{-1} , respectively, with a high deacetylation degree of 96.85% confirming the excellent quality and high solubility of chitosan. The XRD analysis reveals a semi crystalline and amorphous structure in both chitosan powder and membrane, respectively, indicating that the membrane was adequately prepared. TGA and DSC reveal strong heat resistance, making them an excellent ferrate (VI) synthesis alternative.

The prepared membrane was used as a separation in a two-compartment electrochemical cell designed for the electrochemical synthesis of sodium ferrates (Na_2FeO_4). A comprehensive parametric study was performed to determine the optimal operating conditions for ferrate synthesis. The parameters examined included: current density, electrolyte concentration (NaOH), electrolysis time, reaction temperature, and electrode composition and shape. The produced ferrates were analyzed by UV-Visible, IR and XRD spectroscopy, TGA, cyclic voltammetry (CV), chromite titration, and scanning electron microscopy SEM.

Electrochemically synthesized sodium ferrate(VI) achieved notably high concentrations of 0.19 M and 0.23 M when using chitosan membranes, respectively, under optimized conditions. For the chitosan membrane, the optimal parameters included a 24 M sodium hydroxide electrolyte, a current density of 60 mA/cm^2 , an electrolysis duration of 210 minutes, a temperature of 30°C, and an iron electrode containing 0.12% carbon.

The successful generation of ferrate (VI) in both systems demonstrates the effectiveness of chitosan membranes, which were introduced for the first time in ferrate (VI) electro-synthesis. These membranes, being cation exchange (chitosan) materials, offer green, non-toxic, and environmentally friendly alternatives that significantly enhanced the

yield and concentration of ferrate (VI).

The high yield of ferrates (VI) facilitates the formation of its solid form and ensures its long-term stability during storage. Ferrate (VI) characterization displays similarities between our findings and those reported by other researchers. The cyclic voltammetry indicates the detailed ferrate production mechanism through anodic peaks at -1.18 V, -0.96 V, -0.78 V, and -0.67 V. A UV–Vis characteristic peak at a wavelength of 504.5 nm while FTIR spectra shows a characteristic peak at wave number of 865.98 cm^{-1} ; the SEM image confirmed the crystalline structure shown in the XRD results at 30° . The synthesized sodium ferrate has high thermal stability in its powder form goes up to 155°C .

These results indicate that the membranes used are not only efficient, but also very promising for green electrochemical applications, particularly for the synthesis of environmentally friendly oxidants such as ferrates.

Furthermore, the dry synthesis of potassium sulfate-ferrate was optimized in terms of energy conservation thanks to its realization under ambient conditions and improved their yield, purity and stability. A maximum purity of 98.85% was obtained under optimal conditions including a particle diameter between 160 and $200\mu\text{m}$. The process includes an optimal pre-drying of iron sulfate heptahydrate for 10 minutes at 90°C , followed by a 60 minute reaction at a temperature of 30°C . The final product, ferrate (VI), is then dried for 15 minutes at 100°C . After, a triple wash of the ferrate (VI) is carried out to remove residual impurities and ensure better stability of the final compound. The characterization results show a UV-Vis peak of 506.9 nm, an FTIR peak at 815.84 cm^{-1} that characterizes the Fe-O bond in ferrate (VI) with a crystalline form confirmed by DRX at 28° .

Ferrate (VI) demonstrates remarkable efficiency in wastewater treatment. At a concentration of 0.1%, it allows a reduction of 94.56% in chemical oxygen demand (COD) and 97.31% in 5-day biological oxygen demand (BOD₅). Furthermore, at a concentration of 0.08%, it achieves a removal rate of 91.15% for nitrates and 97.22% for nitrites. Finally,

ammonium removal can reach a maximum value of 94.5% at a ferrate concentration of 0.1%. while 100% of bacterial removal was achieved at low ferrate concentration. The result obtained demonstrates the promising efficiency of ferrate synthesized by both methods. This approach opens new perspectives for sustainable wastewater treatment using eco-compatible technologies.

REFERENCES

1. Macova, Z., Bouzek, K., Hives, J., Sharma, V.K., Terryn, R.J., Baum, "Research progress in the electrochemical synthesis of ferrate (VI)", *Electrochim Acta*, 54 (10), (Apr-2009), pp 2673-2683.
2. Scholder, R., Bunsen, H.V., Zeiss, W., "Über orthoferrate IV", *Z. Anorg. Allg. Chem*, vol 283, (1956), pp. 330-337.
3. Scholder R., "Über alkali-oxo-metallate (V) der elemente chrom, mangan,eisen und kobalt,Bull". *Bulletin de la Société Chimique de France* Vol 7,(1965),pp. 1112-1114.
4. Ostrosi, E., "Synthèse des ferrates (VI) de métaux alcalins en utilisant le chlore comme oxydant ". thèse de doctorat . Institut National Polytechnique de Lorraine france,(2007).
5. Kumar, P., Jechan, R., Suresh, L., Kumar, K., "A critical review of ferrate(VI)-based remediation of soil and groundwater". *Environmental Research* ,160, (January2018), pp.420-448.
6. Mellor, J.W., "A Comprehensive Treatise on Inorganic and Theoretical Chemistry", Longmans, Green & Co., London, (1924),pp. 929–937.
7. Eisen teil, D., "Gmelins Handbuch Verlag Chemie, Weinheim", (57), (1932), pp.912.
8. Becquerel, A. . "Ann. Chim. Phys", (51), (1834), pp. 105.
9. Poggendorf, J.C., "Prog. Ann"(54), (1841), pp.372.
10. Bouzek, K., Schmidt, M.J., Wragg, A.A., Bergmann, H. "Electrochemical ferrate (VI) production - anode material aspects", *Institution of Chemical Engineers Symposium Series*,145,199, pp. 153-160. doctoral thesis
11. Adrian James, D., " ELECTROCHEMICAL PREPARATION AND APPLICATION OF THE FERRATE (VI) ION FOR WASTEWATER TREATMENT ", doctoral thesis (7), (1995), UNIVERSITY OF SOUTHAMPTON.
12. Talaiekhazani, A., Samimi-Sedeh, S., & Hassanzadeh, A. *An Overview on Production and Applications of Ferrate(VI)*. *Jundishapur Journal of Health Sciences*, 8(3), e34904. (2016).
13. Ockerman, L.T., Schreyer, J.M., "Chem. Soc". Vol (73), (1951), p. 5478.
14. Toušek, J., "PhD Thesis», CT, Prague, (1959).
15. Helferich, B., Lang, K.," *Allg. Chem*", vol (263), (1950), p.169.
16. Venkatadri, A.S., Bauer, H.H., Wagner, W.F. J., "Transpassive dissolution of iron to Ferrate (VI) in concentrated alkali hydroxide solutions." *Electrochimica acta*, 30(2), (February1985), pp.173-18.

17. Kazama, F., Ferment, J., "Respiratory inhibition of *sphaerotilus* by potassium ferrate". *Journal of fermentation and Bioengineering*, 67(6), (1989), pp.369-373.
18. . Ansaf, V.K., Sukanya K., Lakshmi P., Malhotra, M., "Application of Ferrate for Advanced Water and Wastewater Treatment", (10 June 2020).
19. Libor, M., Zajíček, P., Kolařík, J., Mackuľak, T., Filip, J.. "Ferrates as Powerful Oxidants in Water Treatment Technologies", (2020) ,pp 177-201
20. Caliphs.M.Z., . "Production, Characterization and Application of Ferrate(VI) in Water and Wastewater Treatments". *Brazilian Journal of Analytical Chemistry*, 6(25), November 2019.
21. Wagner, W.F., Gump, J.R., Hart, E.N., "Factors affecting the stability of aqueous potassium ferrate(VI) solutions". *Analytical Chemistry*, 24, (1952), pp .1497-1498
22. Rai, P. Lee, K., Kailasa, J., . Kwon, S. K, Tsang, E., Kim, Y.S., K. H., "Heavy metals in food crops: Health risks, fate, mechanisms, and management", "Environ Res". 160, (2018), pp 420-448 .
23. Zhong, H.Z., Chen, R.Y., Zheng, X., Chen, Z., "Electro-generated FeO_4^{2-} using modified chitosan cation exchange membrane". *J Electrochem* 12(1) (2006) 35–39.
24. Cataldo Hernandez, M.A., May, A., Bonakdarpour, A., Mohseni, M., Wilkinson, D.P., "Analytical quantification of electrochemical ferrates for drinking water treatments". *Can J Chem*, (2016), 13-Sep.
25. Al Umairi, A. R., How, Z. T., Gamal El-Din, M., "Enhanced primary treatment during wet weather flow using ferrate as a coagulant, coagulant aid and disinfectant," *J. Environ. Manage.*, vol. 290, (2020), no. Novembre.
26. Liu, C., Zhou, Z., Yuan, B., Liu, S., Li, F., Sharma, V.K., "Synthesis of ferrate (VI) in two cathodes and one anode cell: enhanced efficiency and treatment of thiocyanate in wastewater". *Ph D J Environ Eng* (2018) 144(10):04018105.
27. Gan, W., Sharma, V. K., Zhang, X., Yang, L., Yang, X., "Investigation of disinfection byproducts formation in ferrate(VI) pre-oxidation of NOM and its model compounds followed by chlorination," *J. Hazard. Mater.*, vol. 292, (2015), pp. 197–204.

28. Mura, S., Malfatti, L., Greppi, G., Innocenzi, P., "Ferrates for water remediation", *Rev Environ Sci Biotechnol*, 16(1), (2017), p.p 15–35.
29. Thompson, G.W., Ockerman, L., Schreyer, J.M., "Preparation and purification of potassium ferrate VI". *Journal of the American Chemical Society*, 73(3), (1951), pp.1379-1381.
30. Jiang, J-Q., Lloyd, B., "Development of ferrate (VI) salt as an oxidant and coagulant for water and wastewater treatment". *Water Research*. 36, (2002), pp.1397-1408.
31. Talaiekhosani, A., Bagheri, M., Reza Talaei, M., Jaafarzadeh, N., "an overview on production and applications of ferrate (VI) ", *Jundishapur J Health Sci*, (July 2016), 8(3): e34904.
32. El maghraoui, A., Zerouale, A., Ijjaali, M., "synthesis process of stable BaFeO_4 by dry method. *International Journal of Chemistry and Materials Research* 2015 Vol. 3, No. 4, 100-106.
33. El maghraoui, A., Zerouale, A., and Ijjaali, M., "Process for the Synthesis of Ferrate (VI) Alkali Metal Dry", *Advances in Materials Physics and Chemistry*, (2015), Vol.5 No.1.
34. Talaiekhosani, A., Bagheri, M., Reza Talaei, M., Jaafarzadeh, N., "an overview on production and applications of ferrate (VI) ", *Jundishapur J Health Sci*, (July 2016), 8(3): e34904.
35. Kanari, N., Filippov, L., Diot, F., Mochón, J., Ruiz-Bustinza, I., Allain, E., Yvon, J., "Synthesis of potassium ferrate using residual ferrous sulfate as iron bearing material" *Journal of Physics: Conference Series*, 2013, Volume 416, Article Number 012013
36. Bin, L., Guangdong, Z., Tiexin, C., Jianshi, Du., "Synthesis of Potassium Ferrate by Chemical Dry Oxidation and Its Properties in Degradation of Methyl Orange". *Asian Journal of Chemistry*, Volume 25, Number 1 (2013), pages 27–31
37. El maghraoui, A., Zerouale, A., and Ijjaali, M., "Synthesis of Stable Alkaline Ferrates (VI) by Dry Process: Quantitative and Qualitative Assessment." *International Journal of Thin Film Science and Technology*, 2023, Volume 12, Issue 3

38. Denvir, A., Pletcher, D.,” Electrochemical generation of ferrate. Part I: Dissolution of an iron wool bed anode”, J. Appl. Electrochem., (26),(1996,) pp. 815-822.
39. Ben Dhieb, F., “Développement et caractérisation de films biodégradables à base d’acide polylactique et de chitosane”, thèse de doctorat (2014), canada
40. Bouzek, K., Schmidt, M.J., Wragg, A.A., Bergmann, H.,” Electrochemical ferrate (VI) production - anode material aspects”, Institution of Chemical Engineers Symposium Series,145,199, pp. 153-160.
41. Alsheyab, M., Jiang, J.Q., Stanford, C., “Electrochemical generation of ferrate (VI): Determination of optimum conditions”, Desalination, vol. 254, no. 1–3, (2010), pp. 175–178.
42. Barişçi, S., Ulu, H. Särkkä, F., Dimoglo, A., Sillanpää, M., “Electrosynthesis of ferrate (VI) ion using high purity iron electrodes: Optimization of influencing parameters on the process and investigating its stability,” Int. J. Electrochem. Sci., vol. 9, no. 6, (2014), pp. 3099–3
43. Zhengwei, Z., Shunping, F., Haiqun, C., & Jing, J., (with Jun Wu contributing from Nanjing University). “Trials of Treating Decentralized Domestic Sewage from a Residential Area by Potassium Ferrate (VI)”. Water, Air, & Soil Pollution, 2017, Volume 228, Article 316.
44. Cataldo-Hernández, M., Stewart, M., Bonakdarpour, A., Mohseni, M., Wilkinson, D.P., “Degradation of ferrate species produced electrochemically for use in drinking water treatment applications”. (2017) Can J Chem Eng.
45. M. Diaz; K.Doederer; J.Keller; M.Cataldo; B.-C.Donose;Y.Ali; P.Ledezma ;“Towards in situ electro-generation of ferrate for drinking water treatment: A comparison of three low-cost sacrificial iron electrodes”, J. Electroanal. Chem., vol. 880, (2021) p. 114897.
46. Klein, J., Kupec, R., Stöckl, M., Waldvogel, S.R., “Degradation of lignosulfonate to vanillic acid using ferrate”. Adv Sustain Syst (2023) 2200431.
47. EL MAGHRAOUI, A., ZEROUALE, A., IJJAALI, M., “K₂FeO₄ Electrochemically Stable Synthesis Process,” Int. J. Chem. Mater. Res., vol. 3, no. 3, (2015), pp. 79–85.

48. Benhabiles ,M. S., Salah, R., . Lounici, H., Drouiche, N., Goosen, M. F. A., Mameri, N., “Antibacterial activity of chitin, chitosan and its oligomers prepared from shrimp shell waste,” *Food Hydrocoll.*, vol. 29, no. 1, (2012), pp.
49. Wang, X., Zhou, P., Lv, X., Liang, Y., “Insight into the structure-function relationships of the solubility of chitin/chitosan in natural deep eutectic solvents”, *Mater. Today Commun.*, vol. 27, no. (March 2021), p. 102374.
50. Vedula, S. S., Yadav, G. D., “Chitosan-based membranes preparation and applications: Challenges and opportunities,” *J. Indian Chem. Soc.*, vol. 98, no. 2, (2021), p. 100017.
51. Le Roux, K., “Purification de la chitine par hydrolyse enzymatique à partir de coproduits de crevette *Penaeus vannamei*. Caractérisations des produits et optimisation du procédé”, (2012), p. 222.
52. Vedula, S.S., Yadav, G.D., “Chitosan-based membranes preparation and applications: Challenges and opportunities” , *J. Indian Chem. Soc.*, vol. 98, no. 2, (2021), p.100017.
53. Khan, T. A., Peh, K. K., Ch’ng, H. S., “Reporting degree of deacetylation values of chitosan: The influence of analytical methods,” *J. Pharm. Pharm. Sci.*, vol. 5, no. 3, (2002) pp. 205–212.
54. Hajji, S., “Structural differences between chitin and chitosan extracted from three different marine sources,” *Int. J. Biol. Macromol.*, vol. 65, (2014), pp. 298–306.
55. Yu, W., Yang, Y., Graham, N., “Evaluation of ferrate as a coagulant aid/oxidant pretreatment for mitigating submerged ultrafiltration membrane fouling in drinking water treatment,” *Chem. Eng. J.*, vol. 298, (2016), pp. 234–242.
56. Matet ,M., “Preparation of chitosan-based films by melting”. Doctoral thesis, *Ecole Polytechnique de Montréal PolyPublie* (2014).
57. Yunho, L., Min, C., Jee Yeon., K., Jeyong, Y., “Chemistry of ferrate (fe(vi)) in aqueous solution and its applications as a green chemical,” *Journal of Industrial and Engineering Chemistry*, vol. 10, no. 1. pp. 161–171, 2004.
58. Jia-Qian, J., Shaoqing, Z., Michael, P., Christian, M., “Exploration of Ferrate(VI) Potential in Treating Lake Constance Water”. *Environments (MDPI)*, 2023, Volume 10, Issue 2, Article 25

59. Rejsek, F., "Analyse des eaux : Aspects réglementaires et techniques . Scéren (CRDP AQUITAINE) (2002). Coll. Biologie technique. Sciences et techniques de l'environnement. 360p.
60. Talaiekhosani, A., Bagheri, M., Reza Talaei, M., Jaafar zadeh, N., "an overview on production and applications of ferrate (VI). Jundishapur J Health Sci July 8(3), (March 22-2016) e34904.
61. Munyengabe, A., Production, Z.C., "Characterization and application of ferrate (VI) in water and wastewater treatments", Braz J Anal Chem 6(25), (2019), 40–57.
62. Metahri M.S. "Elimination simultanée de la pollution azotée et phosphatée des eaux usées traitées par des procédés mixtes cas de la step de la ville de tizi-ouzou", thèse de doctorat, Université Mouloud Mammeri, Tizi-Ouzou, (2012), 172p.
63. Rodier, J., "L'Analyse de l'eau - Eaux naturelles, eaux résiduaires, eau de mer : chimie, physico-chimie, microbiologie, biologie, interprétation des résultats. 8^{ème} Edition. DUNOD, Paris, (2005) 1381p.
64. Belaid, N., "Evaluation des impacts de l'irrigation par les eaux usées traitées sur les plantes et les sols du périmètre irrigué d'El Hajeb-Sfax: salinisation, accumulation et phyto-absorption des éléments métalliques". Thèse de doctorat, Université de Limoges, (2010), 236p.
65. Tabet, M., "Etude physico-chimique et microbiologique des eaux usées et évaluation du traitement d'épuration". Thèse de doctorat, Université Guelma, Algérie, (2015), 161p
66. Kendouci, M.A., Etude de risque de pollution des eaux souterraines de la ville de Béchar et valorisation du sable en vue de son utilisation en traitement des eaux usées, thèse de doctorat. (2018), USTO-MB, Algérie
67. Schriver-M., "La gestion durable de l'eau : Ressources, Qualité, Organisation". DUNOD, Paris, (2012), 250p. ISBN : 978-2-10-10-055026-5.
68. Cardot, C., "Techniques appliquées au traitement de l'eau", Edition ELLIPSES, (2001), ISBN : 978-2-7298-0494-7, 248p.
69. Quevauviller P., Thomas O., Van der Beken A., "Wastewater quality monitoring and treatment". John Wiley & Sons, Ltd, 394p. (2006), ISBN: 978-0-471-49929-9.

70. Ohanssian, K., "Optimisation de filières de traitement des eaux résiduaires industrielles par couplage de procédés physico-chimiques thermiques et biologiques". Thèse de doctorat, Université d'Aix Marseille, France,(2019), 244p.
71. El-Sawy, S.M., Abu-Ayana, Y.M., AbdelMohdy, F.A., "Some chitin/chitosan derivatives for corrosion protection and wastewater treatments". *Anti-Corros Methods Mater* (2001), Vol. 48 Iss 4 pp 227 – 235
72. El Knidri ,H., Belaabed, R., Addaou, A., Laajeb, A., Lahsini, A., "Extraction, chemical modification and characterization of chitin and chitosan", *Int J Biol Macromol*, 120: (2018),1181–1189.
73. Awaliah, T.P., Asnawati, D., Hamdiani, S., "Effectivity of water soluble chitosan from Rajungan shell waste as corrosion inhibitor on iron in 1 M HCl". *The first Progress in Science and Technology Research Symposium (PSTRS)*. (2020), *J Phys: Conf Ser IOP Publishing* 1594, 012004
74. Kumari, S., Ratha, P., Sri Hari Kumar, A., Tiwari, T.N., "Extraction and characterization of chitin and chitosan from fishery waste by chemical method". (2015), *Environ Technol Innov* 77–85
75. Triunfo, M., Tafi, E., Guarnieri, A., Scieuzo, C., Hahn, T., Zibek, S., Salvia, R., Falabella, P., "Insect chitin-based nanomaterials for innovative cosmetics and cosmeceuticals". (2021), *Cosmetics* 8, 40. MDPI.
76. Mathew, G.M., Mathew, D.C., Sukumaran, R.K., Sindhu, R., Huang, C., Binod, P., Sirohi, R., Kim, S., Pandey, A "sustainable and eco- friendly strategies for shrimp shell valorization". (2020), *Environ. Pollut ENPO* 115656
77. Hussein, M.H.M., El-Hady, M.F., Sayed, W.M., Hefni, H., "Preparation of some chitosan heavy metal complexes and study of its properties". (2012), *Polym Sci Ser A* 54(2):113–124
78. Cheng, J., Zhu, H., Huang, J., Zhao, J., Yan, B., Ma, S., Zhang, H., Fan, D., "The physicochemical properties of chitosan prepared by microwave heating". *Food Sci Nutr* published by Wiley Periodicals (2020), 8:1987–1994.
79. Huthman, A.S., Buhari, F., Olagunju, J., Odawn, A., Huthman, O.I., "Chemical analysis and characterization of shrimp chitosan in shrimp shell waste from lagos lagoon". *Nizeria Int j chem pharm*, (2013), sci 2:377–385

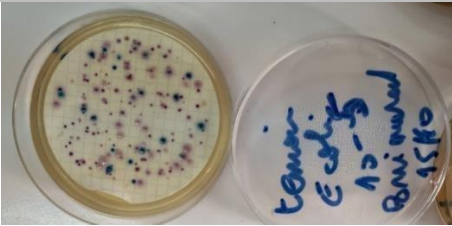
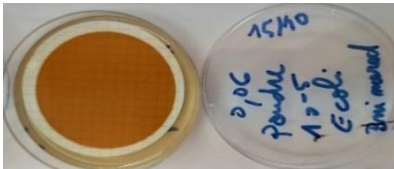
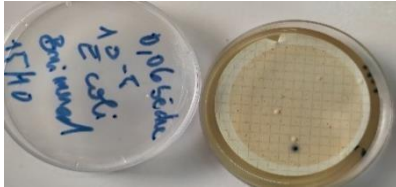
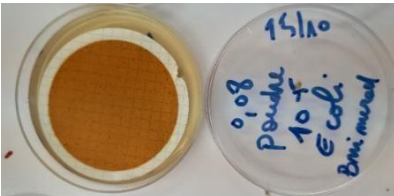

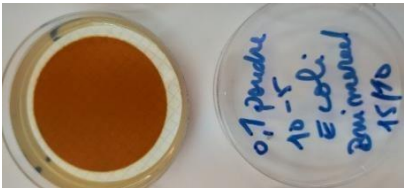
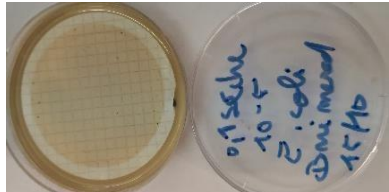
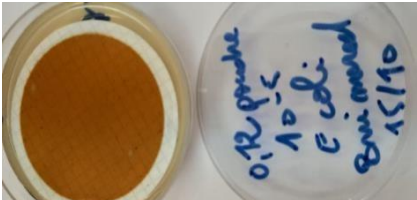
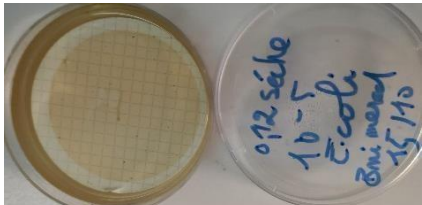
80. Varun, T.K., Senani, S., Jayapal, N., Chikkerur, J., Roy, S., Tekulapa-lly, V.B., Gautam, M., Kumar, N., "Extraction of chitosan and its oligomers from shrimp shell waste, their characterization and antimicrobial effect". *Vet World* (2017), 10(2):170–175
81. Mohanasrinivasan, V., Mishra, M., Paliwal, J., Singh, S., Selvarajan, E., Suganthi, V., "Studies on heavy metal removal efficiency and antibacterial activity of chitosan prepared from shrimp shell waste". *3 Biotech* (2014), 4:167–75
82. Sudatta, B.P., Sugumar, V., Varma, R., Nigariga, P., "Extraction, characterization and antimicrobial activity of chitosan from penshell, *Pinna bicolor*". *Int J Biol Macromol BIOMAC* (2020), 16048
83. Boukhlifi, F., "Quantitative analysis by IR: determination of chitin/chitosan DD". chapter Khan M, Morari G, Nascimento D, El-Azazy M (ed) 04 March *Mod Spectrosc Tech Appl*, (2020)
84. Tolesa, L.D., Bhupender, S., Ming-Jer, L.G., "Chitin and chitosan production from shrimp shells using ammonium-based ionic liquids". *Int J Biol Macromol* (2019), 130:818–828
85. Feketeföldi, B., Cermenek, C., Spirk, A., Schenk, C., Grimmer, M., Bodner, M., Koller, V., Ribitsch, V.H., "Chitosan-based anion exchange membranes for direct ethanol fuel cells birgit". *J Membra Sci Technol* (2016), 6:1
86. Liu, Y., Cai, Z., Ma, M., Sheng, L., Huang, X., "Effect of eggshell membrane as porogen on the physicochemical structure and pro tease immobilization of chitosan-based macroparticles", *Carbohydr Polym*, (2020), 242:116387.
87. Luo, Z., Strouse, M., Jiang, J.Q., Sharma, V.K., "Methodologies for the analytical determination of ferrate (VI): a review". *J Environ Sci Health, Part A: Toxic/Hazard Subst Environ Eng* 46(5), (2011) ,453–460.
88. licht, S., naschitz, V., Halperin, L., Halperin, N., lin, L., chen, J., ghosh, S., liu, B., "Analysis of ferrate (VI) compounds and super iron Fe (VI) battery cathodes: FTIR, ICP, titrimetric, XRD, UV/VIS and electrochemical characterization", *J Power Sources* 101, (2001), 167–176.

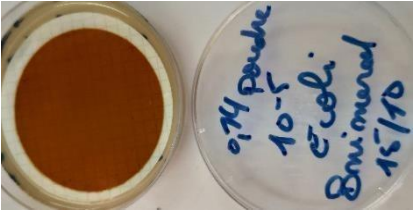
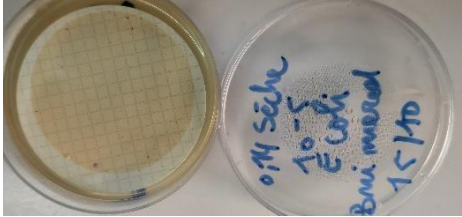




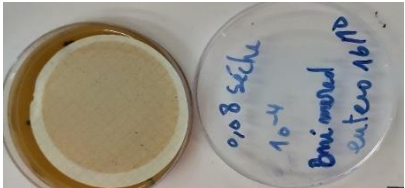




89. Simonović, D., Pešovski, B., Krstić, V., “electrochemical synthesis of ferrate (VI) for the wastewater treatment”. Mining & Metallurgy Engineering Bor No. 3–4 , (2018), str. 49–54.
90. Sari, M., Tamrin, Kaban, J., Alfian, Z., “Comparison of morphology and compatibility of chitosan membrane and Chi-Pec-Gp”, AIP Conference Proceedings 2049, 020048, (2018).
91. Sreelekshmi, R.S., Lincy, A., Jose, J.J., “Shelf-life specific moisture variation in chitosan of genus *fenneropenaeus* distributed along Arabian Sea, INDIA”. bioRxiv, (2022) ,preprint this version posted May 16 <https://doi.org/10.1101/2022.05.15.491996>.
92. Bellouti, F., “Préparation de chitosane à partir des carapaces de crevettes : étude et caractérisations”, thèse de doctorat, (2018).
93. Ait Boulahsen, M., Chairi, H., Laglaoui, A., Arakrak, A., Zantar, S., Bakkali, M., Hassani, M., “Optimization and characterization of gelatin and chitosan extracted from fish and shrimp waste” (2018) , E3S Web of Conferences 37, 02006.
94. Alishahi, A., Mirvaghefi, A., Tehrani, M.R., Farahmand, H., Shojao sadati, S.A., Dorkoosh, F.A., Elsabee, Z.M., “Enhancement and characterization of chitosan extraction from the wastes (2011), Journal of Environmental Polymer Degradation, 19(3):776-783.
95. Dhanashree, B.G., Basavaraj, S.H., “Two-phase extraction, characterization, and biological evaluation of chitin and chitosan from *Rhizopus oryzae* ”. J Appl Pharm Sci 8(11): (2018),116–122.
96. Zhang, H., Kong, M., Jiang, Q., Hu, K., Ouyang, M., Zhong, F., Qin, M., Zhuang, L., Wang, G., “Chitosan membranes from acetic acid and imidazolium ionic liquids: effect of imidazolium structure on membrane properties”, J Mol Liq, (2021), 340:117209.
97. Ben Seghir, B., Benhamza, M. H., “Preparation, optimization and characterization of chitosan polymer from shrimp shells”. Original paper Food Measure cross mark.
98. Barişçi, S., Ulu, F., Särkkä, H., Dimoglo, A., Sillanpää, M., “Electrosynthesis of ferrate (VI) ion using high purity iron electrodes: Optimization of influencing


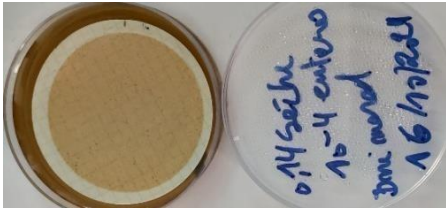
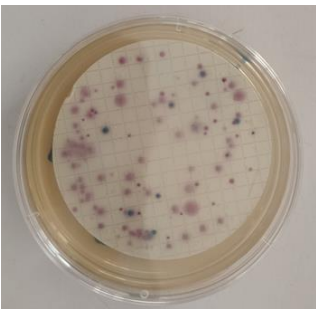
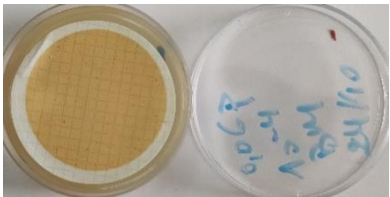
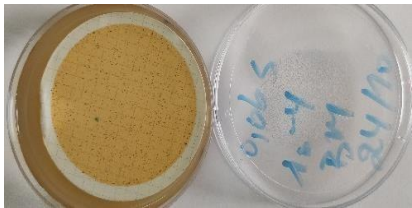
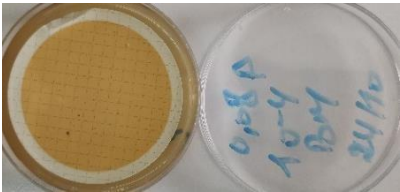
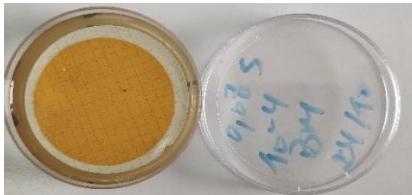

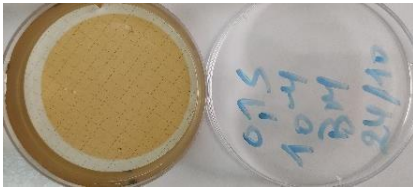
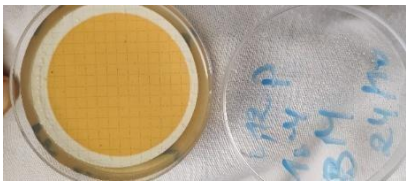
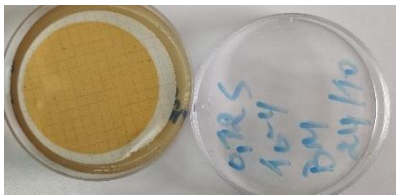
- parameters on the process and investigating its stability,” *Int. J. Electrochem. Sci.*, vol. 9, no. 6, (2014) pp. 3099–3117.
99. İlka, S., Ramanauskaitė, A., Bilican, B.K., Mulerčikas, P., Çam, D., Serdar Onses, M., Torun, I., Kazlauskaitė, S., Baublys, V., Aydın, Ö., Zang, L.S., Kaya, M., “Usage of natural chitosan membrane obtained from insect corneal lenses as a drug carrier and its potential for point of care tests”, *Mater Sci Eng C*, Volume 112, (July 2020), 110897.
 100. Gabriele, F., Donnadio, A., Casciola, M., Germani, R., Spreti, N., “Ionic and covalent crosslinking in chitosan-succinic acid membranes: effect on physicochemical properties”, *Carbohydr Polym*, (2021) ,251:117106.
 101. Feketeföldi, B., Cermenek, C., Spirk, A., Schenk, C., Grimmer, M., Bodner, M., Koller, V., Ribitsch, V.H., “Chitosan-based anion exchange membranes for direct ethanol fuel cells birgit”. *J Membra Sci Technol* (2016) 6:1.
 102. Nguyen, T.V.A., ThiBinh, P., ThiXuan, M., Thanh Thuy, M.T., “The effect of NaOH concentration on ferrate Electrosynthesis”. *Vietnam J Chem*, (2024), 1–9.
 103. Simonović, D., Pešovski, B., Krstić, V., “Electrochemical synthesis of ferrate (VI) for the wastewater treatment”. *Mining & Metallurgy Engineering Bor* No. 3–4 , (2018) str. 49–54.
 104. Yanga, E.L., Shi, J.J., Liang, H.C., “On-line electrochemical production of ferrate (VI) for odor control”. *Electrochim Acta*, 63:, (2012) ,369–374.
 105. Barışçi, S., “Electrochemical ferrate (VI) synthesis with cast iron shavings and its potential application for household graywater recycling”. *J Environ Eng* 144(9): (2018) 04018073.
 106. El Maghraoui, A., Zerouale, A., Ijjaali, M., Sajieddine, M., “Synthesis and characterization of ferrate (VI) alkali metal by electro chemical method”. *Adv. Mater. Phys. Chem*, 3, (2013) , 83–87.
 107. Lee, Y., Cho, M., Kim, J.Y., Yoon, J., “Chemistry of ferrate (Fe(VI)) in aqueous solution and its applications as a green chemical”. *J Ind Eng Chem* 10(1):, (2004) ,161–171.
 108. Sanjari, A.J., Asghari, M., “A review on chitosan utilization in membrane synthesis”. *ChemBioEng Rev*, 3(3): (2016) 134–158.


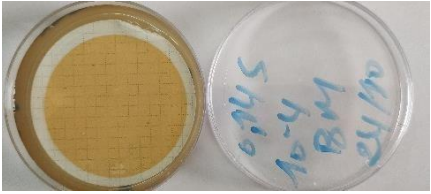

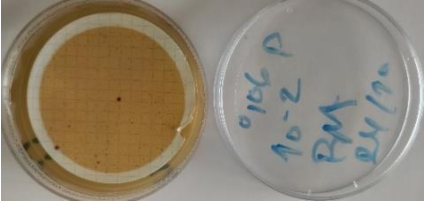
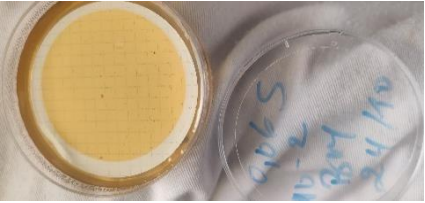


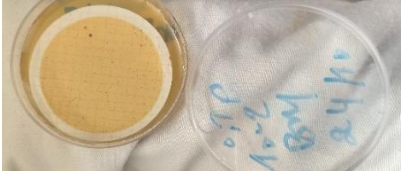
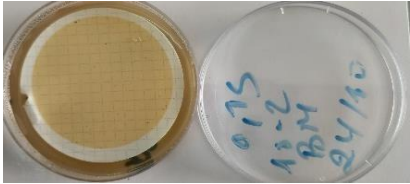
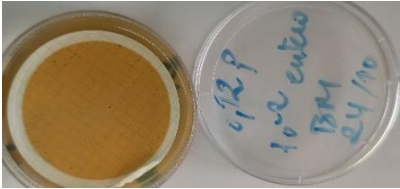
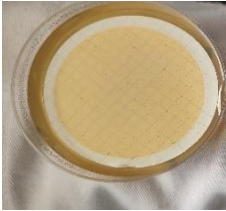
109. Herasa, A., Rodri'guez, N.M., Ramos, V.M., Agullo, E. N., "methylene phosphonic chitosan: a novel soluble derivative". *Carbohydr Polym* 44 (2001) 1–8.
110. Munyengabe, A., Zvinowanda, C., "Synthesis and chemical stability studies of sodium ferrate (VI) solution". *Asian J Chem*,(2019), 31(12):3029–3034.
111. Xu, Z., Wang, J., Shao, H., Tang, Z., Zhang, J., "Preliminary investigation on the physicochemical properties of calcium ferrate (VI)". *Electrochem commun* ,(2007), 9:371–377.
112. Caliphs, M.Z.V., "Production, Characterization and Application of Ferrate (VI) in Water and Wastewater Treatments". *Brazilian Journal of Analytical Chemistry*, 6 (25), (November 2019).
113. Hrnčiarikova, L., Gál, M., Kerekeš, K., Híveš, J., "Voltammetric and impedance study of the influence of the anode composition on the electrochemical ferrate(VI) production in molten NaOH", *Electrochim. Acta*, vol. (2013) pp. 581–586,.
114. Gunawan, G., Prasetya, N.B.A., Pratista, H.A.E, "Ferrate synthesis using NaOCl and its application for dye removal". *Open Chem* ,(2022) ,20:1142–1154.
115. Machala, L., Zboril, R., Sharma, V.K., Filip, J., Schneeweiss, O., Homonnay, Z., Mossbauer characterization and in situ monitoring of thermal decomposition of potassium ferrate (VI), K_2FeO_4 in static air conditions". *J Phys Chem B* ,(2007) ,111:4280–4286
116. Alsheyab, M., Jiang, J.Q., Stanford, C., "On-line production of ferrate with an electrochemical method and its potential application for wastewater treatment - A review," *J. Environ. Manage.*, vol. 90, no. 3, (2009), pp. 1350–1356.
117. Al Umairi, A. R., How, Z.T., Gamal El-Din, M., "Enhanced primary treatment during wet weather flow using ferrate as a coagulant, coagulant aid and disinfectant", *J. Environ. Manage.*, vol. 290, no. (November 2020).
118. Liu, K., Yi, Y., Zhang, N., "Anodic oxidation produces active chlorine to treat oilfield wastewater and prepare ferrate (VI)". *J Water Process Eng* 41: ,(2021), 101998.

APPENDIXES

Beni Mered WWTP			
Electrochemical Fe (VI) powder		Dry ferrate (VI) powder	
E.coli and coliforms			
witness			
0.06%			
0.08%			
0.1%			
0.12%			

0.14%		
enterococci		
Witness		
0.06%		
0.08%		
0.1%		
0.12%		

0.14%		
Beni Messous WWTP		
Electrochemical ferrate (VI) powder		Dry ferrate (VI) powder
E.coli and coliforms		
		
0.06%		
0.08%		
0.1%		
0.12%		

0.14%		
enterococci		
witness		
0.06%		
0.08%		
0.1%		
0.12%		
0.14%	